

Aus dem Institut für Experimentelle und Klinische Pharmakologie und
Toxikologie
der Universität zu Lübeck
Direktor: Prof. Dr. med. M. Schwaninger



UNIVERSITÄT ZU LÜBECK

**Therapeutic effects mediated through the hydroxycarboxylic acid
receptor 2 in an autoimmune disease of the skin.**

Inauguraldissertation
zur
Erlangung der Doktorwürde
der Universität zu Lübeck
- aus der Sektion Medizin –

vorgelegt von
Jakob Friedrich Vielhauer
aus Troisdorf

Lübeck 2021

1. Berichterstatter: Prof. Dr. med. Markus Schwaninger
2. Berichterstatter: Priv.-Doz. Dr. rer. nat. Kathrin Kalies

Tag der mündlichen Prüfung: 15.06.2021

Zum Druck genehmigt. Lübeck, den 15.06.2021

- Promotionskommission der Sektion Medizin -

Dedicated to my parents and my brother.

Table of contents

1.0 Summary.....	1
1.1 Zusammenfassung	2
2.0 Introduction.....	4
2.1 Epidermolysis bullosa acquisita	4
2.2 Dimethyl fumarate.....	8
2.3 HCA₂ receptor.....	13
2.4 Neutrophil effector functions, diapedesis and the role of L-selectin.....	17
2.5 Objective of this thesis.....	21
3.0 Material.....	22
3.1 Equipment	22
3.2 Consumables	23
3.3 Reagents.....	24
3.4 Medium, Buffers and Solutions.....	26
3.5 Antibodies.....	27
3.6 Software.....	28
4.0 Methods.....	29
4.1 Animal experiments.....	29
4.2 FACS analysis	34
4.3 Histological approaches	39
4.4 Statistical analysis.....	41
5.0 Results.....	43
5.1 Validation of antibodies used during flow cytometry in EBA.....	43
5.2 Verifying successful disease induction in immunohistochemical stainings of epidermolysis bullosa acquisita skin samples	49
5.3 Epidermal thickness measurement.....	51
5.4 HCA₂ expression in epidermolysis bullosa acquisita.....	53

5.5 DMF and inflammatory cells in the skin.....	61
5.7 The role of L-selectin in conveying the DMF treatment effect.....	64
5.8 Evaluation of gender and HCA ₂ dependency of DMF treatment	67
5.9 Effects of ketogenic and niacin free diet on EBA	71
6.0 Discussion.....	75
6.1 HCA ₂ carrying cells and their importance in EBA	75
6.2 Neutrophil effector functions and L-selectin	80
6.3 Gender effects in immunology.....	82
6.4 Effect of diets in EBA and DMF treatment.....	85
7.0 References.....	90
8.0 Appendix.....	97
8.1 Abbreviations	97
8.2 List of tables	100
8.3 List of figures	100
8.4 Tierversuchsgenehmigung.....	101
9.0 Curriculum vitae	102
10.0 Danksagung.....	105

1.0 Summary

The therapy of autoimmune diseases remains a challenging task, often involving immunosuppressive agents. In multiple sclerosis (MS) therapy, amongst others, dimethyl fumarate (DMF) has proven its efficacy clinically. The primary metabolite of the drug, monomethyl fumarate (MMF), is a hydroxycarboxylic acid receptor 2 (HCA₂) agonist and experimental approaches proved receptor dependency of the treatment effect in a mouse model of MS. Currently this knowledge is extended to understand the role of the receptor in detail and broaden the spectrum of HCA₂ agonists in clinical use.

The objective of this dissertation was to clarify the importance of the receptor in epidermolysis bullosa acquisita (EBA), an autoimmune disease of the skin, as first data also indicated an HCA₂-dependent effect. The impact of receptor activation on the abundance of different cell types, their distribution in the body and receptor expression upon treatment was assessed. In addition, baseline activation via nutritional receptor agonists and the role of gender on the course of disease was investigated.

After verifying successful disease induction, the HCA₂-dependent treatment effect of DMF described beforehand could be reproduced with reduced affected body surface in animals receiving the drug.

Consistent with published data, a large proportion of neutrophils expressed the receptor on the surface and proved to be responsive to treatment: In the skin fewer neutrophils were detected upon drug administration during EBA. Furthermore, classical and non-classical monocytes, also expressing the receptor on the cell surface in large proportion, were identified as possible mediators of the treatment effect as their distribution was interfered by treatment. In secondary lymphoid organs DMF administration resulted in higher numbers of these cell. Interestingly, $\gamma\delta$ T cells were found elevated in the skin upon DMF treatment.

Concluding from these data, an impact of HCA₂ on migration patterns was hypothesised. In the process of neutrophil migration L-selectin possesses a central role. Levels of the molecule detected on the cell surface inversely correlate to their activation and migration potential. In animals receiving DMF treatment, a significant rise in L-selectin could be detected in neutrophils and non-classical monocytes in the blood.

Their reduced migration thus possibly explains ameliorated skin pathology.

Concerning endogenous receptor activation, an impact on disease scores could not be found in animals fed with ketogenic diet elevating the production of endogenous ligands. When comparing animals with access to a nicotinic acid low diet to those with the usual chow enriched in this compound, a significant reduction in serum levels of nicotinic acid could be detected. The impact of these findings on the clinical course of EBA needs further evaluation.

Lastly, female animals showed significantly lower counts of neutrophils and non-classical monocytes whereas natural killer, $\alpha\beta$ T and $\gamma\delta$ T cells were more abundant, indicating that gender interfered with the autoimmune process.

1.1 Zusammenfassung

Autoimmunerkrankungen sind ein bedeutender Morbiditätsfaktor in der Gesellschaft und ihre Behandlung stellt bis heute eine Herausforderung dar. Dimethylfumarat (DMF) ist derzeit eine etablierte Erstlinientherapie der Multiplen Sklerose (MS), auch wenn die molekulare Basis für die Wirkung nicht geklärt ist. In einem Tiermodell konnte jedoch gezeigt werden, dass der Effekt durch den Hydroxycarbonsäure-Rezeptor 2 (HCA₂) vermittelt wird.

Ziel dieser Arbeit war es, herauszufinden ob die Aktivierung des Rezeptors auch in einer anderen Autoimmunkrankheit, der blasenbildenden Hauterkrankung Epidermolysis bullosa acquisita (EBA), einen Einfluss auf den Krankheitsverlauf ausübt. Des Weiteren sollte der molekulare Einfluss der Rezeptoraktivierung evaluiert werden. Dazu wurde die Verteilung verschiedener HCA₂ tragender Zellen während der Erkrankung und im Hinblick auf die Behandlung, sowie der Einfluss endogener und alimentärer Agonisten untersucht.

Zunächst konnte gezeigt werden, dass die Population neutrophiler Granulozyten, welche zu einem großen Teil den HCA₂-Rezeptor auf ihrer Oberfläche exprimieren, besonders stark auf eine Aktivierung desselben reagieren. Ihre Anzahl in der Haut wurde durch die Gabe von DMF deutlich verringert. Ebenso konnte gezeigt werden, dass Monozyten hinsichtlich ihrer Verteilung durch eine Rezeptoraktivierung beeinflusst werden, da in der Interventionsgruppe eine höhere Anzahl dieser Zellen in den sekundär lymphatischen Organen zu finden war.

Außerdem beeinflusste die Gabe von DMF die Verteilung von gamma-delta ($\gamma\delta$)T-Lymphozyten. Diese im Zusammenhang mit Autoimmunerkrankungen besonders im Fokus stehenden Zellen konnten in ihrer Zahl im Vergleich zur Vehikelgabe signifikant häufiger in der Haut gefunden werden.

Aufgrund der erhobenen Daten war ein Einfluss von HCA₂ auf die Migration von Zellen naheliegend. Bei neutrophilen Granulozyten spielt insbesondere das auf der Zelloberfläche exprimierte Molekül L-Selektin eine herausragende Rolle in der Extravasation. Die Expression von L-Selektin auf der Oberfläche kann als Marker für die Bereitschaft der Migration sowie den Aktivierungsstatus der Zelle verwendet werden und korreliert jeweils invers mit diesen. Es konnte gezeigt werden, dass bei neutrophilen Granulozyten sowie einer Gruppe von Monozyten (nicht-klassische Monozyten) in der DMF Behandlungsgruppe vermehrt L-Selektin exprimiert wird. Insgesamt stellt dies eine mögliche Erklärung für die geringere Anzahl dieser Effektorzellen in der Haut, und dadurch verminderte Krankheitsaktivität dar.

Zudem wurde der Einfluss endogener und alimentär zugeführter Rezeptoragonisten untersucht. Hier zeigte sich, dass eine ketogene Diät und dadurch erhöhte endogene Bildung von Betahydroxybutyrat, einem Rezeptoragonist, keinen Einfluss auf den Verlauf der EBA besaß. In einem zweiten Experiment wurde die normale, mit Nikotinsäure angereicherte Diät mit einer Zubereitung, welche deutlich weniger Anteile dieses Agonisten enthält, verglichen. Es konnte eine deutliche Reduktion des Plasmanikotinsäurespiegels gezeigt werden, sodass die Anreicherung des Futters kritisch zu bewerten ist. Insgesamt bedarf es jedoch weiterer Experimente, insbesondere um den Einfluss dieser Ergebnisse auf den klinischen Verlauf der EBA einschätzen zu können. Bei der nach Geschlecht getrennten Auswertung der Daten konnten Unterschiede im Verteilungsmuster HCA₂-tragender Zellen während der EBA beobachtet werden. So war die Anzahl von neutrophilen Granulozyten und nicht-klassischen Monozyten bei weiblichen Tieren während der EBA vermindert. Natürliche Killerzellen, sowie $\alpha\beta$ - und $\gamma\delta$ T-Lymphozyten konnten bei männlichen Tieren vermehrt nachgewiesen werden.

2.0 Introduction

2.1 Epidermolysis bullosa acquisita

General information, clinical presentation & diagnosis

Epidermolysis bullosa acquisita is a rare autoimmune disease of the skin. In literature, an incidence of 0.2 – 0.5 cases per one million residents is recorded¹. In the early 1970s characteristics and diagnostic criteria of the pathology have been put forward². In general, EBA belongs to the group of autoimmune blistering diseases and the four following major clinical criteria need to be fulfilled for diagnosis: 1. Disease onset in adulthood; 2. No family history of epidermolysis bullosa dystrophica (the hereditary form); 3. Spontaneous or trauma-associated blistering of the skin resembling epidermolysis bullosa dystrophica; 4. Exclusion of other bullous diseases.

Further research identified the autoantigen³ : Type VII-Collagen (COL7). The protein plays a crucial role in attaching the epidermis to the underlying basement membrane zone via so-called anchoring fibrils. Autoantibodies directed against the compound then lead to subepidermal blistering as the connection to the basement membrane can no longer be sustained. In most patients, such autoantibodies (immunoglobulins) can be detected bound to the tissue at the dermal-epidermal junction. Less frequently, free autoantibodies can be measured. With regard to subclasses of immunoglobulins, the most abundant type is IgG⁴. Furthermore, linear complement deposition of C3 is commonly observed.

Interestingly, an association between the type of immunoglobulin and the clinical presentation with regard to disease phenotype (see below) can be observed. As response rates of treatment differ between the variants, the molecular characterisation of each patient gains importance.

Clinical presentation of disease is very heterogenous, not only concerning the localisation of skin lesions but also the occurrence of different symptoms, the most common ones are abnormal skin blistering and hair morphology.

In general, two different clinical phenotypes can be differentiated: The “classical”, also called mechano-bullous, phenotype leads to skin fragility, tense blisters and subsequent scarring in trauma-susceptible areas as well as nail and pigment alterations. Non-classical (inflammatory) presentations can resemble many other autoimmune diseases of the skin⁵,

most commonly bullous pemphigoid, showing tight blisters spread all over the body. Due to this resemblance, differentiation to other skin pathologies can be challenging. Overall, about $\frac{2}{3}$ of patients suffer from the non-classical phenotype with a predominance of neutrophils as effector cells⁶. Below, a common clinical presentation of EBA is depicted.



Classical variant of EBA.

- (a) Erythema and tense blisters on the right knee.
- (b) Erythema and erosions on the left hand.

Inflammatory variant of EBA.

- (a) Erythema, erosions, and crusts on the left knee. (b) Blisters and erosions on the right elbow of the same patient

Figure 2.1: Clinical presentation of Epidermolysis bullosa acquisita

Common clinical features of the different variants of EBA is depicted. Adapted from Vorobyev et al.⁷

Due to the heterogeneity of the patient population, conclusive diagnosis of disease should be based on molecular criteria. These include the detection of linear IgG deposition in perilesional skin where binding of antibodies can be observed. Furthermore, a serration pattern analysis should be performed during histopathological analysis. Additionally, biomarkers in the serum should be measured, e.g. circulating anti-COL7 antibodies as they can be used as a marker for disease severity⁸.

Pathophysiology

In general, EBA can be subdivided into three major phases of disease: The induction phase, characterized by loss of tolerance to COL7, an intermediate phase where autoantibodies are continuously released, and finally the effector phase with emphasis on tissue destruction.

Induction phase: Certain human leukocyte antigen (HLA) variations have been demonstrated to be linked to autoimmune diseases and for HLA-DR2 amongst others, associations with multiple sclerosis and EBA⁹ were found.

Even after more than 30 years of intense research, the basis to the loss of tolerance and subsequent disease development still remains unravelled. Yet, it has been demonstrated, especially in mouse models, which cell types are essential for the disease. T cells generally play a central role as their depletion protects animals from developing lesions. In particular, CD4⁺, but not CD8⁺ T cells are crucial for disease induction¹⁰. Furthermore, neutrophils, B-cells and macrophages are needed in the beginning of EBA¹¹.

Continued autoantibody production: Currently, rather few details are known about the autoreactive plasma cells which are responsible for continued production of antibodies against COL7. The rather long period of 8-12 weeks of continued antibody production after immunosuppression targeting B cells (Rituximab) has been explained via the long lifetime of the COL7 specific plasma cells¹². Furthermore, in a therapeutic approach, the lack of neonatal Fc receptor protected animals from developing skin lesions as it regulates the amount of circulating IgG¹³. The therapeutic potential arising from these findings has already been used in patients¹⁴, but still further evaluation is necessary.

Effector phase: The effector phase is probably the best evaluated component of EBA, as most models mimicking the disease in animals reproduce this specific period. Hence, the knowledge presented below is mainly derived from observations made in murine EBA models.

Subsequent to antibody precipitation in the skin, either endogenously produced in patients or injected for *in vivo* experiments, an inflammatory reaction is triggered. First of all, the complement system is activated¹⁵. Subsequently, neutrophils are recruited to the site of inflammation via the cleavage of complement factor 5 (C5) and activated through cell surface receptors, such as integrins and Fc γ -receptors. Downstream to primary activation, a cascade of different kinases, like PI3K, ERK1/2, p38 and Akt mediates neutrophil effector functions¹⁶.

Amongst the various functions executed by this cell type, the production of reactive oxygen species (ROS) and matrix metalloproteinases (MMPs) is of central importance as both directly damage the dermal-epidermal junction^{17,18}, thus inducing blister formation. Interestingly and even of therapeutic potential, patients or mice unable to produce ROS are completely protected from the development of blisters even when EBA is artificially induced via COL7 antigen¹⁷.

Therapy

The treatment of EBA is challenging due to the rarity of disease and heterogenic clinical presentations of skin pathology. No controlled clinical trials are available so far so that the clinical expertise of the medical practitioner becomes even more important.

Established Therapies:

Like in many other dermatological diseases, **corticosteroids** are used in EBA and proved to be effective¹⁹ and, as they are well known, often primal treatment of disease. Especially based on the high prevalence of adverse effects, other treatments should also be considered⁶.

Methotrexate, azathioprine, cyclosporine and colchicine have all only been used in smaller patient cohorts and case series reported beneficial effects of each treatment^{20,21}. The specific mode of action of **intravenously applied immunoglobulins (IVIG)**, which are separated and pooled from human blood sera, is not fully understood. In EBA, reports are especially available on IVIG-therapy in patients in whom other strategies have failed to control disease²². As the results were satisfactory, IVIG can be regarded as a treatment option in EBA.

Immunomodulation of effector cells in EBA, specifically B-cells, using **anti-CD20 antibodies** (e.g. rituximab) is a rather new therapeutic strategy. For EBA, only case studies are available which mostly report a successful remission in patients in whom disease was not controllable beforehand²³. However, serious infections as adverse effects need to be taken into account when considering this treatment possibility.

Novel therapeutics strategies:

The most important drug target in the induction period of EBA are T cells. Their survival, especially in pro-inflammatory situations, is amongst others controlled by so called **heat-shock proteins (HSP)**, specifically HSP-90 which are of central importance for the folding of proteins and thus regulate cellular viability²⁴. First experimental data on T cells with autoimmunity against COL7 showed reduced inflammatory responses upon HSP-90 blocking thus suggesting a potential use of this strategy in EBA²⁵.

As the **complement system** serves a central role in mediating tissue damage during the effector phase of disease, it is not surprising that antibodies directed towards this structure showed positive effects²⁶. However, further research is needed to develop efficient treatment strategies.

In conclusion, EBA is a very heterogenous disease and not only due to its rare occurrence, diagnosis is challenging. Broad research has led to an advanced understanding of the pathophysiology and opened up a great variety of novel therapeutic approaches, especially providing options for patients who have not benefitted from earlier treatment so far.

2.2 Dimethyl fumarate

General information

Dimethyl fumarate (IUPAC name trans -1,2-ethylenedicarboxylic acid dimethyl ester) is the dimethyl ester of fumaric acid. Fumaric acids occur in plants, such as *Fumaria officinalis*, mushrooms and as intermediate products in the citric acid cycle of mammals thus serving a central role in cellular energy production. Dimethyl fumarate (DMF) itself is a crystalline, powder like substance possessing a “fruit-like” taste.

The first description as a drug can be dated back to the 1950s when a German scientist isolated dimethyl fumarate out of plants and successfully used it to treat his own psoriasis²⁷. Ongoing research then led to the introduction of a mixture including different fumaric esters and DMF (Fumaderm[®]) to be licensed for the treatment of psoriasis in 1994. Later, a preparation containing DMF solely (Tecfidera[®]) was licensed for the treatment of a variant of multiple sclerosis, relapse remitting MS (RR-MS).

Multiple sclerosis in general is a chronic, immune-mediated, demyelinating disease affecting nerve fibres of the central nervous system (CNS) thus involving pathology in the brain and spinal cord²⁸. It is the most common chronic disabling disease regarding the nervous system in young adults²⁹ and manifestation mainly occurs between 25 and 35 years.

Clinical manifestation is heterogenic with a large diversity of possible clinical symptoms, determined by the specific location of a lesion in the nervous system. Sensomotoric impairments comprise the most common presentations. For conclusive diagnose, a dissemination in “space and time” is necessary, meaning a variation in the severity and location of symptoms over time³⁰.

In the course of disease, patients can experience different variants of the disease, such as a continuous worsening of impairment (primary progressive MS, PP-MS) or episodes of

worsening (relapses) and emerging impairments followed by improvements (relapse remitting MS, RR-MS). RR-MS is much more common and can be observed in over 80 % of patients²⁸.

Pharmacological characteristics and pharmacokinetics

When taken orally, DMF is rapidly cleaved to monomethyl fumarate (MMF) by esterases in the alkaline environment of the intestine³¹. About 89 % of the drug undergoes this primary degradation process and is finally eliminated via the citric acid cycle. The remaining 11 % are directly attached to glutathione and excreted via the kidneys³².

When measuring metabolites of DMF in the portal vein, no free DMF could be detected while the main degradation product found was MMF³³, proving MMF to be the main active metabolite of oral DMF administration.

The half-life period of MMF is rather short, ranging between 38 minutes (Fumaderm^{®34}) and about 1 hour (Tecfidera^{®35}).

The most common adverse effect of oral DMF treatment is flushing, comprising reddening of the skin or hot flush symptoms. About 37 % of patients receiving the drug report similar conditions and whilst most commonly observed at the beginning of treatment, periodic reoccurrence is possible. Despite the high prevalence, only a small proportion (3 %) of patients had to discontinue administration in the approval study³⁵. The basis to this effect is believed to be conveyed via the HCA₂ receptor³⁶. Furthermore, adverse effects, related to the gastrointestinal tract are rather common and include diarrhoea, nausea and abdominal pain³⁵.

The clinically most serious, yet very rare, adverse effect of treatment is leukopenia, a fundamental reduction of white blood cells and thus severe immune deficiency, which can lead to the reactivation of viruses. The disease caused by proliferation of this virus is called progressive multifocal leukoencephalopathy (PML) and has a high mortality rate. Reports of a case led to the release of a so-called “Rote-Hand-Brief” in 2013, a publication by the Drug Commission of the German Medical Association reporting recent serious drug safety issues³⁷. The recommendations include a periodic screening of patients treated with Tecfidera for reductions in white blood cells.

Mechanisms of action

The mechanism of action of DMF/MMF is not yet fully elucidated. Different pathways have been discussed to convey the treatment effect amongst which the following are most intensively researched:

Nuclear factor (NF)- κ B pathway inhibition: NF- κ B is a protein complex and transcription factor found in almost all animal cells. Amongst others, it is involved in the regulation of cellular survival, immune response, cytokine production and synaptic plasticity reacting to numerous stimuli of cellular stress³⁸. To exert its impact on these cellular functions, translocation to the nucleus is mandatory. In different cell types of the skin and immune cells, such as T- and mononuclear cells³⁹⁻⁴¹, this translocation was inhibited upon DMF, but not MMF treatment⁴². In accordance with these findings, downstream functions, i.e. cytokine and chemokine production, controlled by NF- κ B were also reduced⁴³. Because of the rapid metabolism of DMF to MMF with no free DMF measurable in the blood, the impact of these results is discussed controversially.

Nuclear factor erythroid-derived 2 (Nrf2) pathway activation: Nrf2 is a transcription factor which controls the expression of numerous anti-inflammatory proteins, such as NAD(P)H oxidoreductases⁴⁴ and glutathione-S-transferases⁴⁵. Under homeostatic conditions, the protein is located in the cytosol and constantly degraded and resynthesized which is facilitated by binding to the KEAP1 protein. However, when oxidative stress occurs, the bond cannot be upheld and Nrf2 travels to the nucleus where the transcription for antioxidative genes is initiated⁴⁶. This mechanism explains the beneficial effects observed in the nervous systems and protection from oxidative stress in keratinocytes.

DMF and MMF can covalently bind to KEAP1 preventing it from controlling the degradation of Nrf2, which can then travel into the nucleus and exert its effect on antioxidative genes.

The significance of this effect was proven in an EAE model in mice, where the beneficial effect of DMF treatment on disease scores was Nrf2-dependant⁴⁷.

Modulation of Glutathione (GSH): GSH is an important regulator of oxidative stress and as described above, free DMF is rapidly bound to it in the intestine. Due to the depletion in free and thus also cellular GSH, several pro-inflammatory cytokines are down-regulated⁴⁸. It is believed that this can cause a shift towards a more anti-inflammatory response of T-helper cells⁴⁹. Again, the impact of this mechanism is not yet elucidated as it would only occur in mucosal cells of the intestine, where free DMF is present.

Hydroxycarboxylic acid receptor 2 (HCA₂) activation: MMF is an agonist of the HCA₂ receptor and *in vivo* as well as *in vitro* studies have shown a receptor dependant neuroprotective effect upon activation (c.f. section HCA₂ receptor).

Apart from these intensively investigated mechanisms, various other pathways have been postulated to be affected upon DMF/MMF^{50,51} treatment and ongoing research has to clear their relevance in mediating the drug effect.

Effect on different cell types

In general, many different effects of DMF or its metabolites, of which MMF is most important, on multiple cell types have been described *in vitro*. However, some of these data are derived from experiments where cells were directly treated with DMF⁵² and, as described above, few to no free DMF can be detected in the peripheral blood of patients³³ so that the interpretation of the results remains difficult.

Furthermore, the clinical significance has only been validated for very few cells types. An overview of the effects of DMF on different cell types is depicted in Figure 2.2.

In the following, the effect of DMF/MMF on those cell types most significant to EBA and MS are outlined.

Neutrophils, being of central importance in multiple diseases, have been studied intensively:

Many central effector functions are limited in their effectiveness upon treatment, the most important ones are ROS production, migration and NET formation⁵². Recently, the underlying mechanisms have partly been highlighted. They involve HCA₂ receptor activation⁵³ and multiple MAPK- and ERK1/2 pathways.

Keratinocytes are rather well characterized with regard to their responsiveness upon DMF or MMF treatment. Both substances suppress proliferation and differentiation in this cell type *in vitro*⁵⁴. Furthermore, DMF treated cells express fewer chemokines and surface markers, such as ICAM-1 which is needed for adhesion⁵⁵.

From patients treated with DMF in MS, it is known that the drug has profound effects on the count of various **lymphocyte**-types and can significantly reduce total counts of leukocytes with a risk of leukopenia⁵⁶.

However, the underlying mechanisms mainly remain unravelled. In general, an immunomodulating effect with a shift towards a rather anti-inflammatory cellular situation can be noted upon treatment. More specifically, CD8⁺ T cells⁵⁷, memory B- and memory T cells⁵⁸ are reduced whilst regulatory T- and B-cells are found elevated⁵⁸. The basis to these effects

can be explained via reduced cytokine production and inhibitory effects on activation and proliferation of T cells as well as on the expression of antigen presentation and costimulatory markers on B cells^{59,60}. Furthermore, DMF can directly induce apoptosis, preferably in T cells⁶¹.

Two main functions are inhibited upon DMF treatment in **endothelial cells**. First, cell-to-cell interactions are impaired as the expression of adhesion molecules, such as ICAM-1, VCAM-1 and E selectin, is inhibited⁶². Secondly, migration of immune cells is reduced, as VEGF receptors are downregulated and angiogenesis limited^{63,64}.

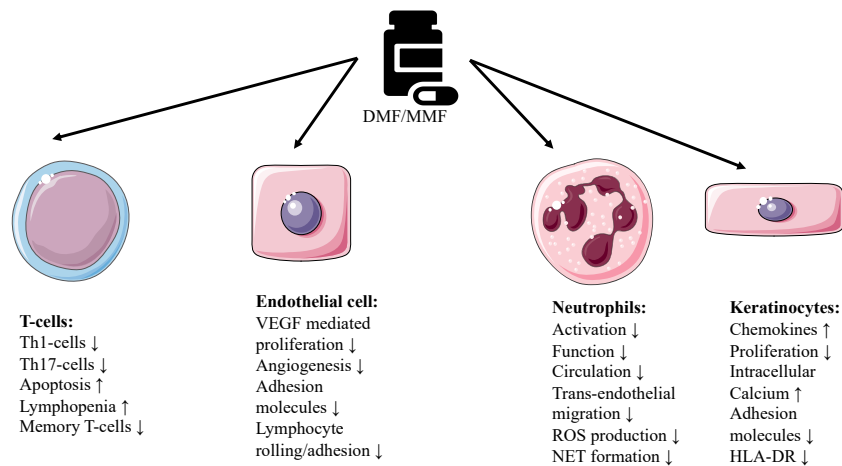


Figure 2.2: Effects of DMF on different cell types.

Upon ingestion, most of the administered DMF is rapidly converted to MMF. The full pharmacokinetic profile of DMF and MMF remain to be elucidated. ↑: upregulation/activation/increase; ↓: downregulation/ inactivation/decrease in certain experimental models. Adapted and modified from Meissner et al.⁶⁵ DMF, dimethyl fumarate; HLA-DR, human leucocyte antigen-antigen D related; NET, neutrophil extracellular trap; ROS, reactive oxygen species; Th, T helper; VEGF, vascular endothelial growth factor; For further details and references see respective section of each cell type in introduction.

Efficacy of DMF treatment

As described above, DMF is an established treatment option for patients with psoriasis and has lately been authorized for the use in multiple sclerosis.

In psoriasis, a significant correlation between drug administration and clearance of skin lesions is described⁶⁶. Currently, treatment guidelines recommend systemic DMF therapy for moderate-to-severe psoriasis as a first-line option⁶⁷.

With regard to multiple sclerosis therapy, treatment using DMF is a rather recent development and thus fewer clinical data are available. However, in this disease too, DMF

proved its efficacy⁶⁸ and is valued as a first-line therapy by the European and German guidelines on multiple sclerosis⁶⁹.

Concerning EBA, despite a lack of clinical data, *in vivo* results from a mouse model of disease proved a significant reduction of skin lesions upon DMF treatment in established disease and a prophylactic impact of administration⁵². Due to the rarity of disease, a validated treatment protocol is not established yet and further clinical trials need to clarify the role of DMF as a therapeutic agent.

Conclusively, DMF is a therapeutic agent used for the treatment of various, in particular autoimmune-mediated, diseases and is of central importance in multiple sclerosis and psoriasis as a first-line drug. Despite common use, the precise underlying mode of action still remains speculative even though intensive research has clarified potential molecular targets.

2.3 HCA₂ receptor

The hydroxycarboxylic acid receptor 2 (HCA₂) receptor (also GPR109A, PUMA-G, NIACR1 or HM74a) is a G-protein coupled receptor whose signalling is transduced via the G_{αi}- subunit. It is expressed in various species including humans, rodents, cats and cattle^{70,71} and could be detected on immune cells (neutrophils⁷², microglia⁷³, monocytes / macrophages⁷³, dendritic cells⁷⁴, Langerhans cells⁷⁵) and other cell types, such as keratinocytes⁷⁵, adipocytes⁷⁶ as well as epithelial cells⁷⁷ and pancreatic β-cells⁷⁸.

Three endogenous ligands have been described differing in their pharmacological profile: Butyrate, nicotinic acid (NA) and β-hydroxybutyrate (BHB). However, endogenous receptor activation is only accomplished in the serum via BHB, produced in higher amounts during fasting or ketogenic diets. For the other ligands, blood levels do not reach the threshold for HCA₂ stimulation⁷⁹. Recently it has been demonstrated that these HCA₂ ligands are also derived from the degradation of bacteria belonging to the microbiome. The investigators state that this contributes to the maintenance of homeostasis and regulates the immune system⁸⁰.

Apart from endogenous ligands, the receptor can be activated via MMF, the active metabolite of DMF which itself is not a receptor agonist. Furthermore, multiple partial- and full-agonists have been described (i.e. MK-0354⁸¹) and their role as therapeutic agents is currently investigated. For detailed information on receptor agonists see “IUPHAR guide to pharmacology”⁸².

Effect of receptor activation in different diseases

Activation of the receptor has shown to be relevant in the pathogenesis and also treatment of various diseases.

Neuroprotective effects of HCA₂: In a model of ischemic brain damage, niacin treatment reduced the volume of stroke in a receptor-dependant manner, most probably mediated through downregulation of pro-inflammatory monocytes/ macrophages, more specifically Ly6C^{Hi} monocytes⁷³. The relevance of this neuroprotective effect could also be shown in spinal cord injury, where accumulation of activated, pro-inflammatory monocytes was reduced via receptor activation. The authors hereby explain the significant better locomotor function upon treatment⁸³.

In the treatment of multiple sclerosis, DMF plays an important role as first-line therapy (see section DMF). Recently, the effect seen upon drug administration has been linked to the HCA₂ receptor as Chen *et al.* demonstrated a loss of neuroprotection in receptor-deficient mice⁵³. The reduced number of infiltrating neutrophils upon DMF treatment suggests the effect to be conveyed via altered immune cell migration into the nervous system.

Furthermore, a different pathway via which the HCA₂ receptor mediates neuroprotection has been described: In microglial cells, via AMP-activated kinase pathways, NF-κB signalling is suppressed, resulting in reduced pro-inflammatory cytokine production⁸⁴.

HCA₂ in dermatological diseases: The most common, albeit benign, adverse effect of DMF treatment is flushing. It has been demonstrated that the effect is mediated via keratinocytes and Langerhans cells through the HCA₂ receptor⁸⁵.

Moreover, few data exist on the importance of the receptor in dermatological diseases. The effect of DMF on various cell types, which is also conveyed via HCA₂, suggests an involvement in drug effects, for example in the treatment of psoriasis⁶⁷. Currently, this assumption has not been validated experimentally, so that the clinical importance remains speculative.

HCA₂ in internal medicine and oncology: Nicotinic acid has been used for the treatment of hyperlipidaemia and the receptor was found to be involved in the anti-lipolytic and anti-atherosclerotic effects observed⁸⁶.

Furthermore, due to the expression in squamous cell carcinoma, a dermatological tumour, the receptor may be involved in cancer development⁸⁷. These data are supported by a recent publication stating the involvement of mitochondrial dysfunction in cancer which is associated to HCA₂-activating metabolites⁸⁸.

Additionally, a variety of different receptor mediated effects has been put forward in different diseases: acute pancreatitis⁸⁹, proteinuric kidney disease⁹⁰, hepatic steatosis⁹¹ and inflammatory bowel syndrome⁹².

Downstream cascade

HCA receptors in general, and HCA₂ in particular, couple to G_i-type G proteins which inhibit adenylyl cyclase activity. More specifically, the G_i- subunit of G proteins is inactivated following receptor activation and thus adenylyl cyclase activity is reduced, resulting in reduced cleavage of ATP to cAMP⁹³. In adipocytes, lipolysis is controlled via this pathway as lipolytic enzymes are phosphorylated and thus activated when high cAMP levels activate protein kinase A (PKA). Consequently, HCA₂ results in reduced lipolytic activity in adipocytes⁹⁴.

Besides its importance in metabolism, the impact of the receptor on immune cells is focus of intense research: Multiple inflammatory stimuli, such as lipopolysaccharide (LPS), IFN- γ , TNF- α or IL-1 β ⁹⁵, lead to increased receptor expression on the cell surface, enhancing the significance of the receptor. Interestingly, pre-stimulated cells treated with receptor agonists show a reduction in the release of inflammatory stimuli which can be explained via alterations in NF- κ B dependant signalling⁹⁶. Furthermore, HCA₂ activation regulates apoptosis in neutrophils⁷² and modulates the inflammatory status in subtypes of microglial and monocytic cells⁸⁴.

These effects, partly explained by HCA₂ signalling directly, are also mediated through prostaglandin expression, yet another pathway controlled by the receptor⁷³. The release of prostaglandins triggers the expression of a transcription factor (peroxisome proliferator-activated receptor/ PPAR gamma⁹⁷) and as prostaglandins are vasoactive, this pathway explains flushing, a common unwanted effect seen upon DMF therapy⁷⁵.

For immune cells, multiple downstream signalling pathways have been described: Upon receptor activation, Ca^{2+} ions are released intracellularly. This effect is mediated through G_i coupled phospholipase C activation⁹⁸. Concerning the downstream cascade to this pathway, different mechanisms have been discussed: On the one hand, Ca^{2+} -sensitive phospholipase A_2 activation explains the rapid release of prostanoids (prostaglandin E_2 and D_2) observed upon niacin treatment⁹⁹. On the other hand, phosphorylation and thus activation of mitogen activated protein kinases (MAPK), in particular extracellular signal-regulating kinase 1/2 (ERK 1/2) and Akt has proven its importance *in vitro*¹⁰⁰. Which of the two mechanisms predominates has not yet been evaluated conclusively.

The termination of receptor activity is dependent on arrestin-3 and G protein-coupled receptor kinase 2 as knockout experiments of these two structures showed a significant reduction in internalization¹⁰¹. Figure 2.3 depicts a graphic summary of the cascade downstream to HCA_2 activation.

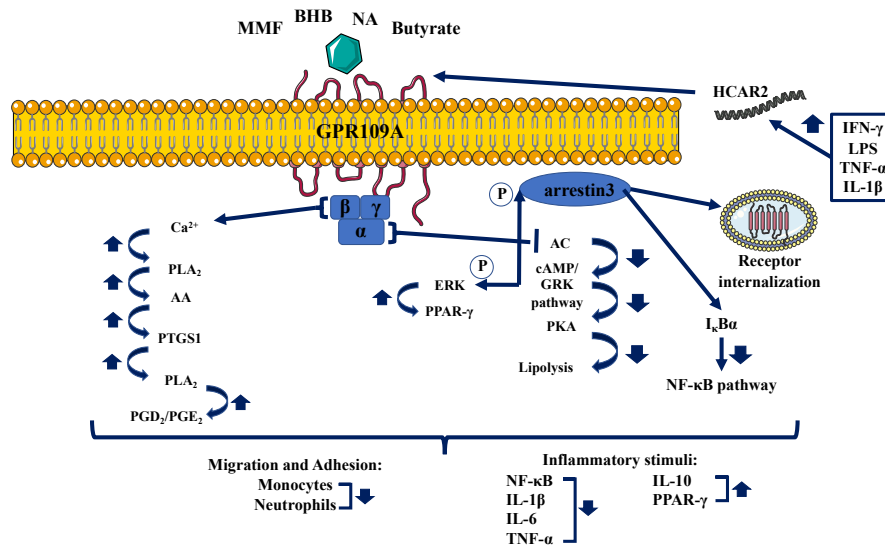


Figure 2.3: HCA_2 receptor downstream cascade.

The HCA_2 receptor (G-protein coupled receptor 109A, GPR109A) can be activated via monomethyl fumarate (MMF), beta-hydroxybutyrate (BHB), nicotinic acid (NA) and butyrate. Upon activation, distinct units of the G-protein coupled receptor are activated. On the one hand, activation leads to a rise in intracellular calcium levels (Ca^{2+}) and thus signalling via phospholipase A_2 (PLA₂) resulting in elevated release of prostaglandins D_2 and E_2 ($\text{PGD}_2/\text{PGE}_2$). On the other hand, via the $G_{\alpha i}$ -unit, adenylate cyclase (AC) activity is inhibited and via the cyclic adenosine monophosphate (cAMP) and G protein coupled receptor kinase (GRK) pathway, lipolysis is reduced in adipose tissue. Furthermore, this pathway mediates the phosphorylation of extracellular signal-regulated kinases (ERK) and arrestin3. In further consequence, peroxisome proliferator-activated receptor gamma (PPAR- γ), as well as nuclear factor kappa-light-chain-enhancer of activated B cells (NF- κ B) levels are controlled. Furthermore, arrestin3 supervises receptor internalization. Finally, migration and adhesion in monocytes and neutrophils is inhibited upon receptor downstream signalling and the amount of various pro-inflammatory stimuli in immune cells is reduced. Modified and adapted from Offermanns & Schwaninger¹⁰² and Chai et al.¹⁰³. IFN- γ , interferon- γ ; LPS, lipopolysaccharide; TNF- α , tumour necrosis factor α ; IL, interleukin; PKA, protein kinase a, AA, arachidonic acid; PTGS1, prostaglandin synthase 1, P, phosphorylation.

In summary, numerous different effects of HCA₂ receptor activation have been described, stating its central role in various diseases, but also for the maintenance of homeostasis. Even though the overall impact of receptor activation in different diseases remains unknown, the characterisation of its downstream cascade holds the opportunity for future therapeutic approaches.

2.4 Neutrophil effector functions, diapedesis and the role of L-selectin

Neutrophil effector functions

Neutrophils are of major importance for host defence. They are the most abundant leukocyte population in humans, accounting for up to 65% of all white blood cells¹⁰⁴. With a number of different effector-functions, the major task of this cell type, belonging to the innate immune system, is antimicrobial clearance. Neutrophils can migrate to the site of inflammation or infection (chemotaxis, c.f. section “L-selectin”) and, via release of cytokines, amplify the cellular response of several other cell types themselves. In addition to the recruitment and activation of other cells, they are capable of executing three directly antimicrobial features: Phagocytosis (ingestion of particles), degranulation (release of proteins with antimicrobial properties, such as myeloperoxidases, NADPH oxidases, collagenases) and generation of neutrophil extracellular traps (NETs, formation of a “web” of fibres which trap and inactivate pathogens¹⁰⁵). Furthermore, recent studies have identified neutrophils as participants in the adaptive immune response, important to the production of immunoglobulins by interactions with B cells¹⁰⁶ providing even more evidence for their importance in host defence.

Inadequate activation and misguided execution of effector functions can lead to the relapse of serious infections, observed for example in patients with chronic granulomatosis, a disease where phagocytic ability is impaired¹⁰⁷. In addition to dysregulations in host defence against pathogens, neutrophils also play an important role in the pathogenesis of chronic inflammatory diseases. In sputum samples derived from asthma patients, more than $\frac{3}{4}$ of cells detected were neutrophils¹⁰⁸. The portrayed *in vivo* observations in humans are underlined by multiple data from experimental models of different chronic inflammatory diseases. In EAE, clinical signs are significantly delayed or, in some

animals, prevented when mice are depleted of neutrophils after immunization. However, when depletion is conducted at an earlier time point before immunization, no changes in the disease course can be ascertained¹⁰⁹. These results indicate that neutrophils play a crucial role in the effector phase of EAE but not during the induction period, which is rather driven by CD4⁺ T cells¹¹⁰.

For numerous dermatological diseases, especially those associated with autoimmune blistering, the key role of neutrophils has been shown experimentally¹¹¹. The effect of neutrophil depletion is well described in two models of bullous pemphigoid (BP) and EBA. When neutrophils are recruited to a different site of inflammation in the body and are thus absent in the skin¹¹² or when their effector functions are blocked¹⁷, animals are protected from the formation of lesions and do not develop the autoimmune disease upon antibody injection¹¹³.

These data have been the basis to further research on blocking neutrophil functions in autoimmune diseases. Here, the use of DMF, which is converted to MMF when administered orally, proved to have considerable effects. Müller *et al.* found numerous effector mechanisms to be changed upon DMF treatment: ROS production and NET formation, both key functions in host defence are impaired in neutrophils incubated with DMF⁵². Chemotaxis and subsequent activation of cells are also changed upon treatment. Despite direct changes in effector functions, a number of activation pathways are altered upon DMF explaining the profound effects described above. Different elements of mitogen-activated protein kinases, such as p38, protein kinase B (also known as Akt) and ERK1/2 are modulated. However, which of the different cascades mediates the effect is stimulus-dependant⁵². Interestingly, these pathways are downstream elements to the HCA₂ receptor¹⁰² giving another link between impaired neutrophil functions and receptor activation. However, the results presented need to be interpreted carefully as DMF is no direct HCA₂ agonist. Furthermore, and more importantly, upon oral administration, the drug is quickly and nearly completely converted into MMF. Not only in peripheral blood of humans³², but also in the portal vein of mice³³, and thus directly after gastro-intestinal uptake, no free DMF but only its metabolites are detectable. Despite these limitations, a recent *in vivo* study using human blood also found NET formation and ROS production to be consistently inhibited upon oral DMF treatment using Fumaderm[®], a formula eligible for the treatment of psoriasis¹¹⁴. The findings ask for further evaluation of these specific effector functions especially with regard to HCA₂ mediated impacts.

Studies concentrating on MMF and other receptor agonists also reveal profound effects on neutrophil behaviour. Apoptosis, for example, is accelerated in mature neutrophils which, unlike immature ones or eosinophils, express the receptor on their cell surface. Blocking of G_i proteins abolishes the effect⁷² and the impact on cell death in wild-type neutrophils is lost in populations deficient for the HCA₂ receptor⁵³. However, the overall impact of reduced cell counts due to increased apoptosis in disease severity remains unclear, as the distribution of neutrophils from other compartments of the body quickly balances out the changes at the site of inflammation.

Despite regulation of cell numbers via apoptosis, neutrophil function is also interfered at earlier timepoints. *In vivo* findings of reduced counts in the spinal cord of EAE diseased animals when treated with DMF led to further *in vivo* evaluation with regard to effects mediated through the receptor.

Neutrophil diapedesis and the involvement of L-selectin

Receptor activation for example via MMF, a direct agonist of the receptor, proved to interfere with neutrophil movement. For example, *in vitro* assays of adhesion and chemotaxis stated a significant reduction in both functions when cells were treated with MMF. Furthermore, an *in vivo* experiment revealed lowered amounts of neutrophils in the spinal cord upon DMF treatment in mice with EAE. Both effects were lost in animals (and neutrophils *in vitro*) depleted from the HCA₂ receptor proving the effect to be receptor dependent⁵³.

Before neutrophils leave the blood vessel (= diapedesis) to execute their effector functions in tissues, a complex process of interaction with the endothelium takes place, which is not entirely understood to date¹¹⁵. Diapedesis can be subdivided into different phases during which specific proteins are involved.

In postcapillary venules, a weak adhesive interaction between neutrophils and endothelial cells is responsible for their primary approximation. During this phase, which is called “rolling”, molecular and physical forces play an important role. Due to their size and weight, neutrophils are aligned on the outside of the blood stream close to the vessel-forming endothelium. In close proximity, they can thus build up low-affinity interactions with receptors expressed on the luminal wall. The most important receptor family governing rolling are glycoprotein adhesion molecules, called selectins. Three members can be distinguished, L-selectin (also CD-62L, expressed exclusively on leukocytes), P-selectin (on platelets and endothelial cells) and E-selectin (only on endothelial cells). For

leukocyte (and thus neutrophil) adhesion, L-selectin, which is constantly expressed on the cell surface, binds to sialylated carbohydrates on endothelial cells. The expression of this ligand is controlled by a variety of inflammatory signals, such as LPS and endogenous proinflammatory cytokines (TNF- α ; IL-1- β ¹¹⁶). The process described marks the first, essential step in neutrophil diapedesis as it enables stronger adhesive interactions to be built which are needed for the consecutive phase in the cascade, called “adherence”. Here the intracellular adhesion molecule (ICAM) 1 on the endothelium is an important ligand for neutrophils to form a firm attachment¹¹⁷. The third and final part of diapedesis, “transmigration”, is a multistep process which involves a variety of adhesion molecules, such as the platelet-endothelial cell adhesion molecule (PECAM)-1, enabling neutrophils to pass through the endothelial monolayer and basement membrane without adhering to intercellular junctions¹¹⁸. In order to complete transmigration and finally enter the extravascular space where effector functions can be carried out, a chemoattractant gradient is necessary¹¹⁹.

The sophisticated interactions during diapedesis are intensively controlled at various points in order to stop or enhance the inflammatory response mediated by neutrophils. The lack or blocking of the molecules needed for diapedesis results in reduced extravasation. With the ulterior motive to reduce effector functions in diseases where pathology is mediated by neutrophils, intense research has been directed towards a better understanding of how transmigration works. Here, especially L-selectin as a key player has been studied. Recent research focused upon a target unique to L-selectin, the so-called ectodomain. The structure can be shed resulting in a downregulation of L-selectin and subsequent reduced infiltration of neutrophils. The shedding is mediated by various stimuli, amongst others, peptides from bacteria, TNF or osmotic stress can induce the process. Not only is diapedesis in neutrophils centrally interfered when the ectodomain is shed, but as the molecule also controls other effector functions, activation of the cells in general is reduced. The presence of L-selectin is currently even used to judge the activation status of neutrophils and referred to as the gold standard for *in vivo* and *in vitro* experiments as it is inversely correlated to the execution of effector functions¹²⁰.

2.5 Objective of this thesis

Recently, the importance of the HCA₂ receptor has been highlighted in mediating the treatment effect of DMF in multiple sclerosis as a knockout cohort showed no response to treatment. Likewise, in a pilot study of EBA diseased mice, evidence was found for a receptor dependent treatment effect.

On a cellular level, neutrophils are particularly responsive to HCA₂ activation and the effect observed in mice suffering from EAE was partly explained by reduced infiltration of cells into the CNS. Concerning the molecular cascade downstream to the receptor, the full influence of receptor activation on cellular functions in effector cells remains unknown in particular with regard to the specific pathways responsible in different diseases.

In this thesis, the HCA₂ receptor and its impact in another autoimmune disease, EBA, should be elucidated. The following issues were of primary interest:

- Can the initial evidence for receptor dependency in EBA be validated in a larger cohort, independent of the sex?
- Which population of receptor carrying cells is especially responsive to EBA and is there a possible molecular explanation for reduced infiltration?
- What else influences treatment outcomes? Is there a gender dependency or changes via baseline activation, for example up to nutritional intake of receptor agonists?

3.0 Material

3.1 Equipment

Device	Specification	Company
Agarose gel documentation system		Phase GmbH, Lübeck (G)
Agarose gel electrophoresis system	Sub-Cell GT	Bio-Rad Laboratories, Munich (G)
Autoclave	Systec V-65	Systec, Linden (G)
Centrifuges	Mikro 200 R	Andreas Hettich, Tuttlingen (G)
	Mikro 120 5415 R	Eppendorf, Hamburg (G)
	Avanti J-E GR412	Beckman Coulter, Brea (USA)
	Universal 320 R	Thermo Fischer Scientific, Waltham (USA)
	Omnifuge 2.0 RS	Andreas Hettich, Tuttlingen (G)
Chemiluminescence recorder	Fusion Solo S	Heraeus, Hanau (G)
CO ₂ Incubator	BD210	VWR International, Radnor (USA)
Counting chamber	MCI-18M	Binder, Tutlingen (G)
	Fuchs-Rosenthal	Sanyo, Moriguchi (JP)
Flow cytometer (core facility CanaCore Lübeck)	FACS LSR II	Marienfeld-Superior, Lauda-Königshofen (G)
Fluorescence lamp	EL-6000	BD Biosciences, San Jose (USA)
Freezers	-80°C: KM- DU73Y1	Leica-Microsystems, Wetzlar (G)
	-20°C: MediLinie	Panasonic, Osaka (JP)
Gel casting apparatus	Hand casting Ste	Liebherr, Biberach an der Riß (G)
Heating block	QBT2	Bio-Rad Laboratories, Munich (G)
Horizontal shaker	MTS4	Grant Instruments, Royston (GB)
Cryotome	CM 3050	IKA-Werke, Staufen (G)
Light Source	Polychrome V	Leica Microsystems, Wetzlar (G)
Magnetic heating stirrer	Combimag	FEI Munich, Munich (G)
Microscopes	Fluorescence Microscope: DMI 6000B	IKA-Werke, Staufen (G)
	Fixed-Stage-	Leica Microsystems, Wetzlar (G)
		Carl Zeiss Microscopy,

	Microscope Axio Examiner.D1	Jena (G)
Microwave		Samsung, Seoul (COR)
Multipette	Multipette plus	Eppendorf, Hamburg (G)
pH meter	pH 531	WTW, Weilheim i. OB (G)
Pipettes	Reference/Research (10, 100, 200, 1000 µl)	Eppendorf, Hamburg (G)
Pipetting aid	Pipetus	Hirschmann, Eberstadt (G)
Polyacrylamide gel electrophoresis (PAGE)-System	Mini-PROTEAN	Bio-Rad Laboratories, Munich (G)
Rinsing cannula	1428 LL	Acufirm Ernst Kratz, Dreieich (G)
Rocking shaker	WT17	Leica Microsystems (G)
	DRS-12	neoLab, Heidelberg (G)
Rolling mixer	RM5	CAT, Ballrechten-Dottingen (G)
Scales	ABT 100-5 M	Kern& Sohn, Balingen (G)
	MC1 LC 220 S & MC1 LC 4200 S	Sartorius, Göttingen (G)
Shaking incubator	HAT Multitorn Standard	Infors, Bottmingen (G)
Sterile bench	Safe 2000	Thermo Fisher Scientific, Waltham (USA)
Thermomixer	Thermomixer compact	Eppendorf, Hamburg (G)
Vibratome	VT 1200S	Scientific Industries, New York (USA)
Vortex shaker	Reax 2000	Heidolph, Schwabach (G)
Water treatment system	Milli-Q Reference	Merck, Darmstadt (G)

3.2 Consumables

Product	Specification	Company
Cannula	BD Microlance 3 23 G, 26 G, 27 G	BD, Franklin Lakes (USA)
Cell strainer	Falcon cell strainer 70 µm	Thermo Fisher Scientific, Waltham (USA)
Cover glasses	24 x 50 mm	Th. Geyer, Renningen (G)
Disposable blades	Cryotome: Type 818	Leica Microsystems, Wetzlar (G)
	Vibratome: Classic blades	Wilkinson, High Wycombe (G)
Filter paper	Whatman	GE Healthcare Life Sciences, Little Chalfont (GB)
Grease pencil	DAKO Pen	Agilent Technologies, Santa Clara (USA)

Infusion cannula	Safety-Multifly 21G	Sarstedt, Nümbrecht (G)
Ketone body test strip kit	Keto-Diabur Test 5000	Roche, Basel (CH)
Microscope slides	Superfrost™ Plus	Thermo Fisher Scientific, Waltham (USA)
Microvette	CB 300	Sarstedt, Nümbrecht (G)
Multipette tips	Combi tips advanced (2,5 / 5 / 10 ml)	Eppendorf, Hamburg (G)
Multiwell plates	CELLSTAR® (6- / 24-well)	Greiner Bio-One International, Kremsmünster (AUT)
Nicotinic acid low diet	0.05 mg/kg nicotinic acid, C 1025 Special Chow	Altromin, Lage (G)
Nitrile gloves	Peha-soft nitrile FI-NO	Hartmann, Heidenheim (G)
Pasteur pipette	Glass, 230 mm	Glaswaren Karl Hecht, Sondheim v. d. Rhön (G)
Pipette tips	10 / 200 / 1000 µl	Sarstedt, Nümbrecht (G)
Polypropylene containers	CELLSTAR® 15 ml, 50 ml	Greiner Bio-One International, Kremsmünster (AUT)
Reaction tubes	0,2 / 0,5 / 1,5 / 2 ml	Eppendorf, Hamburg (G)
Scalpel	Type 10 / 11 / 22	Feather, Osaka (JP)
Serological Pipettes	CELLSTAR® (5 / 10 / 25 / 50 ml)	Greiner Bio-One International, Kremsmünster (AUT)
Sterile filter	Millex GV 0,22 µm	Merck, Darmstadt (G)
Syringes	1 / 5 / 10 / 20 / 50 ml	BD, Franklin Lakes (USA)
Vinyl gloves	Vinyl 2000 PF	Meditrade, Kiefersgelden (G)

3.3 Reagents

Reagent	Company
1,4-Diazabicyclo[2.2.2]octane (DABCO)	Carl Roth, Karlsruhe (G)
2-Amino-2-hydroxymethyl-propane-1,3-diol (TRIS)	Carl Roth, Karlsruhe (G)
2,2,2-Tribromethanol (Avertin)	Sigma-Aldrich, St. Louis (USA)
3,3'-Diaminobenzidin (DAB)	Vector Labs, Burlingame (USA)
4-(2-Hydroxyethyl)-1- piperazine ethanesulphonic acid (HEPES)	Sigma-Aldrich, St. Louis (USA)
4',6-Diamidino-2-phenylindole (DAPI)	Sigma-Aldrich, St. Louis (USA)
Agarose (<i>Low Melt</i>)	Carl Roth, Karlsruhe (G)
Agarose (NEEO Ultra Quality)	Carl Roth, Karlsruhe (G)
Ammonium persulfate (APS)	Sigma-Aldrich, St. Louis (USA)
Bovine Serum Albumin (BSA)	GE Healthcare Life Sciences, Little Chalfont

	(UK)
Calcium-monohydrate	Merck, Darmstadt (G)
Cell lysis buffer (10x)	Cell Signalling Technologies, Danvers (USA)
Dimethyl fumarate (DMF)	Sigma-Aldrich, St. Louis (USA)
Dimethyl sulfoxide (DMSO)	Sigma-Aldrich, St. Louis (USA)
Dulbecco's PBS (phosphate buffered saline)	Biowest, Nuaille (F)
Embedding medium	Leica Microsystems, Wetzlar (G)
Erythrocyte lysis buffer (Cat No./ID: 79217)	Qiagen, Venlo (NED)
Ethanol, 70 % (v/v), denatured	Th. Geyer, Renningen (G)
Ethanol, absolute	J. T. Baker, Center Valley (USA)
Ethylenediaminetetraacetic acid (EDTA)	Sigma-Aldrich, St. Louis (USA)
Glycerol	Carl Roth, Karlsruhe (G)
Glycine	Carl Roth, Karlsruhe (G)
Hydrochloride (HCl, 1 M)	Carl Roth, Karlsruhe (G)
Iscove's Modified Dulbecco's Medium	Thermo Fisher Scientific, Waltham (USA)
Isopropanol	J. T. Baker, Center Valley (USA)
Ketamine 10 %	bela-pharm, Vechte (G)
Keto-Diabur Test 5000 for ketone bodies in mouse urine	Roche, Basel (CH)
Liberase™ TL medium	Sigma-Aldrich, St. Louis (USA)
Methanol	Th. Geyer, Renningen (G)
Methocel® 90 HG	Sigma-Aldrich, St. Louis (USA)
Monopotassium phosphate (KH ₂ PO ₄)	Merck, Darmstadt (G)
Monosodium phosphate (NaH ₂ PO ₄)	PanReac AppliChem, Darmstadt (G)
Mowiol 4-88	Carl Roth, Karlsruhe (G)
Optimal cutting temperature compound (OCT compound)	Thermo Fisher Scientific, Waltham (USA)
Paraformaldehyde (PFA)	Merck, Darmstadt (G)
Potassium chloride (KCL)	Merck, Darmstadt (G)
Rompun® (Xylazine, 2 %)	Bayer Vital, Leverkusen (G)
RPMI 1640 with L-glutamine, Phenol Red, without HEPES	Thermo Fisher Scientific, Waltham (USA)
Sodium acid	Sigma-Aldrich, St. Louis (USA)
Sodium hydroxide (NaOH)	J. T. Baker, Center Valley (USA)
Special mouse diets:	
Ketogenic (ketogenic diet, KD; sniff EF R/M ketogenic diet with 80% long chain fatty acids in dry mass and 8 % protein, #E15149-30)	Ssniff Spezialdiäten, Soest (G)

Control (control diet, CD, sniff M-Z,
containing 48 % carbohydrates, 15 % fat and
37 % protein, #E15000-00)

Ssniff *Spezialdiäten*, Soest (G)

Nicotinic acid free diet (Altromin C 1025
Niacin free diet <0.05 mg/kg Nicotinic acid)

Altromin, Lage (G)
Uhu, Bühl/Baden (G)

Superglue

TRIS-HCL

Carl Roth, Karlsruhe (G)

Viability Dye for FACS, Conjugate: APC-
Cy7

eBioscience, Santa Clara (USA)

Cat. #: 65-0865-14

3.4 Medium, Buffers and Solutions

Buffer/ Solution

Blocking buffer

Ingredients

3 ml FACS- buffer + 30 µl Anti-Mo
CD16/CD32

Cover medium for object slides
(Mowiol/DABCO)

3.6 M Glycerine
0.43 mM Mowiol
0.2 M Tris-HCL (pH 8.5)
22.3 mM DABCO

DMF

Dimethyl fumarate solved in
0.8 % Methocel™ /H₂O

FACS-buffer
(5 % FCS)

500 ml PBS (sterile) + 50 ml heat
inactivated Fetal calf serum (FCS)

Liberase medium

25 mg/ml; 0,5 ml RPMI + 0,48 µl
Liberase (diluted in Iscove's Modified
Dulbecco's Medium (Gibco (no FCS)

PBS-acidic

PBS

PBS; pH 7.4

0.02 % (w/v) Sodium acid
137 mM NaCl
2.7 mM KCl
10 mM Na₂HPO₄
2mM KH₂PO₄

PFA (4 %); pH 7.4

PBS

4 % (w/v) Paraformaldehyde
pH 7.4 calibrated via NaOH titration

RPMI medium (Roswell Park Memorial
Institute)

RPMI 1640

With L-Glutamine, Phenol Red, without
HEPES; Company: Thermo Fisher
Scientific

RPMI medium with FCS (5%)

500 ml PRMI 1640 + 50 ml heat
inactivated Fetal calf serum (FCS)

TBS-Tween-20 (TBS-T), pH 7.6

20 mM TRIS
137 mM NaCl

	0.1 % (v/v) Tween-20
TRIS-acetate-EDTA (TAE)-Buffer (30x)	1.2 M TRIS 30 mM EDTA pH 8.3 adjusted using conc. acetic acid
TRIS-buffered saline (TBS), pH 7.6	20 mM TRIS 137 mM NaCl

If not specified differently, all solutions, buffers and media were prepared using ultra-pure water (MiliQ)

3.5 Antibodies

Antibody (Clone)	Supplier (Cat-Nr.)	Dilution
Primary antibodies:		
Anti-mouse CD16/CD32, rat-IgG, monoclonal (93)	Thermo Fisher Scientific, Waltham (USA; 16-0161-81)	1:100
Anti-mouse C3, rat-IgG, monoclonal (20439M0716-A)	HycultBiotech, Wayne (USA; HM1045)	1:400
APC anti-mouse CD11c (N418)	Biolegend, San Diego (USA; 117310)	1:400
APC Trgv1.1 (V γ 1.1; 2.11)	Biolegend, San Diego (USA; 141107)	1:800
APC-Cy7 anti-mouse CD45R (RA3-6B2)	Biolegend, San Diego (USA; 103224)	1:200
Brilliant Violet 421™ anti-mouse NK-1.1 (PK136)	Biolegend, San Diego (USA; 108741)	1:200
Brilliant Violet 421™ Trgv3 (V γ 3; 536)	BD Pharmingen, San Diego (USA; 743238)	1:100
Brilliant Violet 510™ anti-mouse CD45 (30-F11)	Biolegend, San Diego (USA; 103138)	1:800
Brilliant Violet 650™ anti-mouse/human CD11b (M1/70)	Biolegend, San Diego (USA; 101239)	1:200
FITC anti-mouse CD3 (145-2C11)	Biolegend, San Diego (USA; 100306)	1:400
PE Trgv2 (V γ 2; UC3-10A6)	Biolegend, San Diego (USA; 137705)	1:200
PE/ anti-mouse CD62L (MEL14)	Biolegend, San Diego (USA; 104406)	1:800
PE/Cy7 anti-mouse Ly-6C (HK1.4)	Biolegend, San Diego (USA; 128018)	1:800
PerCP-Cy5.5 gdTCR (REA633)	Miltenyi, Bergisch-Gladbach, (G; 130-109-801)	1:200
PerCP/Cy5.5 anti-mouse Ly-6G (1A8)	Biolegend, San Diego	1:200

PE/Cy7 anti-mouse CD127 (REA 680)	(USA; 127616) Miltenyi, Bergisch-Gladbach, (G; 130-110-376)	1:200
Secondary Antibody		
Anti-rabbit IgG, donkey-IgG AlexaFluor® 488, polyclonal	Thermo Fisher Scientific, Waltham (USA; A-21206)	1:400
Anti-rat IgG, donkey-IgG Cy3, polyclonal	Jackson ImmunoResearch, Ely (UK, (712-165-150)	1:400

3.6 Software

Program	Company
Evolution Capt Solo 6 17.0	Vilber Lourmat, Collégien (F)
FACS DIVA software (BD Biosciences)	BD Biosciences, Franklin Lakes (USA)
Fiji (Image J)	Open Source Project (http://fiji.sc)
FlowJo 10.3	BD Biosciences, Franklin Lakes (USA)
LAS AF Imaging Software	FEI Munich, Munich (G)
Live Acquisition Software	FEI Munich, Munich (G)
Office 365	Microsoft, Redmont (USA)
Offline Analysis Software	FEI Munich, Munich (G)
Prism Version 5.0	GraphPad, La Jolla (USA)
Servier Medical Art	Servier, Neuilly-sur-Seine (F)

4.0 Methods

4.1 Animal experiments

General housing conditions

Mouse experiments were carried out in close cooperation and under supervision of Dr. Julian Assmann and Dr. Melanie Wannick (Institute for Experimental and Clinical Pharmacology and Toxicology, Lübeck). In general, all experiments followed the guidelines of the Schleswig-Holstein Federal state “Ministeriums für Energiewende, Landwirtschaft, Umwelt und ländliche Räume”. Animals used during the experiments were either bred at the University of Lübeck (Gemeinsame Tierhaltung) or derived from an external breeder particularly Charles River (Germany). Different genotypes of black 6 mice (C57BL/6) were used during the experiment: wild-type (WT) and knockout (KT) animals were littermates from heterozygous matings with their specific genotype marked as Hcar2^{+/+} or Hcar2^{-/-}. Animals bred exteriorly are indicated as WT animals.

The animals were kept in house 66 (CBBM) of the University of Lübeck. Food (standard rodent diet: Altromin diet for mice, #1314) and tap water were provided *ad libitum*. Mice aging between 8 to 12 weeks, that were housed in individually ventilated cages (IVC) in groups of 1 to 5 animals on a surface area of 500 cm² (female individuals were never kept alone during any experiment) were used for the experiments. In the course of treatment, a 12-hour circadian rhythm was adhered to and the animals were transferred to the experimental lab for a familiarization period prior to the start of each experiment. Mouse lines used during the experiments are listed in the table below:

Table 4.1: Mouse lines used during the experiments and their specifications.

Mouse line	Specification	MGI-ID (Mouse genome Informatics Database)	Reference
Hcar2 ^{-/-}	Hcar2 ^{tm1Soff}	2653103	Tunaru et al. ¹²¹
Hcar2 ^{mRFP}			Hanson et al. ⁷⁵
Wildtype (WT)	C57BL/6NCRL		Charles River

EBA and DMF treatment of mice

The basis to all experiments was the induction of EBA in both HCA₂ wild type and knockout animals, which was carried out under supervision of Dr. Melanie Wannick and Dr. Julian Assmann.

Prior to each experiment, animals were randomized into a treatment and vehicle group and subsequently divided to achieve an equilibrated population for each cage concerning genotype. EBA was induced using anti-mice collagen Type VII antibodies (anti-mColVIIc IgG) which were prepared by Dr. M. Wannick. Each animal was treated on day 0 (100 µg); 2 (100 µg) and 4 (60-100 µg) via intraperitoneal injection (i.p.). following oral application of DMF or vehicle treatment.

During the treatment experiments, all animals were orally gavaged every 12 hours. With the help of a buttoned cannula (individual for each treatment) either DMF (50 mg/kg body weight; prepared freshly every day) or vehicle treatment (0.8 % Methocel in H₂O) were administered starting 2 days prior to disease induction and continuing until the day of tissue and organ harvesting. The treatment volume (10 µl/g body weight; final dose 50 mg/kg body weight; indicated in each figure) was defined on a daily basis via morning weighing of each animal. The data collected were furthermore used to scan for weight loss during the experiment. After disease induction, mice lost weight which they typically regained during the first 5 days of EBA (course of weight see Figure 4.1). However, if an animal's weight dropped too rapidly or it did not regain the starting weight, an exclusion from the experiment needed to be considered. The Society for Animal Protection (TVT) published termination criteria for mouse experiments. These were used as references during the experiments described below: rapid weight loss (>20 % during a few days), long lasting weight reduction and consecutive emaciation, continuing loss of hair, ragged fur, cowering body position, distended abdomen, lethargy (> 3 days), diarrhoea (> 3 days), cough, gasping, lung sounds, nose efflux, icterus, anaemia, CNS symptoms (shivering, head bending, wiggling, convulsion, circular movement, paresis, paralysis), bleeding, anuria or discolouration of urine, self-mutilation, injuries resulting in reduced food uptake¹²².

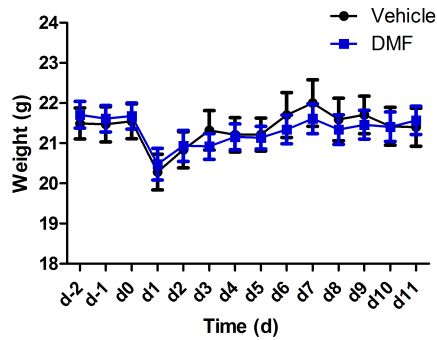


Figure 4.1: Course of bodyweight during EBA Experiment.

Mice received a total of 3 i.p. injections of 100 µg anti-collagen VII-IgG every second day starting on day 0. Body weight was assessed daily in order to monitor animals for weight loss and determined the amount of DMF or vehicle administered. Data are shown as mean + SEM, n = 18-20, p < 0.05 for time, 2-way ANOVA with Bonferroni post-test was performed, F-ratio: 0.1460; total degrees of freedom: 417.

In order to keep a steady suspension, the tube containing DMF was continuously homogenized using a rolling table during oral gavage. Treatment prepared in advance for the second gavage of the day was being stored at 4 °C under permanent homogenization. Scoring of disease activity started on day 4 after EBA induction and was thenceforward ascertained every third day. For this procedure each animal was anesthetised applying Ketamine (10 mg/kg) / Xylazine (15 mg/kg) via i.p. injection. During narcosis the complete body surface was compartmentalized into different sections and each examined with regard to flush, hair loss, scaling and skin erosions. For each section a score of affected skin surface was raised (indicated as a proportion of the complete section in percentage) and then referred to the complete body surface area. Table 4.2 shows the different body parts with regard to their proportion to the whole skin area. To ensure invariable scoring conditions, data were collected partly blinded by Dr. M. Wannick with regard to treatment and fully blinded with regard to genotype. Only after the experiments, the genotypes were matched to the scoring results. With regard to oral gavage, blinding could not be carried out due to the distinct physical appearance of the two solutions; whilst the DMF solution has a milky aspect, the vehicle treatment is transparent. However, the blinding for genotype was maintained and scoring was carried out prior to oral gavage to ensure blinding of the scorer.

Concluding an experiment (Day 5 or Day 11 of disease) mice were deeply anesthetised (validated via interdigital reflex response) using Ketamine (10 mg/kg) / Xylazine (15 mg/kg) and euthanized via cervical dislocation for tissue and organ harvesting. For further experiments, blood, abdominal lymph nodes, spleen and both ears as skin samples were

extracted and either directly prepared for FACS-analysis or fixed using 4 % PFA or liquid nitrogen. Until further use, the organs were then stored at -80 °C (cryosections) or at 4 °C (histological stainings, PFA-fixed).

Body part	% of skin surface	Affected area of body part in %	
		Mouse 1	Mouse 2
Ear (left)	2.5	100	75
Ear (right)	2.5	90	60
Eye (left)	0.5	100	55
Eye (right)	0.5	100	80
Snout	2.5	90	24
Head & Neck	9	76	0
Front leg (left)	5	64	4
Front leg (right)	5	40	16
Rear leg (left)	10	4	25
Rear leg (right)	10	3	12
Tail	10	6	6
Trunk	40	8	0
Oral Mucosa	1.5	0	0
Total are affected:	100	24.54	9.95

Table 4.2: Scoring of affected body surface area on day 13 of disease.

Different body parts and their proportion to the whole skin are used for scoring during EBA. Affected body surface area was ascertained individually for each body part and then later calculated for the whole surface area (left column). Results from the scoring of one mouse receiving a ketogenic diet (Mouse 1) and one receiving control diet (Mouse 2) on day 13 of disease. In order to calculate the total area of affected skin, each score is multiplied with the respective relative proportion of skin and then all values are added up. It is commonly observed in EBA that the skin of ears, eyes and snout are explicitly affected, however the score shown for mouse 1 is considered relatively high. For comparison, an animal with distinctively fewer body surface area is shown.

Ketogenic and nicotinic acid-free diets in EBA

In order to assess the effect of nutritional baseline HCA₂ activation on EBA, mice were fed using a ketogenic or a niacin free diet. For all experiments a control group was treated equally but using control diet only. Chow was available *ad libitum*. As individual feeding of mice could not be carried out appropriately, the distinct experimental groups were housed individually with regard to the diet they received.

Ketogenic diet: Prior to the induction of EBA mice were first fed using a 50 % ketogenic diet (KD, sniff EF R/M ketogenic diet with 80% long chain fatty acids in dry mass and 8 % protein, #E15149-30) mixed with normal chow/ control diet (CD, sniff M-Z, containing 48 % carbohydrates, 15 % fat and 37 % protein, #E15000-00) for 3 days to habituate them. The animals were then subsequently fed for 11 days using the ketogenic diet only (100 % KD). Concluding a total of 2 weeks on ketogenic/ control diet, EBA was induced as described above. Throughout the course of the experiment, sufficient chow supply with the specific diet was guaranteed. During the experiment, the clinical manifestation of EBA was evaluated every third day starting on day 4 of the disease as described above. Successful induction of ketosis was verified by testing the ketone body excretion in spontaneous mouse urine using Keto-Diabur Test 5000 (Roche) stripes three days prior to disease induction (Figure 5.24). To assure an identical hygienic status for all animals, those derived from external breeders were kept in the housing of the “Gemeinsame Tierhaltung” of the University of Lübeck for two weeks prior to the experiments.

Nicotinic acid free diet: Trials using a nicotinic acid free diet were carried out with a special chow (Altromin C 1025 Niacin free diet <0.05 mg/kg Nicotinic acid) in comparison to control diet (Altromin Standard mouse diet #1314; containing 36 mg/kg Nicotinic acid) provided by the “Gemeinsame Tierhaltung” Lübeck. Throughout the experiment, sufficient chow supplies were guaranteed. The animals were fed for two different time periods (12 or 28 days) prior to the collection of plasma samples which were then sent to Labor Dr. Bayer (Leinfelden-Echterdingen, Germany) where analysis of the NA levels and other niacin metabolites was carried out. The blood samples were collected by puncture of the right ventricle of the heart after deep anaesthesia (Ketamine (10 mg/kg) and Xylazine (15 mg/kg)) via intraperitoneal injection. Using a 20G needle and a syringe, filled with 150 µl, 50 mM EDTA to prevent the blood from clotting, between 500 and 1000 µl could be drawn per animal. Furthermore, body weight data were ascertained from all animals.

4.2 FACS analysis

Cell and tissue isolation

The experiments were performed fully blinded and only after conclusion, the data derived were matched to the different groups.

For FACS analysis cells were isolated from blood, spleen, lymph nodes and skin (ears).

At first mice received deep anaesthesia using Ketamine (10 mg/kg) and Xylazine (15 mg/kg) via intraperitoneal injection with a 26G needle. The depth of the anaesthesia was verified by reflex level measurement (interdigital).

At first, blood samples were collected by puncture of the right ventricle of the heart. Using a 20G needle and a syringe, filled with 150 μ l, 50 mM EDTA to prevent the blood from clotting, between 500 and 1000 μ l could be drawn per animal. After removing the needle from the syringe to avoid shearing force induced cell destruction, the blood was directly transferred into 1,5 ml Eppendorf tubes and shaken softly for steady mixing of the blood with EDTA.

In order to retrieve the remaining organs for analysis the peritoneal cavity was opened longitudinally. The spleen was removed and stored in a 1.5 ml tube containing 1 ml FACS buffer. Subsequently, the pelvic lymph nodes were extracted together with the surrounding tissue and stored in the same way as the spleen.

At last, both ears were cut at the basis and stored in one tube. The animals were sacrificed via cervical dislocation, directly following the procedure.

All samples were stored in 1.5ml Eppendorf tubes on ice for further processing.

Cell preparation for FACS analysis

Blood: In order to purify white blood cells, the samples were added to 7 ml of erythrocyte lysis buffer (Qiagen GmbH) in 15 ml tubes, blended and incubated at room temperature for 10 minutes following the manufacturer's instructions. Lysis was stopped by adding 3 ml of FACS-buffer. The samples were then centrifuged for 10 minutes at 1200 rpm and 4 °C in a benchtop centrifuge. These steps were carried out twice in order to obtain adequate lysis.

After the second repetition cells were resuspended in 200 μ l of cold FACS buffer and stored on ice for further analysis. The cell number was ascertained via trypan blue exclusion staining and cell counting in a Fuchs-Rosenthal counting chamber. Depending

on the measurements scheduled, the number of cells per millilitre was then adjusted using FACS buffer.

Spleen and lymph nodes: The first step of cell preparation from spleen and lymph nodes included homogenization of the tissue on a 70- μ m cell strainer using the plunger of a 2 ml syringe. The samples were collected in 50-ml Falcon tubes. After flushing the filter using 20 ml PBS, they were centrifuged for 10 minutes and 1200 rpm at 4 °C using a benchtop centrifuge. The supernatant was removed and cells were resuspended in 250 μ l FACS buffer. Erythrocyte lysis was performed once for the cells derived from the spleen as described above for blood samples. Afterwards the remaining cells were transferred into a 15-ml Falcon and counted.

Ears: The organ was first halved along the cartilage and then cut into small pieces before adding 0.5 ml RPMI-Medium (without FCS) and 0.5 ml liberase™ medium (Sigma, 1.2 mg/ml) diluted in Iscove's Modified Dulbecco's Medium (Gibco) to the Eppendorf tube. Using a shaker, the samples were incubated for 90 minutes at 37 °C and 800 rpm. The pieces were then pushed through a 70- μ m cell strainer into a 50-ml Falcon tube, flushed with 20 ml PBS and stored on ice until all samples were processed. After 10 minutes of centrifugation (4 °C, 1200 rpm), the supernatant was removed and the sediment resuspended in 1 ml cold FACS buffer for counting. The samples were then stored on ice.

FACS preparation

Subsequent to the individual preparation, all samples were centrifuged, the supernatant removed and the remaining cells resuspended in 100-250 μ l of FC-block for 30 minutes (4 °C, dark; purified Anti-Mouse CD16/CD32 in FACS buffer 1/100). This step was necessary in order to prevent false positive (non-specific) binding of immunoglobulins to endogenous Fc receptors to ensure antigen specific binding in FACS analysis and reduce background signal. The reaction was stopped by adding 100-250 μ l of FACS buffer. Following another centrifugation (10 minutes, 1200 rpm, 4°C), removing of the supernatant and transfer to a 96-well plate, primary antibodies were added to the samples and homogenized (for example, 70 μ l antibody in FACS buffer suspension). "Unstained" or control samples were treated with the corresponding amount of FACS buffer without antibodies. Prior to the experiments, the optimum concentration for each antibody was assayed via a titration run as shown in the results section. For this purpose, tissue from non-diseased but otherwise identical animals was used.

After incubation of 30 minutes (4 °C, dark), FACS buffer (250 µl) was added. Following centrifugation (10 minutes, 4 °C, 1200 rpm) and removing of the supernatant the cells were mixed and incubated with 100 µl of viability dye in PBS (APC/APC-Cy7; dilution 1:1000) for 30 minutes (4 °C, dark; unstained or control samples were incubated with FACS buffer only).

Following this procedure, the cells were washed using 100 µl FACS buffer, centrifuged (4 °C, 10 minutes, 1200 rpm) and resuspended in 200 µl cold FACS buffer. The measurements were made in the core facility of the University of Lübeck (CanaCore) hence all samples were stored on ice and transported in the dark.

Analysis of FACS data

For cell analysis, the flow cytometer (BD LSR II) in the Cell Analysis Core Facility (CanaCore) was used. With 4 lasers, 18 different colours could be measured in total, however only 7-9 of these were needed to acquire well distinguishable signals. The following fluorochromes were utilized (corresponding wavelength of $E_{m_{max}}$ = Emission maximum): Tomato (RFP, 607 nm), Brilliant™ violet (BV) 510 (510 nm), BV 650 (650 nm), BV 421 (421 nm), PE (R-phycoerythrin; 578 nm), PE-Cy™7 (Tandem conjugate: PE + cyanine dye (Cy7); 785 nm), PerCP-Cy™5.5 (Tandem conjugate: Peridinin-Chlorophyll-protein + Cyanine dye Cy5.5; 695 nm), APC (Allophycocyanin; 660 nm), APC Cy™7 (Tandem conjugate: APC + Cyanine Dye Cy7; 785 nm), FITC (Fluorescein isothiocyanate; 520 nm). The individual antibody panel setup, showing which fluorochrome was used for which surface marker, is depicted in the respective results section of each experiment.

Cell measurement in the flow cytometer was carried out together with Dr. M. Wannick as profound knowledge is needed for data acquisition in order to receive reliable results. Prior to the experiments, antibodies were chosen with regard to their maximum excitation and emission spectra and compensation for spectral overlapping was carried out using cell samples, analysed with FACS Diva and FlowJo software. First of all, using an unstained sample, voltages for the different fluorescence channels were set. Forward (FSC) and side scatter (SSC) were then adjusted so that the cell population could be delineated clearly. Next, compensation was carried out in order to remove the signal of one fluorochrome in a neighbouring channel. For this purpose, single colour stainings were performed and measured in FACS. The compensation values for each channel were subsequently adjusted

so that only those cells positive for the individual staining were marked and as little signal as possible was acquired in other channels. During the experiments (especially CD62L expression), isotype controls were used to account for nonspecific staining.

In order to mark and exclude dead cells from analysis, they were irreversibly labelled using Viability Dye eFluor® 780 (Thermo Fisher). This amine-reactive dye binds proteins which are, due to impaired membrane stability, much more accessible in dead cells compared to living ones as the dye is capable of entering the cells.

Gating strategy

The specific gating strategy for each experimental setup is described in the respective results section of the data acquired.

The general approach for cell distinction is described below:

First of all, FSC and side SSC were used to exclude debris which typically has lower FSC levels (Figure 4.2 A). Then, FSC-Height versus FSC-Area excluded doublets and clumps (B). Distinction can be made as single cells typically fall along a diagonal line through the plot, whereas doublets and clumps show increased area relative to their height. After this, viable cells were first distinguished as viable single cells (Fixable Viability Dye vs. FCS; C) and subsequently as viable CD45⁺ single cells (Fixable Viability Dye vs. CD45; D). Based on the expression of CD45, the cell population chosen comprised all living leukocytes.

In further analysis, the subpopulations of specific immune cells were then identified due to their distinct cluster of differentiation surface expression. Neutrophils were characterised as CD45⁺CD11b⁺Ly6G⁺ (E), non-classical monocytes as CD45⁺Ly6G⁻CD11b⁺Ly6C^{Lo}, classical monocytes as CD45⁺CD11b⁺Ly6G⁻Ly6C^{Hi}, $\gamma\delta$ T cells as CD45⁺CD3⁺ $\gamma\delta$ TCR⁺, $\alpha\beta$ T cells as CD45⁺CD3⁺ $\gamma\delta$ TCR⁻ and NK cells as CD45⁺CD3⁻NK1.1⁺. However, as not all cells could be analysed at the same time due to potential overlapping of the fluorochromes in different channels, two antibody set-ups (“panels”) were used during the experiments. They are depicted in the result section of each experiment.

Subsequent to the definition of the individual cell populations via surface markers, their relative amount was measured using FlowJo software. For analysis, data were displayed for each population in relation to viable single cells or viable single CD45⁺ cells (leukocytes).

Experiments targeting HCA₂ expression were carried out using an *Hca2*^{mRFP} reporter line where expression of the receptor can be assayed via monomeric red fluorescent protein (mRFP; Em_{max} 607 nm).

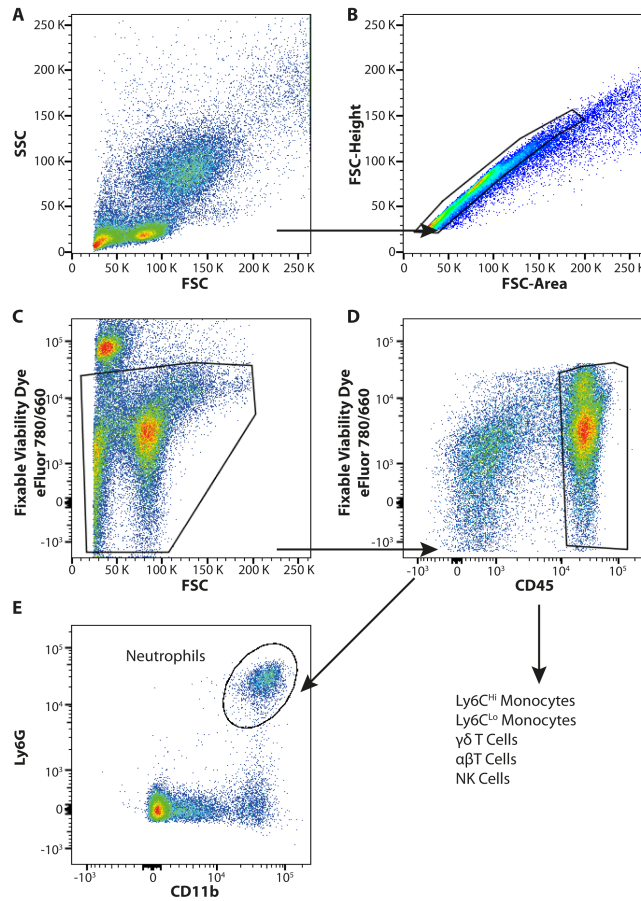


Figure 4.2: Gating strategy of flow cytometry analysis.

Isolated cells of different tissues were gated for viable cells and the expression of CD45. All determined leukocytes were analysed for CD45⁺CD11b⁺Ly6G⁺ neutrophils, CD45⁺CD11b⁺Ly6G⁻Ly6C^{Lo} monocytes, CD45⁺CD11b⁺Ly6G⁻Ly6C^{Hi} monocytes, CD45⁺CD3⁺γδTCR⁺ γδT cells, CD45⁺CD3⁺γδTCR⁻ αβT cells and CD45⁺CD3⁻NK1.1⁺NK cells. The number of cells is shown as percent of viable cells. Representative dot blots of blood cells are shown.

4.3 Histological approaches

The experiments were performed fully blinded and only after conclusion, the data derived were matched to the different groups.

Vibratome

Sample preparation: Vibratome sections were derived from mouse ears using a Leica Vibratome. The samples were collected at different time points of the experiments, primarily frozen using liquid nitrogen and then stored at -80 °C. The day before cutting, the samples were transferred to a 4 °C fridge for optimal cutting conditions.

Prior to cutting the tissue needed to be embedded in low melt agarose, which was preheated via a microwave until melted. The specimen was then placed in a 6-well plate, aligned for cutting and then fluid agarose was poured on top until completely covered. After cooling and hardening, the embedded samples were glued onto the base of the vibratome using superglue.

While cooling, the vibratome was prepared by adding PBS to the sample chamber so that the specimen would be completely submerged and a new surgical blade was installed for precise cutting.

Sections: All samples were cut beginning from the basis of the ear. First of all, the cartilage was removed by cutting thicker sections. As soon as one of the slides taken comprised a complete ear section, the cutting speed was limited to a thickness of 100 µm and a speed of 0.5 mm/s as this proved to be the ideal setting for optimal histological assessment in previous experiments. Sections were then cut continuously. Directly after cutting, the samples were transferred to a 24-well plate containing 0.02 % NaAcid in PBS with the help of a brush and stored at 4 °C in the dark until staining.

Cryosections

Cryosections were made using unfixed, -80 °C frozen mouse ears (primarily frozen in fluid nitrogen directly after organ harvesting), which were transferred to a -20 °C freezer the day before cutting. The samples were aligned and embedded in cutting fluid (optimum cutting temperature compound) which typically freezes very quickly and can then be adhered to the platform of the cryotome using superglue. Resembling to the vibratome sections, cryosections were taken and discarded until the whole organ was covered in one slide

taken. Hereafter, 10 µm thick sections were taken continuously. Following this step, 4 samples were transferred to each object slide, dried at room temperature and then stored at -20 °C in the dark for further use.

Immunostaining/Immunohistochemistry

The best picture quality was achieved using 1% BSA in PBS and acetone fixing. First all sections were thawed and fixed in -20 °C cold acetone for 10 minutes. After two washing steps of 5 minutes in PBS, each individual section was surrounded with a water repellent layer, using DakoPen. For 1 hour all samples were then blocked using a 1 % BSA solution in PBS (200 µl/ slide).

Following blocking, the primary antibody against C3 (clone 11H0, Hycult Biotech) was added at a dilution of 1:400 in 1 % BSA in PBS for incubation overnight at 4 °C (dark). The next day, appropriate secondary antibodies were applied after two steps of washing with PBS for 5 minutes (for example: Alexa 488-labeled anti-rat IgG, dilution 1:400, Thermo Fisher, Cy3-labeled anti-rabbit IgG, dilution 1:400, Jackson ImmunoResearch) together with 4',6-diamidino-2-phenylindole (DAPI, concentration: 2 µg/ml) and incubated for 1 h at room temperature in the dark. DAPI is a fluorescent stain binding to adenine-thymine regions, used to label DNA in cells. Two washing steps using PBS for 5 minutes each (dark) were carried out prior to adding the mounting medium (Mowiol/DABCO; 70-80 µl/object slide) and coverslips. Microscope pictures were acquired after one night of hardening (4 °C, dark) utilising a Leica DMI6000B fluorescence microscope. Fluorescence intensity as well as epidermal thickness were specified using ImageJ.

Epidermal thickness measurement using neutrophil antibody peroxidase staining

Ear sections were taken as described above, stored in formalin, embedded in paraffin and cut into 10-µm thick sections using a cryotome.

Samples were taken from 3 individual experiments on day 16 after disease induction with both knockout and wild-type animals which were treated with DMF (50 mg/kg, p.o.) or vehicle twice a day.

After cutting, the sections were deparaffinized using Xylol solution (2x 5 min) and subsequently washed in decreasing ethanol solution baths (absolute ethanol decreasing to

40 % ethanol; each washing step carried out for 5 minutes). After one H₂O washing step, the samples were rinsed and stored in TRIS-buffered saline (TBS).

In order to demask antigen epitopes which were crosslinked due to formalin fixation beforehand, the samples were incubated in 100 °C hot citrate buffer for 20 minutes and again rinsed with TBS after cooling down.

A 20-minute incubation step with 1 % H₂O₂ / TBS was performed to reduce endogenous peroxidase activity and thus non-specific background staining.

Subsequently, blocking steps using 8 % skim milk (2 h incubation), Avidin and Biotin (both 15 min) were performed in order to prohibit endogenous non-specific Fc receptor and biotin binding.

The primary antibody was incubated overnight (Rat- α -7/4; dilution 1:800 in 3 % BSA/ TBS), all samples rinsed afterwards and incubated using the secondary antibody (Goat- α -Rat-Biotin; dilution 1:600 in 3 % BSA/ TBS) for 45 minutes.

An avidin-biotin-complex (ABC) staining (Vectastain ABC kit) was carried out to amplify signal intensity (2 drops of reagent A in 2.5 ml TBS + 2 drops of reagent B in 2.5 ml TBS, 30 min incubation time; afterwards 50 μ l Vectastain ABC Reagent incubation for 10 min).

3,3'-Diaminobenzidin (DAB) substrate was added for 5 minutes. Afterwards, mounting medium (Mowiol/DABCO; 70-80 μ l/object slide) and coverslips were added and microscope pictures acquired after one night of hardening (4 °C) utilising a Leica DMI6000B fluorescence microscope. The epidermal thickness was then measured at diseased sites and

the average diameter was calculated as a mean value from three representative measurements from each section of epidermis.

4.4 Statistical analysis

Data analysis was carried using GraphPad Prism (Version 5.0). Prior to analysis, Gaussian distribution of the data was checked (Shapiro-Wilk-Test). If a Gaussian distribution could be verified, subsequent analysis was carried out using Student's t-test for experiments with two independent groups. When more than two independent groups (i.e. genotype and treatment as variables) were assessed, a one- or two-way analysis of variance (ANOVA) was applied.

For data sets where a significant main effect was reached, the distinct groups were compared applying post-hoc analyses, such as Bonferroni, Dunnett's or Tukey's test. Data sets not showing a Gaussian distribution were analysed using the nonparametric Kruskal-Wallis test combined with Dunn's multiple comparisons post-hoc test.

All data are displayed as mean value \pm standard error of the mean (SEM) and p-values of less than 0.05 are considered as showing a significant difference (*p < 0.05, **p < 0.01 and *** p < 0.001). Bar graphs are shown using Box-Whisker plots according to Tukey.

5.0 Results

5.1 Validation of antibodies used during flow cytometry in EBA

Antibody titration

Antibody titration was carried out for fluorophores which have not been used in our laboratory before to find out the ideal antibody concentration. A known number of cells was stained using decreasing antibody concentrations beginning with the concentration suggested by the vendor (referred to as 1). By adding FACS buffer, 5 different dilutions were created: 1; 0.5; 0.25; 0.125 and 0.0625 as relative concentrations compared to the vendor's recommendation. Equal amounts of cells were subsequently stained and measured in the flow cytometer. The acquired signals were then gated for the specific populations of interest (see section FACS analysis in methods) and the amount of positive and negative cells was identified.

From the results gathered for each individual concentration the staining index (SI¹²³) was calculated using the following formula:

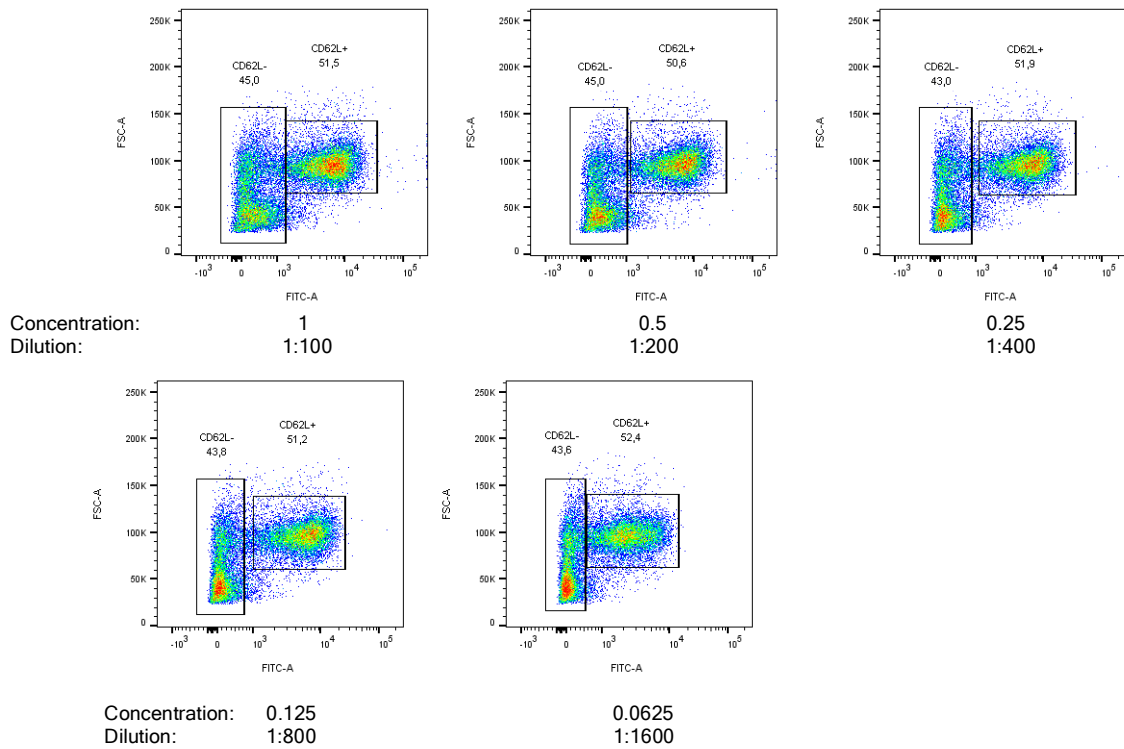
$$SI = \frac{Med_{pos} - Med_{neg}}{[(84 \%_{neg} - Med_{neg})/0.995]}$$

Med_{pos} indicates the measured median fluorescent intensity (MFI) of the positive population and Med_{neg} the MFI of the negative population. The difference between both values was divided by the standard deviation (a measure of the amount of variation in a data set)¹²⁴.

In order to find the optimum antibody concentration, the values for staining index were plotted (antibody concentration against staining index). The graph point with the highest staining index mapped the ideal concentration and at this point minor changes occurring due to experimental deviance did not change the SI significantly. Hereinafter titration data for the L-selectin antibody as well as for characterization of the $\gamma\delta$ T cell population using the T cell receptor gamma variable regions are shown.

First, the titration of the antibody directed against CD62L (L-selectin) was carried out. The results are depicted below.

A



B

Conc	Dilution	CD62L+	CD62L-	CD62L- Percentile	SI
1	1:100	5616	367	816	11.632
0.5	1:200	5509	310	641	15.628
0.25	1:400	5416	242	518	18.653
0.125	1:800	5279	203	434	21.864
0.0625	1:1600	2231	158	325	12.351

C

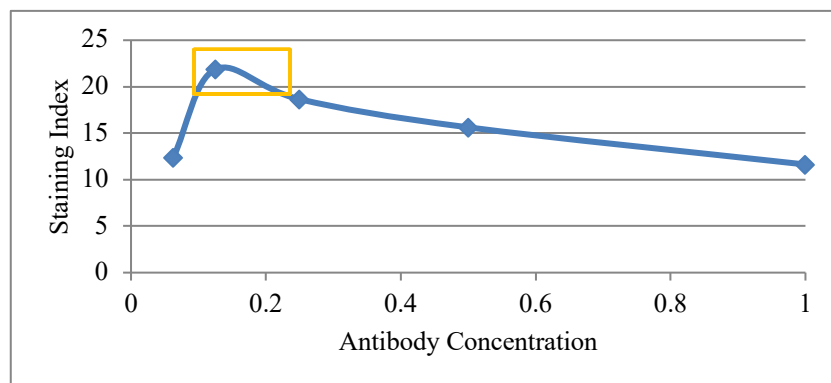


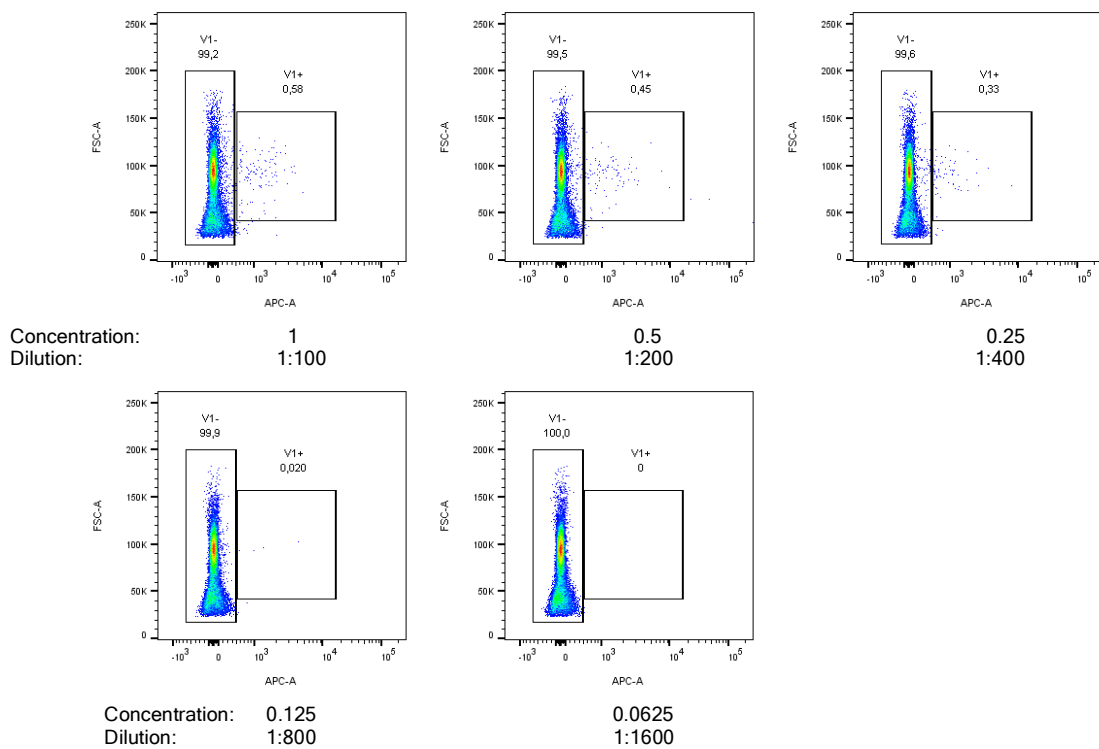
Figure 5.1: Antibody titration FACS L-selectin (CD62L) antibody.

FACS-data acquired for titration of the L-selectin targeting antibody (Biolegend Clone MEL-14, Cat. # 104406, conjugated to fluorescein isothiocyanate = FITC). A: FITC is plotted against the area (FSC-A) of the cells; gated for viable single cells. 5 different dilutions were made (1:100 = vendor's recommendation; Concentration = relative concentration compared to vendor's recommendation, Dilution = dilution of antibody in FACS-buffer); B: Staining index (SI) calculated for each dilution; C: Line plot for SI against Antibody concentration, the orange box indicated the best range of antibody concentration.

Corresponding to the experimental findings, the ideal concentration to be used during further experiments was chosen. Generally, the graph point with the highest staining index mapped the ideal concentration as minor changes occurring due to experimental variation would not change the SI significantly and thus comparable results would be obtained. The vendor recommended an antibody dilution of 1:100 (concentration 1), in our experimental setup, the highest staining index for the CD62L antibody was identified as 1:800 (concentration 0.125)

Furthermore, the titration was carried out for the T cell receptor gamma variable region 1 (Trgv1.1) targeted antibody. The graphic results are depicted below.

A



B

Conc	Dilution	Trgv1.1+	Trgv1.1-	Trgv1.1- Percentile	SI
1	1:100	1127	7.7	68.1	18.4388
0.5	1:200	1082	6.42	65.5	18.11446
0.25	1:400	789	2.57	56.5	14.50951
0.125	1:800	974	2.57	57.8	17.50087
0.0625	1:1600	0	1.28	57.8	-0.02253

C

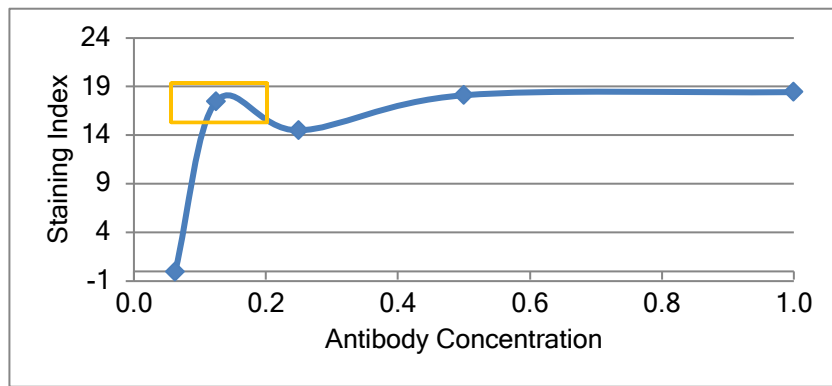


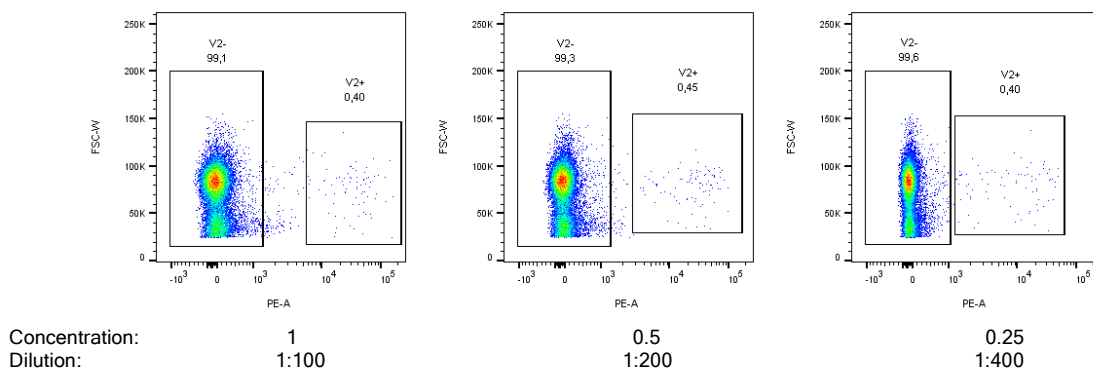
Figure 5.2: Antibody titration T cell receptor gamma variable region 1 (Trgv1.1).

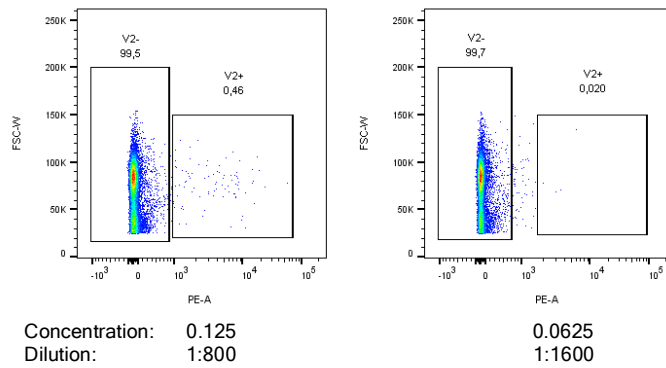
FACS-data acquired for the titration of the Trgv1.1 (Biolegend, Clone 2.11, Cat. # 141007) targeting antibody (conjugated to Allophycocyanin = APC; 5 different dilutions were made (1:100 = vendor's recommendation; Concentration = relative concentration compared to vendor's recommendation, Dilution = dilution of antibody in FACS-buffer); **A:** ABC is plotted against the area (FSC-A) of the cells; gated for viable single cells. **B:** Staining index (SI) calculated for each dilution; **C:** Line plot for SI against Antibody concentration, the orange box indicated the best range of antibody concentration.

The vendor recommended an antibody dilution of 1:100 (concentration 1), in our experimental setup, the highest staining index for the CD62L antibody was identified as 1:800 (concentration 0.125)

T cell receptor gamma variable region 2 (Trgv2) antibody titration was carried out subsequently. The results are shown below.

A





B

Conc	Dilution	Trgv2+	Trgv2-	Trgv2- Percentile	SI
1	1:100	32331	87.4	253	193.7342
0.5	1:200	27215	66.8	205	195.4592
0.25	1:400	9577	33.4	125	103.6668
0.125	1:800	2957	15.4	71.9	51.8034
0.0625	1:1600	2963	11.6	53.9	69.42418

C

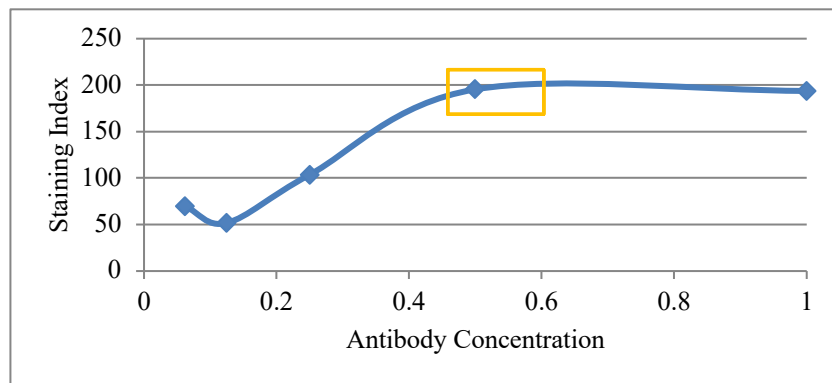


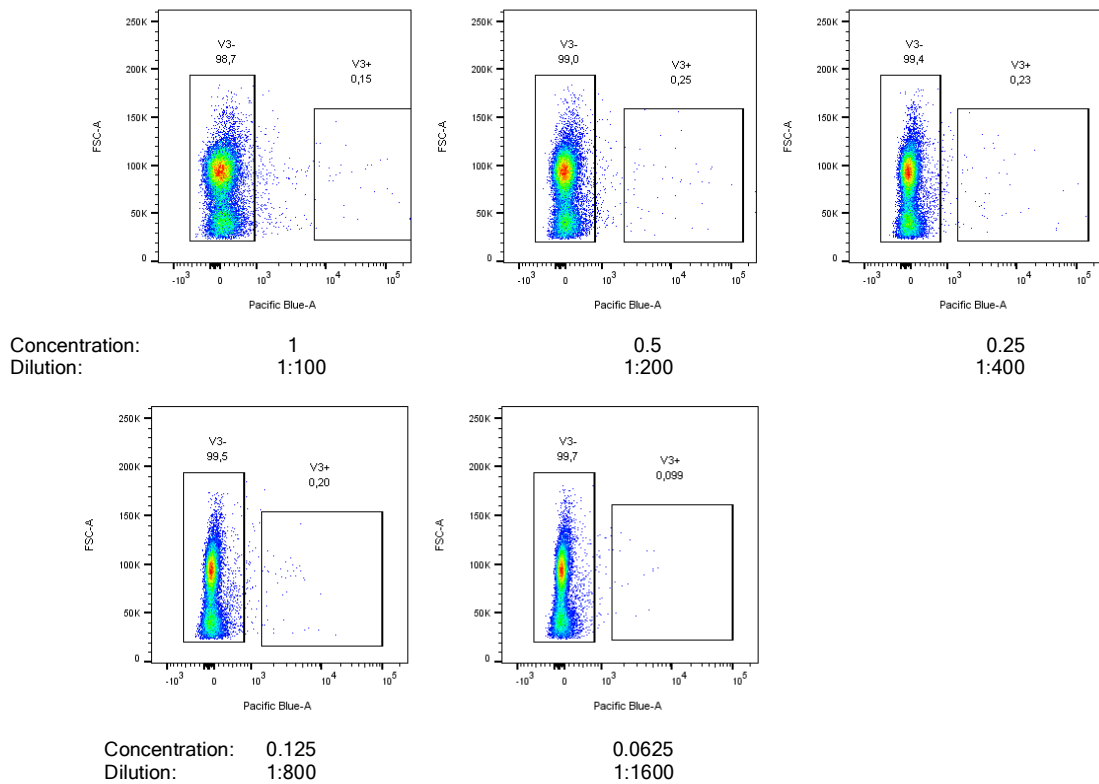
Figure 5.3: Antibody titration T cell receptor gamma variable 2 (Trgv2).

FACS data acquired for the titration of the Trgv2 receptor (Biolegend, Clone UC3-10A6, Cat. # 137705) targeting antibody (conjugated to phycoerythrin = PE; 5 different dilutions were made (1:100 = vendor's recommendation; Concentration = relative concentration compared to vendor's recommendation, Dilution = dilution of antibody in FACS-buffer); **A**: PE is plotted against the area (FSC-A) of the cells; gated for viable single cells. **B**: Staining index (SI) calculated for each dilution; **C**: Line plot for SI against Antibody concentration, the orange box indicated the best range of antibody concentration.

The vendor recommended an antibody dilution of 1:100 (concentration 1), in our experimental setup, the highest staining index for the Trgv2 antibody was identified as 1:200 (concentration 0.5)

Lastly, the titration of the T cell receptor gamma variable region 3 (Trgv3) targeting antibody was carried out.

A



B

Conc	Dilution	Trgv3+	Trgv3-	Trgv3- Percentile	SI
1	1:100	18941	140	321	103.3536
0.5	1:200	5191	102	241	36.42845
0.25	1:400	3259	66.8	175	29.35526
0.125	1:800	2849	53.9	138	33.06926
0.0625	1:1600	1853	51.4	125	24.35587

C

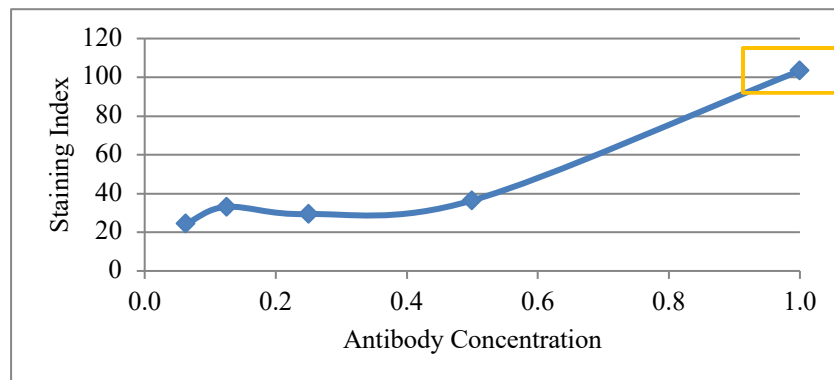


Figure 5.4: Antibody titration for the T cell receptor gamma variable 3 (Trgv3).

FACS data acquired for the titration of the Trgv3 receptor (BD Biosciences, Clone 536, Cat. # 743238) targeting antibody (conjugated to Brilliant Violet 421 = BV421; similar to Pacific Blue, but emission spectrum more narrow); 5 different dilutions were made (1:100 = vendor's recommendation; Concentration = relative concentration compared to vendor's recommendation, Dilution = dilution of antibody in FACS-buffer); **A**: Pacific Blue is plotted against the area (FSC-A) of the cells; gated for viable single cells. **B**: Staining index (SI) calculated for each dilution; **C**: Line plot for SI against Antibody concentration, the orange box indicated the best range of antibody concentration.

The vendor recommended an antibody dilution of 1:100 (concentration 1), in our experimental setup, the highest staining index for the Trgv3 antibody was indeed identified as 1:100 (concentration 1)

5.2 Verifying successful disease induction in immunohistochemical stainings of epidermolysis bullosa acquisita skin samples

Initially, successful induction of EBA had to be verified in skin samples of diseased animals. For this purpose, immunohistochemical stainings were carried out on cryosections derived from each individual in all treatment groups on day 16 of disease in order to detect skin-bound anti-collagen VII antibodies and complement factor C3. Both findings are key elements of experimental EBA in mice but also essential for the diagnosis of disease in patients.

Figure 5.5 shows representative fluorescent microscopic pictures from the different stainings for anti-collagen VII IgG and C3 and a merged image with all stainings together in order to evaluate their distributional pattern.

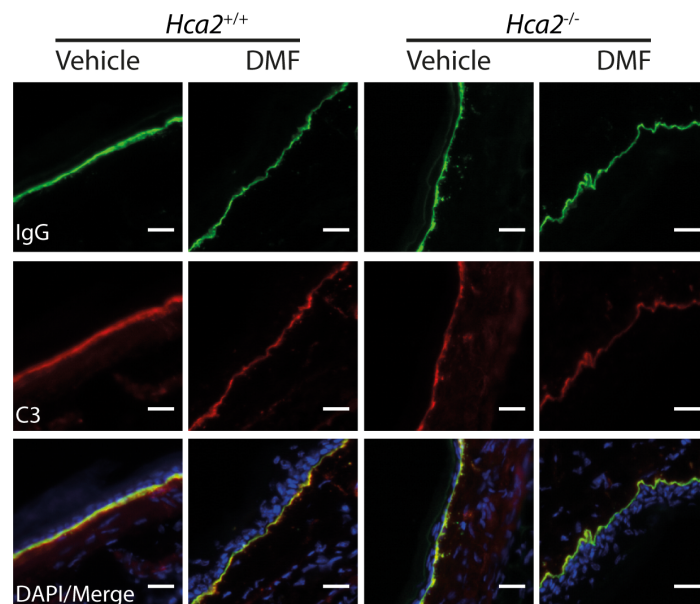


Figure 5.5: Representative immunohistochemical staining of anti-collagen VII-IgG and C3 depositions at the dermal-epidermal junction.

Stainings were made from the dermis of animals with wildtype receptor status ($HCA2^{+/+}$) and knockout littermates ($HCA2^{-/-}$) where antibody transfer EBA was induced. Animals either received vehicle or DMF treatment (50 mg/kg, p.o., twice per day). Immunohistochemical stainings of anti-collagen type VII-IgG and C3 deposition at the dermal-epidermal junction were performed on cryosections of skin samples. Scale bar = 20 μ m.

In all treatment groups, injected anti-collagen VII-IgG antibodies could be detected which were used to mimic an autoimmune production of antibodies directed towards collagen type VII (found at the dermal-epidermal junction) in the antibody-mediated form of EBA. A positive signal thus provided evidence for successful disease induction. Furthermore, the fluorescence intensity of IgG deposition was measured using ImageJ and statistically analysed (Figure 5.6).

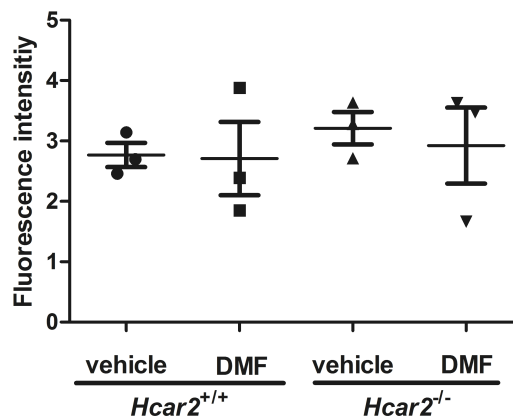


Figure 5.6: IgG deposition at the dermal-epidermal junction.

Similar intensity of IgG-depositions in all groups. Antibody transfer EBA was induced in $Hca2^{+/+}$ and $Hca2^{-/-}$ mice that received oral vehicle or DMF treatment (50 mg/kg, p.o., twice per day). Immunohistochemical stainings of anti-collagen VII-IgG depositions at the dermal-epidermal junction were performed on cryosections of skin samples and fluorescence intensity of depositions was determined by ImageJ. In statistical analysis, no difference in IgG deposition could be found. (n=3 mice, Kruskal-Wallis Test with Dunn's post hoc test).

Analysis of the distinct groups (using Kruskal-Wallis test with Dunn's post hoc test) showed no significant difference. These findings demonstrated that the antibodies successfully travelled to the dermal-epidermal junction after i.p. injection and that the distribution is neither affected by genotype nor by oral treatment during the experiment.

Aside from IgG deposition, skin-bound complement factor C3 was used as a key immunohistochemical finding in EBA, also utilized for disease diagnosis⁷. C3 deposition was measured in the same way as shown for IgG beforehand (Figure 5.7).

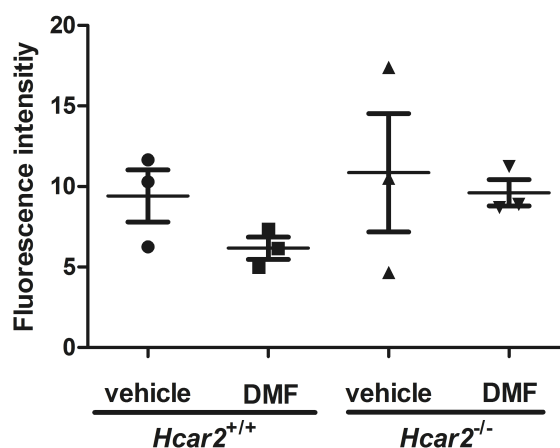


Figure 5.7: C3 deposition at the dermal-epidermal junction.

Similar intensity of C3-depositions in all groups. Antibody transfer EBA was induced in $Hca2^{+/+}$ and $Hca2^{-/-}$ mice that received oral vehicle or DMF treatment (50 mg/kg, p.o., twice per day). Immunohistochemical stainings of C3 depositions at the dermal-epidermal junction were performed on cryosections of skin samples and fluorescence intensity of deposition was determined by ImageJ. In statistical analysis, no difference in C3 deposition could be found. (n=3 mice, Kruskal-Wallis Test with Dunn's post hoc test).

Complement factor deposition could be detected in all groups at the dermal-epidermal junction. Furthermore, no difference in intensity could be found when comparing the groups with regard to treatment and genotype. These findings substantiate the previous findings, indicating that inflammation was evenly present in all samples and thus successful disease induction took place consistently.

5.3 Epidermal thickness measurement

Cell invasion and inflammatory response usually lead to an increase in epidermal thickness in fully developed lesions of EBA. To investigate a possible effect of DMF treatment on the width of the epidermis, ear samples were taken on day 16 of disease (microscopic pictures see Figure 5.9).

In all groups thickening of the skin and split formation could be detected in inflamed areas as a proof of disease activity. The mean value of the epidermal thickness ranged between 72.75 μm ($Hcar2^{+/+}$; vehicle treatment) and 89.82 μm ($Hcar2^{+/+}$; DMF treatment) for the different groups. Using 2-way ANOVA analysis, no significant difference between the treatment or genotype groups could be detected (Figure 5.8). Neither in the measurement of maximum epidermal thickness, nor in the average width, a difference between the different treatment groups or with regard to genotype could be found.

In conclusion, skin inflammation could be induced in each individual animal as a proof of successful EBA induction but epidermal thickening as a result of inflammation did not differ between treatment or genotype.

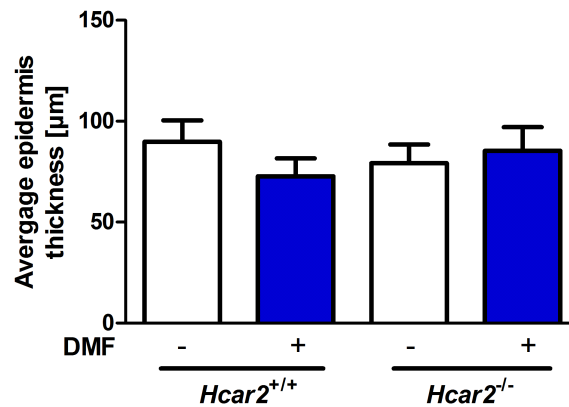


Figure 5.8: Average epidermal thickness measurement.

No significant difference in the average epidermal thickness in EBA with regard to treatment or genotype could be found. Mice received a total of 3 i.p. injections of 100 µg anti-collagen VII-IgG every second day and were treated with DMF or vehicle (50 mg/kg p.o.) every 12 hours. On day 16 of EBA, ear samples were taken, stained with haematoxylin-eosin staining and microscopic pictures were acquired from inflamed areas. Epidermal thickness was measured using ImageJ. Data are shown as mean + SEM, $n=18$, $p < 0.05$, 2-way ANOVA with Bonferroni post-test was performed.

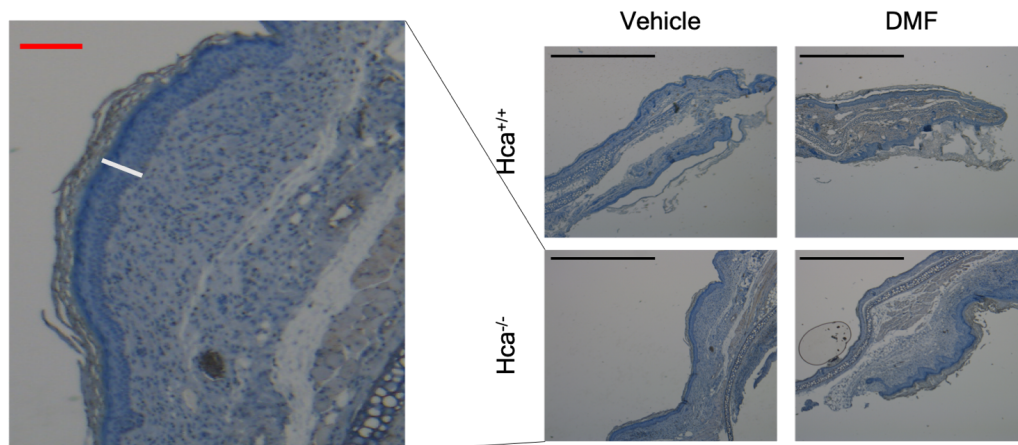


Figure 5.9: Epidermal thickness measurement.

Representative microscopic pictures of haematoxylin- and eosin-stained skin sections. The epidermal thickness measurement was carried out in animals where antibody transfer EBA was induced in *Hca2*^{+/+} and *Hca2*^{-/-} mice that received oral vehicle or DMF treatment (50 mg/kg, p.o., twice per day). Stainings were made using haematoxylin-eosin staining and epidermal thickness was measured. Black scale bar = 1000 µm; red scale bar: 100 µm; white bar: epidermal thickness.

5.4 HCA₂ expression in epidermolysis bullosa acquisita

Spatio-temporal receptor expression on different cell types was analysed in the skin and blood with regard to DMF or vehicle treatment.

To allow a precise evaluation, the reporter mouse line *Hca2^{mRFP}* (*Gpr109^{mRFP}*) was used. Here, monomeric red fluorescent protein (mRFP) expression is controlled by the *Grp109* gene promoter: *Hcar2^{mRFP}* mice were generated by introducing a bacterial chromosome transgene into the genome. This comprises the genomic locus of *Hcar2*⁷⁵ and contains the 3'- and 5' sequences. As the *Hcar2* coding sequence has been exchanged for the mRFP gene, fluorescent expression is accordingly controlled by *Hcar2*. The expression pattern of the receptor can then be quantified using fluorescence analysis, respectively FACS.

The approach revealed that after EBA induction in mice, significantly more immune cells were RFP⁺ in blood compared to naïve mice (Figure 5.10 A). Already on day 5 after the first antibody injection, a significant rise in receptor expressing cells could be detected. In accordance with these findings, higher relative numbers of HCA₂⁺ cells were detected in the skin (Figure 5.10 B).

Furthermore, analysis revealed consistent numbers of RFP⁺ cells over the course of the experiment, showing no difference for blood or skin in these cells comparing days 5 and 11 after disease induction. DMF had no effect on the percentage of immune cells as the relative amount stayed stable with regard to treatment (Figure 5.10).

In lymph nodes or the spleen, no significant difference in RFP expressing cells was found during the experiment, neither with regard to the course of EBA, nor to DMF treatment (Figure 5.11)

Having found an increase in RFP expression, FACS analysis was performed with regard to receptor expression by individual cell populations. The gating strategy is depicted in the section FACS-Analysis in methods and the antibody panel used is shown below (Table 5.10). First, single cells were identified, then viability dye was used to find viable cells, and subsequently viable CD45⁺ cells. Having established this subgroup, further analysis was carried out with individual markers for each specific cell type (described below), such as CD45 and CD11b which are both positive in neutrophils.

Nearly all neutrophils (CD45⁺CD11b⁺Ly6G⁺) and non-classical monocytes (CD45⁺CD11b⁺Ly6C^{Lo}) were found to express the receptor (90-93 % of neutrophils and

84-87 % of non-classical monocytes), but only between 5 and 20 % of the classical monocytes (CD45⁺CD11b⁺Ly6C^{Hi}). Furthermore, T cells were analysed showing a small subpopulation of $\gamma\delta$ T cells (CD45⁺CD3⁺ $\gamma\delta$ TCR⁺) that carried the receptor (2-3 %). In both $\alpha\beta$ T cells (CD45⁺CD3⁺ $\gamma\delta$ TCR⁻) and NK cells (CD45⁺CD3⁻NK1.1⁺) only very few cells were RFP⁺ (0.1 % and 0.5 – 0.8 %, Figure 5.10 C). Apart from classical neutrophils where DMF treatment lowered the fraction of HCA₂ expressing cells, no difference could be observed with regard to treatment.

The abundance of the distinct cell types, especially neutrophils and non-classical monocytes was quantified in blood, skin, spleen and lymph nodes where populations were measured in relation to viable single cells for both DMF and vehicle treated animals. In the following, the results are described for each cell type individually. The impact of DMF on inflammatory cells in the different organs is described in detail in the section “inflammatory cells in the skin”.

Table 5.10.: Antibody panel for HCA₂ expression experiments.

The respective antigen against which the antibody is directed, as well as the conjugate it is linked to in order to identify the signal in FACS analysis later. Furthermore, the company, clone, Catalogue number (Cat. #) and Dilution which was identified in a titration experiment beforehand, are shown. APC, allophycocyanin; CD, cluster of differentiation; HCA₂, hydroxycarboxylic acid receptor 2; Ly, leukocyte; TCR, T cell receptor; NK, Natural killer cell; RFP, red fluorescent protein; BV, Brilliant™ violet; PE, R- phycoerythrin; Per, peridinin-chlorophyll-protein; Cy7, cyanine dye 7; FITC, fluorescein isothiocyanate.

“Antigen”	Conjugate	Clone	Company	Cat. #	Dilution
HCA ₂	(RFP) Tomato				
CD45	BV 510	30-F11	Biolegend	103138	800
CD11b	BV 650	M1/70	Biolegend	101239	200
Ly6C	PE-Cy7	HK1.4	Biolegend	128018	800
Ly6G	PerCP-Cy5.5	1A8	Biolegend	127616	200
CD11c	APC	N418	Biolegend	117310	400
Viability	APC-Cy7		eBioscience	65-0865-14	1000
$\gamma\delta$ TCR	PerCP-Cy5.5	REA633	Miltenyi	130-109-801	200
CD127	PE-Cy7	REA680	Miltenyi	130-110-376	200
CD3	FITC	145-2C11	Biolegend	100306	400
CD45R	APC-Cy7	RA3-6B2	Biolegend	103224	200
NK1.1	BV 421	PK136	Biolegend	108741	200

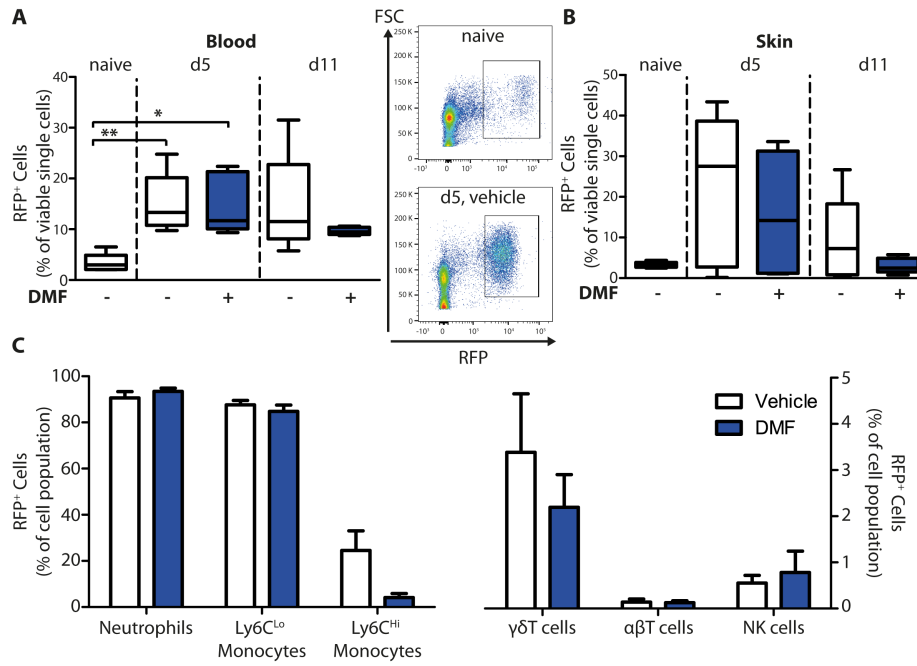


Figure 5.10: HCA₂ receptor expression in blood and skin in different cell types and with regard to treatment.

HCA₂ expression increased in blood and skin upon induction of experimental epidermolysis bullosa acquisita. Quantification of monomeric red fluorescent protein (mRFP)⁺ cells in blood and ear skin of Hca2^{mRFP} mice. The numbers of RFP⁺ cells are shown in percent of viable cells for (A) blood and (B) skin of naive mice or of animals on day 5 (d5) and 11 (d11) after first antibody injection. Mice were treated with vehicle of dimethyl fumarate (DMF) (50 mg/kg, p.o., twice per day). **p* < 0.05; ***p* < 0.01 (*n* = 5 mice, Kruskal–Wallis Test with Dunn’s post hoc test). (A) Representative dot plots from naive mice and animals at d5 (vehicle-treated group) are shown. (C) Quantification of mRFP⁺ cells in immune cell populations of DMF- and vehicle-treated mice at d11. The numbers of mRFP⁺ cells are expressed as percent of CD45⁺CD11b⁺Ly6G⁺ neutrophils, CD45⁺CD11b⁺Ly6C^{Lo} monocytes, CD45⁺CD11b⁺Ly6C^{Hi} monocytes, CD45⁺CD3⁺ $\gamma\delta$ TCR⁺ $\gamma\delta$ T cells, CD45⁺CD3⁺ $\gamma\delta$ TCR⁻ $\alpha\beta$ T cells, and CD45⁺CD3⁻NK1.1⁺ NK cells. Means \pm SEM are depicted (*n* = 5 mice).

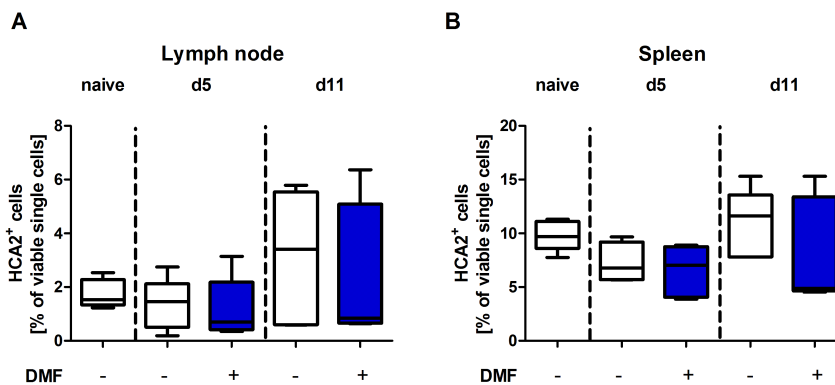


Figure 5.11: RFP⁺ cells in spleen and lymph node.

Quantification of monomeric red fluorescent protein (mRFP)⁺ cells in spleen and lymph nodes of Hca2^{mRFP} mice. The numbers of RFP⁺ cells are shown in percent of viable cells for (A) lymph node and (B) spleen of naive mice or of animals on day 5 (d5) and 11 (d11) after first antibody injection. Mice were treated with vehicle of dimethyl fumarate (DMF) (50 mg/kg, p.o., twice per day). Kruskal–Wallis Test with Dunn’s post hoc test was performed. Means \pm SEM are depicted (*n* = 5 mice).

Population of neutrophils

The analysis of neutrophils revealed a trend towards higher relative amounts in blood (Figure 5.12 A, already on day 5); spleen (Figure 5.12 B, day 11), and lymph nodes (Figure 5.12 C). Explorative statistical analysis comparing equal treatment at different time points revealed a significant difference for vehicle treated animals, in blood, skin and lymph nodes when comparing day 0 with day 5 and day 0 with day 11. In the spleen a change was only detected comparing day 0 and day 11. However, since multiple testing was not considered in this approach, these results need to be interpreted carefully.

Non-explorative statistical analysis for DMF showed no significant effect on the number of cells measured in blood, lymph node or spleen, but there was a trend towards a reduction on day 11 in spleen and blood by treatment (Figure 5.12 A, B, C).

For the analysis in skin however, a significant decrease in neutrophils could be detected upon DMF treatment (Figure 5.16 D, Results and Figure see section DMF and inflammatory cells).

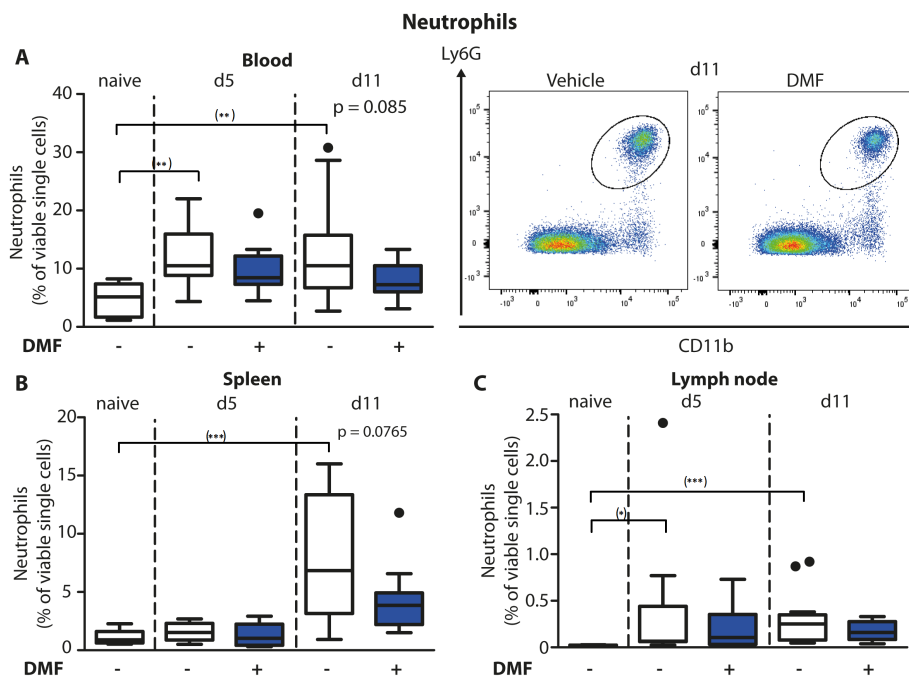


Figure 5.12: DMF treatment of mice does not reduce elevated numbers of neutrophils in blood and lymphoid tissue.

Quantification of $CD45^+ CD11b^+ Ly6G^+$ neutrophil cell population in (A) blood, (B) spleen and (C) lymph nodes of naïve mice or of animals on day 5 (d5) and 11 (d11) after 1st antibody injection. Mice were treated with vehicle or DMF (50 mg/kg, p.o., twice per day). The numbers of cells are shown in percent of viable cells. Representative dot plots of d11 are shown. (* $p < 0.05$; ** $p < 0.01$; *** $p < 0.001$; $n=9-14$ mice, Mann-Whitney test; explorative use of Mann-Whitney test distinguished by use of brackets, for further details see descriptive section above).

Population of classical monocytes (Ly6C^{Hi})

Only few of the classical monocytes were HCA₂ receptor-positive in previous analyses (Figure 5.10 C).

Explorative statistical analysis comparing equal treatment at different time points revealed a significant rise in this cell population for skin (Figure 5.13 C) and spleen (Figure 5.17 A) already at an early stage of EBA (vehicle treated animals; day 0 vs. day 5 and day 0 vs. day 11). For lymph nodes, a difference was only observed at a later time point (Figure 5.17 C; vehicle treatment day 0 vs. day 11). In blood, no changes in cell count could be detected (Figure 5.13 B). However, since multiple testing was not considered in this approach, the results need to be interpreted carefully.

In non-explorative analysis, with regard to DMF treatment, a responsiveness of classical monocytes could be shown in spleen and lymph node (Figure 5.17 A & C) but not in the other organs.

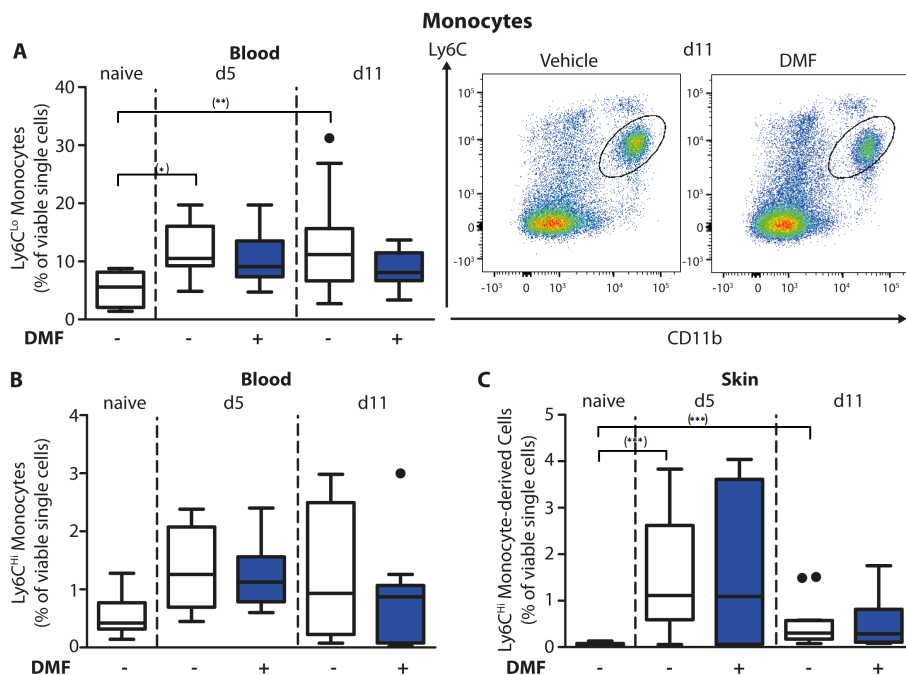


Figure 5.13: DMF treatment of mice does not reduce elevated numbers of monocytes in blood.

Quantification of (A) CD45⁺CD11b⁺Ly6C^{Lo} monocyte and (B) CD45⁺CD11b⁺Ly6C^{Hi} monocyte cell populations in blood and (C) CD45⁺CD11b⁺Ly6C^{Hi} monocyte-derived cells in the skin of naive mice or from animals on day 5 (d5) and 11 (d11) after 1st antibody injection. Mice were treated with vehicle or DMF (50 mg/kg, p.o., twice per day). The number of cells is shown in percent of viable cells. Representative dot plots of d11 are shown. (*p < 0.05; **p < 0.01; n=9-14 mice, Mann-Whitney test; explorative use of Mann-Whitney test distinguished by use of brackets, for further details see descriptive section above).

Population of non-classical monocytes (Ly6C^{L0})

A large proportion of non-classical monocytes showed to express the HCA₂ receptor beforehand (Figure 5.10 C). Explorative statistical analysis comparing equal treatment at different time points revealed a rise in proportion to all single cells at an early disease stage in blood (Figure 5.13 A) and skin (Figure 5.16 C) in vehicle treated animals (day 0 vs. day 5 and day 0 vs. day 11). For the secondary lymphoid organs, a later response on day 11 compared to disease induction (Figure 5.17 B & D; vehicle treated animals) was found. However, since multiple testing was not considered in this approach, the results need to be interpreted carefully.

In non-explorative analysis, DMF had no effect on the number of non-classical monocytes in the organs examined (Figure 5.13 A; 5.16 C; 5.17 B & D).

Population of natural killer cells (NK cells)

The previous experiment showed that only a small proportion of NK cells were RFP⁺ on day 11 of EBA (Figure 5.10 C). Explorative statistical analysis comparing equal treatment at different time points revealed that the relative amount of NK cells only varied significantly in the spleen on day 11 compared to the start of disease (Figure 5.14; vehicle group). In contrast to other cell populations, a reduction in cells could be observed. These findings indicated that NK cells were not responsible for the rise in RFP⁺ cells in blood upon disease induction. In the skin, no NK cells could be detected in FACS analysis. Since multiple testing was not considered in this approach, the results need to be interpreted carefully.

In non-explorative analysis, DMF again had no effect on the number of NK cells in the organs examined (blood, spleen, lymph node; Figure 5.14).

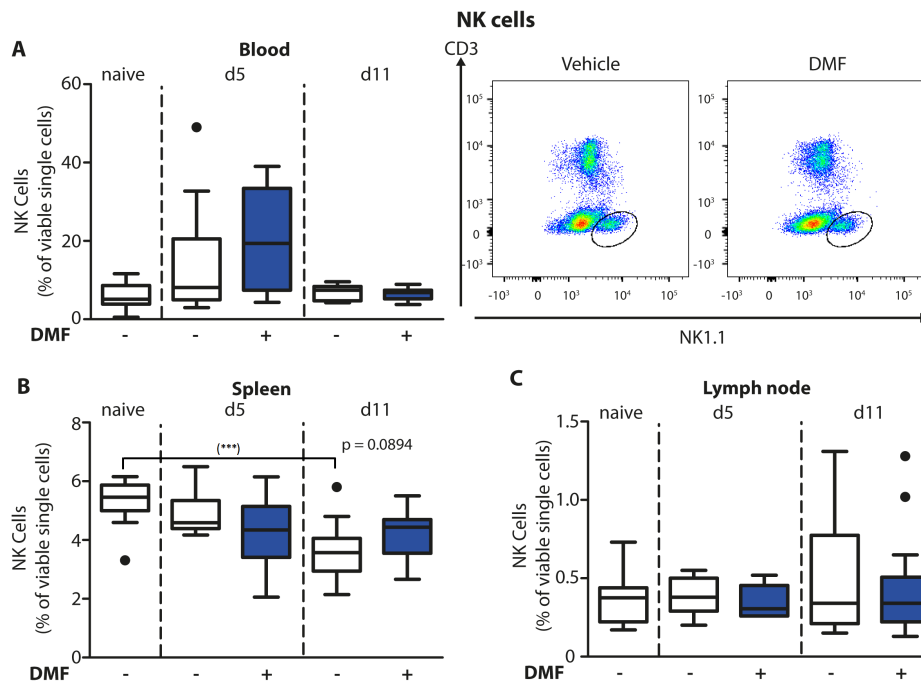


Figure 5.14: DMF treatment of mice does not affect elevated numbers of NK cells.

(A-C) Quantification of CD45⁺CD3⁺NK1.1⁺NK cell populations in (A) blood, (B) spleen and (C) lymph nodes of naïve mice or from animals on day 5 (d5) and 11 (d11) after 1st antibody injection. Mice were treated with vehicle or DMF (50 mg/kg, p.o., twice per day). The number of cells is shown in percent of viable cells. Representative dot plots of d11 are shown (**p < 0.001; n=9-14 mice, Mann-Whitney test, explorative use of Mann-Whitney test distinguished by use of brackets, for further details see descriptive section above).

Population of $\gamma\delta$ T cells

Previous analysis showed that a small subpopulation of $\gamma\delta$ T cells carried the HCA₂ receptor (Figure 5.10 C). Further, explorative statistical analysis comparing equal treatment at different time points, revealed that, in the vehicle group, a significant decrease in cell population was evident for day 11 compared to naïve mice in both spleen and skin (Figure 5.15; Figure 5.16 E). In blood and lymph node a stable number of cells was detected. However, since multiple testing was not considered in this approach, the results need to be interpreted carefully.

In non-explorative analysis, no DMF effect on $\gamma\delta$ T cells was perceivable in blood, spleen and lymph node (Figure 5.15). However, a significant increase in $\gamma\delta$ T cells could be found upon DMF administration in the skin on day 11 (Figure 5.16 E).

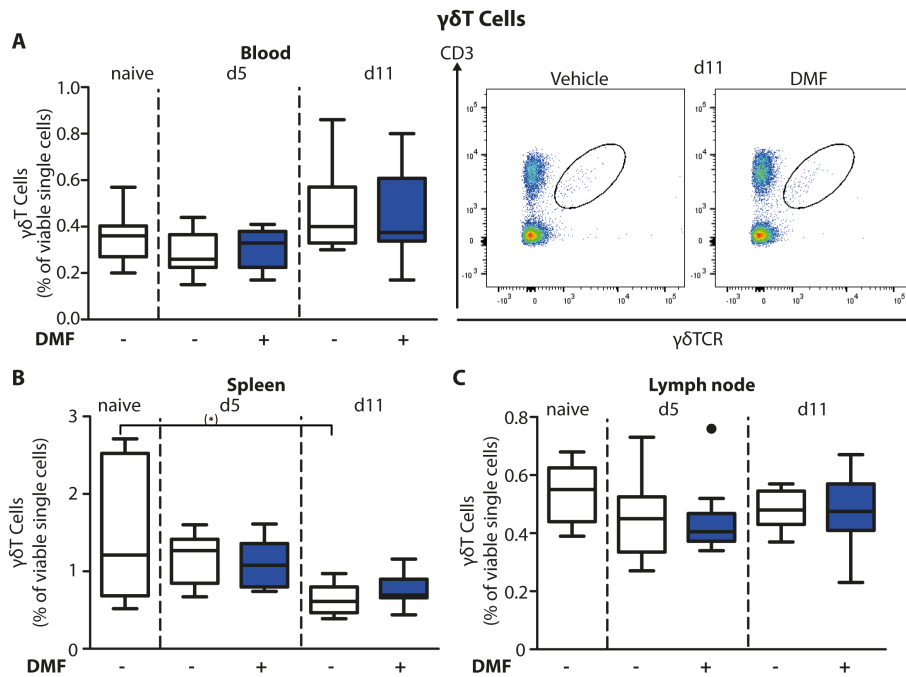


Figure 5.15: DMF treatment of mice does not reduce elevated numbers of $\gamma\delta$ T cells in blood and lymphoid tissue.

Quantification of $CD45^+CD3^+\gamma\delta TCR^+\gamma\delta T$ cells populations in (A) blood, (B) spleen and (C) lymph nodes of naïve mice or from animals on day 5 (d5) and 11 (d11) after 1st antibody injection. Mice were treated with vehicle or DMF (5 mg/kg, p.o., twice per day). The number of cells is shown in percent of viable cells. Representative dot plots of d11 are shown. (* $p < 0.05$; $n = 9-14$ mice, Mann-Whitney test, explorative use of Mann-Whitney test distinguished by use of brackets, for further details see descriptive section above).

In conclusion, spatiotemporal, explorative analysis of HCA₂ expression showed that the significant rise in receptor positive cells found on day 5 after EBA induction coincides with higher relative numbers of neutrophils, non-classical and classical monocytes. These populations also showed high levels of RFP signal.

Furthermore, with regard to DMF treatment and the responsiveness of the different cell types, it could be shown that only elevated neutrophil counts in the skin were influenced by DMF. For classical monocytes, reductions in counts in the spleen and lymph node could be demonstrated. Non-classical monocytes, $\gamma\delta$ T cells and NK cells were not influenced by treatment in blood, spleen, lymph nodes or skin.

5.5 DMF and inflammatory cells in the skin

Müller et al. (2016) have previously established a protective effect of DMF treatment on disease severity in the skin. We aimed to reproduce this finding before the start of further experiments. After the first experiment, similar results to those reported in the literature had been found: DMF treatment significantly inhibited the formation of skin lesions. Disease severity was altered by about 60 % at its peak (Figure 5.16 B). The affected body surface area diminished from a mean value of 6.7 % to 2.9 % under DMF treatment (Figure 5.16 A). Figure 5.16 B shows representative pictures of skin lesions on day 11 of disease.

Flow cytometry analysis was then used on peripheral blood, secondary lymphoid tissue (specifically lymph nodes and spleen) and lesional skin to detect changes in cell numbers. Vehicle and DMF treated animals were characterized with regards to the relative number of cells in relation to viable cells. Three different conditions were covered: naïve (mice without disease induction), 5 and 11 days after disease induction (i.p. injection of anti-collagen type VII).

Immune cells in the skin

At disease onset (day 5), no difference in the populations of neutrophils (Figure 5.16 D), non-classical (Ly6C^{Lo}, Figure 5.16 C) and classical monocytes (Ly6C^{Hi}, Figure 5.13 C) or $\gamma\delta$ T cells (Figure 5.16 E) with regard to treatment could be observed in the skin. NK cells could not be detected in skin measurements.

Analysis at a more advanced disease stage (day 11) showed that significantly fewer neutrophils (Figure 5.16 D) were present in the skin under DMF treatment. Apart from this, a trend towards lower numbers of non-classical monocytes (Figure 5.16 C) was detected. $\gamma\delta$ T cells were significantly more abundant when mice received DMF (Figure 5.16 E). The relative numbers of the other cell types remained similar with regard to treatment.

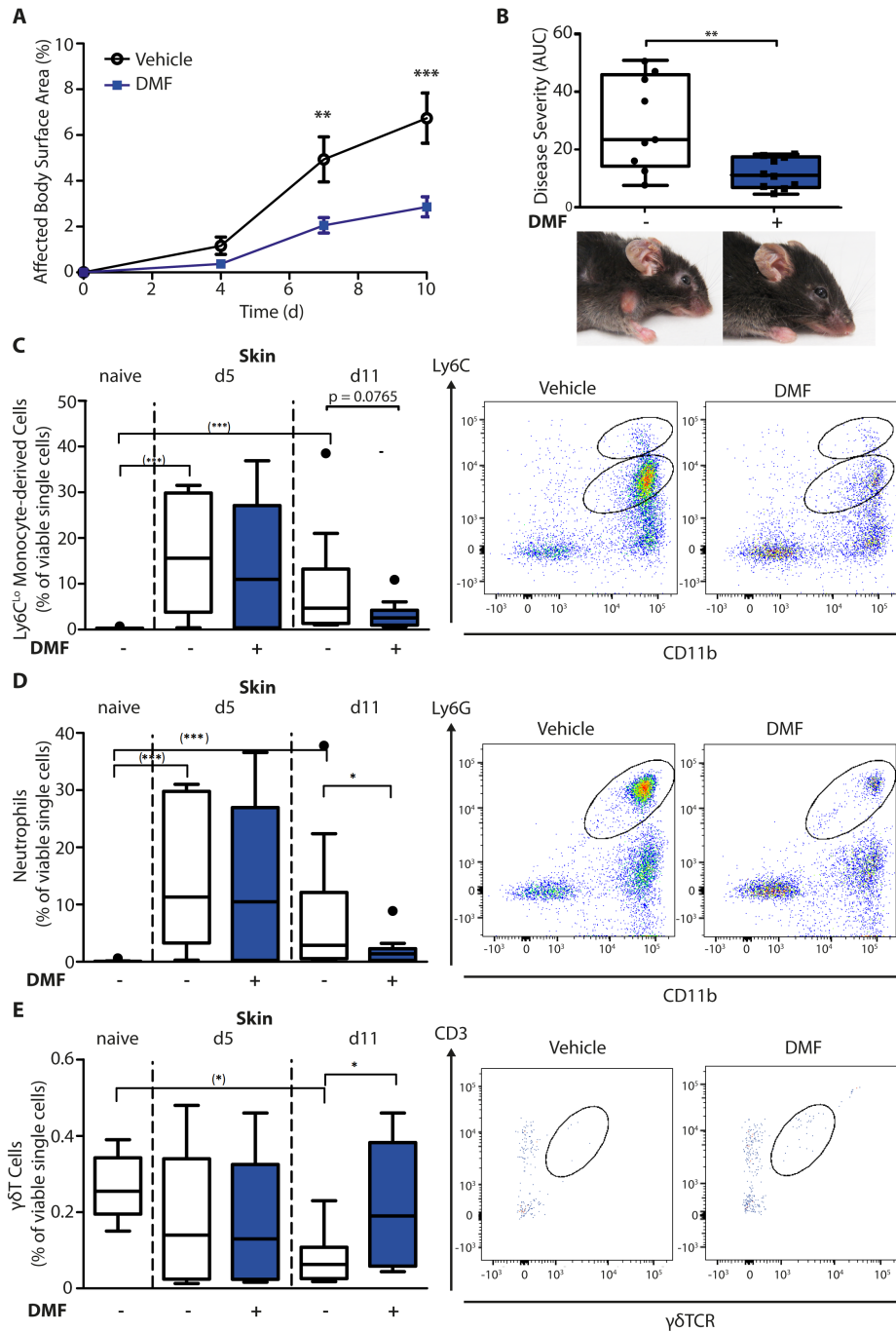


Figure 5.16: Inflammatory cells in the skin.

Dimethyl fumarate (DMF) treatment diminishes disease severity of experimental epidermolysis bullosa acquisita (EBA) by reducing elevated numbers of pro-inflammatory cells in the skin. (a) Clinical course of antibody transfer EBA in wild-type mice that were treated with DMF (50 mg/kg, p.o., twice per day) or vehicle. Two-way ANOVA, $F(1/51) = 8.85$, $**p < 0.01$; $***p < 0.001$ ($n = 9-14$ mice, Bonferroni post hoc test). (b) Disease severity, calculated as area under the curve of the data in (a), and clinical presentation. $**p < 0.01$ (Mann-Whitney test). (c-e) Quantification of immune cell populations in ear skin of naive mice or of animals on day 5 (d5) and 11 (d11) after first antibody injection. The numbers of cells are shown in percent of viable cells for (c) $CD45^+CD11b^+Ly6C^{Lo}$ monocytes, $***p < 0.001$ ($n = 9-14$ mice, Mann-Whitney test). (d) $CD45^+CD11b^+Ly6G^+$ neutrophils, and (e) $CD45^+CD3^+\gamma\delta TCR^+$ $\gamma\delta T$ cells. Representative dot plots of day 11 are shown. $*p < 0.05$; $***p < 0.001$, ($n = 9-14$ mice, Mann-Whitney test, explorative use of Mann-Whitney test distinguished by use of brackets, for further details see descriptive section above).

Immune cells in blood

In contrast to skin analysis, in peripheral blood the relative number of inflammatory cells stayed similar with regard to treatment at both time points despite a trend towards reduced cell numbers in neutrophils (Figure 5.12 A, 5.13 A & B, 5.14 A, 5.15 A).

Immune cells in spleen

Even though no changes could be detected at an early time point, monocytes showed a considerable responsiveness to DMF treatment at day 11 with reduced cell numbers of classical monocytes (Ly6C^{Hi}, Figure 5.17 A) and a trend towards lower counts of non-classical monocytes (Ly6C^{Lo}, Figure 5.17 B) in the spleen. Similar results were observed for neutrophils (trend at day 11; Figure 5.12 B). In contrast to these findings, NK cells showed a trend towards an increase in relative cell numbers at day 11 (Figure 5.14 B). The relative number of $\gamma\delta$ T cells stayed similar in the spleen upon DMF treatment (Figure 5.15 B).

Immune cells in lymph node

Classical monocytes were reduced upon DMF administration on day 11 (Ly6C^{Hi}, Figure 5.17 C). The amount of neutrophils, non-classical monocytes (Ly6C^{Lo}), NK cells and $\gamma\delta$ T cells remained unchanged in the course of EBA (Figure 5.17 D, 5.12 C, 5.14 C, 5.15 C).

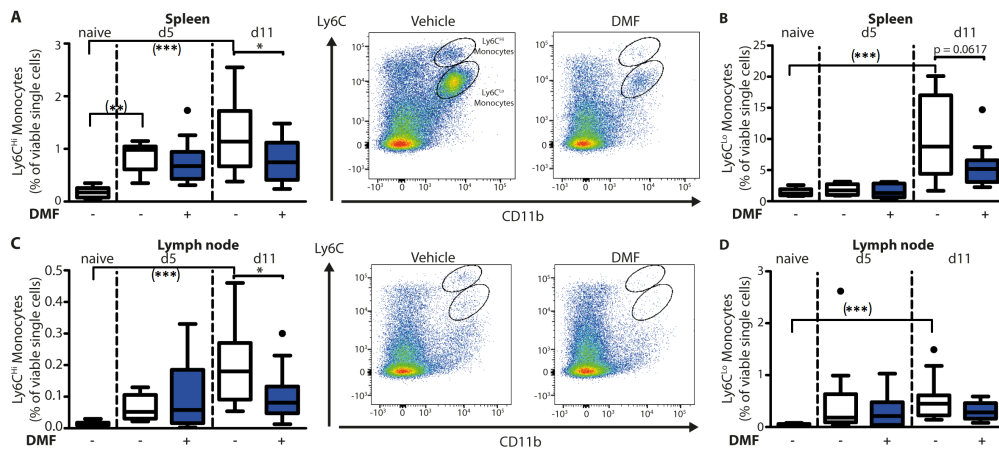


Figure 5.17: Inflammatory cells in spleen and lymph node.

Dimethyl fumarate (DMF) treatment of mice inhibits trafficking of Ly6C^{Hi} monocytes to secondary lymphoid tissues. Quantification of CD45⁺CD11b⁺Ly6C^{Hi} and CD45⁺CD11b⁺Ly6C^{Lo} monocyte populations in spleen (A,B) and lymph nodes (C,D) of naive mice or of animals on day 5 (d5) and 11 (d11) after first antibody injection. The animals received either vehicle or DMF (50 mg/kg, p.o., twice per day). The numbers of cells are shown in percent of viable single cells. Representative dot plots of day 11 are shown. **p* < 0.05; ****p* < 0.001 (*n* = 9–14 mice, Mann–Whitney test, explorative use of Mann–Whitney test distinguished by use of brackets, for further details see descriptive section above).

In conclusion, the number of cells detected showed no difference at EBA induction (day 5). Nevertheless, at a later time point, changes with regard to treatment were especially detected in the skin (neutrophils ↓, $\gamma\delta$ T cells ↑), the spleen (Ly6C^{Hi} ↓) and lymph nodes (Ly6C^{Hi} ↓).

5.7 The role of L-selectin in conveying the DMF treatment effect

On day 11 after the first antibody injection, organs were harvested and analysed via FACS with regard to the expression of CD62L in the two treatment groups. The antibody panel (Table 5.11) used for this experiment is listed below. For the three cell types of neutrophils (differentiated as CD45⁺CD11b⁺Ly6G⁺), non-classical monocytes (CD45⁺CD11b⁺Ly6C^{Lo}) and classical monocytes (CD45⁺CD11b⁺Ly6C^{Hi}), CD62L levels were quantified. For each analysis, an isotype control was carried out (graphic results depicted in Figure 5.18). Non-activated cells express higher amounts of L-selectin on their surface and consequently, low levels of CD62L are a marker for activated or migrating cells.

CD62L in blood

A significant difference between the amount of CD62L-levels on the surface of neutrophils and non-classical monocytes could be detected when comparing vehicle with DMF treated mice. Animals that received DMF showed higher amounts of L-selectin (Figure 5.18 A & B). For classical monocytes, no difference in CD62L expression could be observed with regard to treatment (Figure 5.18 C).

CD62L in secondary lymphoid organs

In the lymphoid organs, no significant differences could be found when comparing vehicle and DMF treated animals. The levels of L-selectin were not altered by treatment in any group of immune cells.

The CD62L levels in secondary lymphoid tissues are depicted in Figure 5.19.

In conclusion, DMF only showed an effect on neutrophils and non-classical monocytes in blood resulting in a higher CD62L expression. As CD62L expression levels and activation status are correlated inversely, the two cells types were thus less activated in blood.

Table 5.11: Antibody panel for L-selectin (CD62L) experiments.

The respective antigen against which the antibody is directed, as well as the conjugate it is linked to in order to identify the signal in FACS imaging later. Furthermore, the company, clone, Catalogue number (Cat. #) and Dilution which was identified in a titration experiment beforehand, are shown. V γ stands for antibodies directed against T cell receptor gamma variable thus identifying $\gamma\delta$ T cell subpopulations. APC, allophycocyanin; CD, cluster of differentiation; Ly, leukocyte; TCR, T cell receptor; NK, natural killer cell; RFP, red fluorescent protein; BV, brilliant™ violet; PE, R-phycoerythrin; Per, peridinin-chlorophyll-protein; Cy7, cyanine dye 7; FITC, fluorescein isothiocyanate.

“Antigen”	Conjugate	Clone	Company	Cat. #	Dilution
CD62L	FITC	MEL-14	Biologend	104406	800
NK1.1	BV 421	PK136	Biologend	108741	200
CD45	BV 510	30-F11	Biologend	103138	800
CD11b	BV 650	M1/70	Biologend	101239	200
Ly6C	PE-Cy7	HK1.4	Biologend	128018	800
Ly6G	PerCP-Cy5.5	1A8	Biologend	127616	200
Viability	APC		eBioscience	65-0864-14	1000
CD45	BV 510	30-F11	Biologend	103138	800
$\gamma\delta$ TCR	PerCP-Cy5.5	REA633	Miltenyi	130-109-801	200
V γ 1.1	APC	2.11	Biologend	141107	800
V γ 2	PE	UC3-10A6	Biologend	137705	200
V γ 3	BV421	536	BD	743238	100

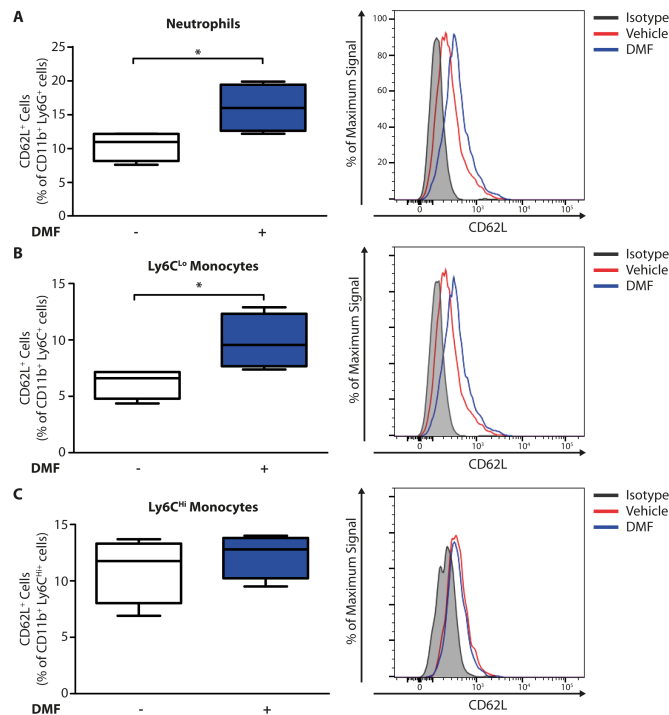


Figure 5.18: DMF treatment inhibits activation of neutrophils and non-classical monocytes.

Quantification of CD62L on immune cell populations in blood of wild-type mice taken on day 11 after 1st antibody injection. Mice were treated with vehicle or DMF (50 mg/kg, p.o., twice per day). The amount of CD62L+ cells is shown in percent of (A) neutrophils, (B) non-classical monocytes and (C) classical monocytes. Representative histograms show isotype control (grey), vehicle-control (red) and DMF-treatment (blue). N = 4 mice/group. Statistical analysis was performed using the Mann-Whitney-Test.

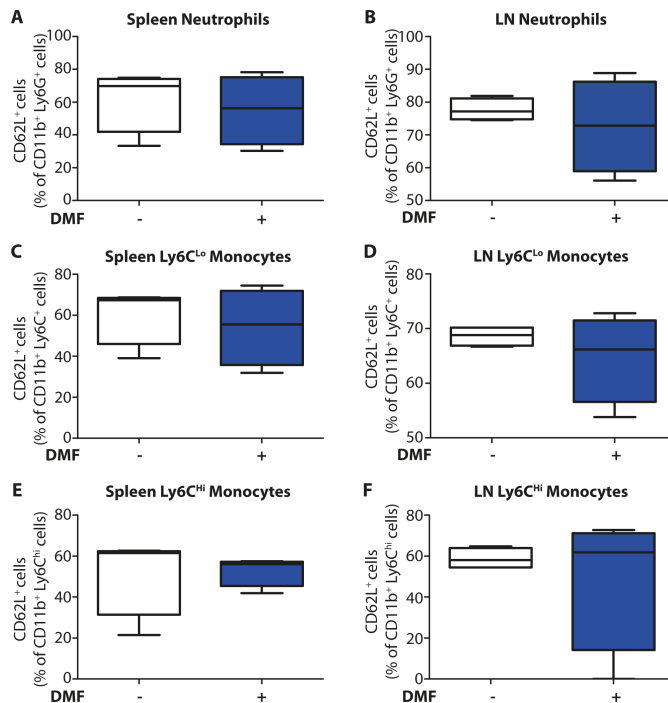


Figure 5.19: DMF treatment does not affect CD62L expression on immune cells in secondary lymphoid tissues.

Quantification of CD62L on immune cell populations in spleen and lymph nodes (LN) of wild-type mice on day 11 after 1st antibody injection. Mice were treated with vehicle or DMF (50 mg/kg, p.o., twice per day). The number of CD62L+ cells are shown in percent of (A) CD45⁺CD11b⁺Ly6G⁺neutrophils, (B) CD45⁺CD11b⁺Ly6C^{Lo}monocytes and (C) CD45⁺CD11b⁺Ly6C^{Hi} monocytes. (n=4 mice, Mann-Whitney test).

5.8 Evaluation of gender and HCA₂ dependency of DMF treatment

HCA₂ dependency of DMF treatment

In EAE it has already been shown that the protective effect of DMF treatment is dependent on the presence of the receptor⁵³. To directly investigate this hypothesis in EBA, the disease was induced in mice deficient in HCA₂ (*Hca2*^{-/-}) to compare the clinical course of the disease with their wild-type littermates (*Hca2*^{+/+}).

For wildtype animals, the same course of disease could be detected as before with a protective effect of DMF treatment. Significant reductions on individual days and throughout the entire observation period (area under the curve; AUC) were found in the treatment group (Figure 5.20 & Figure 5.21)

In the receptor deficient group, no difference was apparent between vehicle and DMF administration on individual days or for the whole experimental period (Figure 5.20 & Figure 5.21). Figure 5.20 B shows representative pictures from the clinical presentation in four experimental groups. Statistical analysis (two-way ANOVA) revealed that the treatment effect is HCA₂-dependent.

Despite these findings, analysis of the data also showed a significant difference between the vehicle treated animals of the wild-type group and their littermates which were receptor deficient. Animals lacking HCA₂ had a less pronounced clinical course of the disease when comparing the AUC (Figure 5.20 C). This might suggest a long-term protective effect of receptor deficiency. Nevertheless, these findings were not reflected in individual analysis of day 16 at the end of the experiment (Figure 5.20 D).

In conclusion, the data showed an HCA₂-dependent treatment effect of DMF in EBA which is consistent with the hypothesis generated from the data acquired earlier and results of trials published in literature^{52,125}.

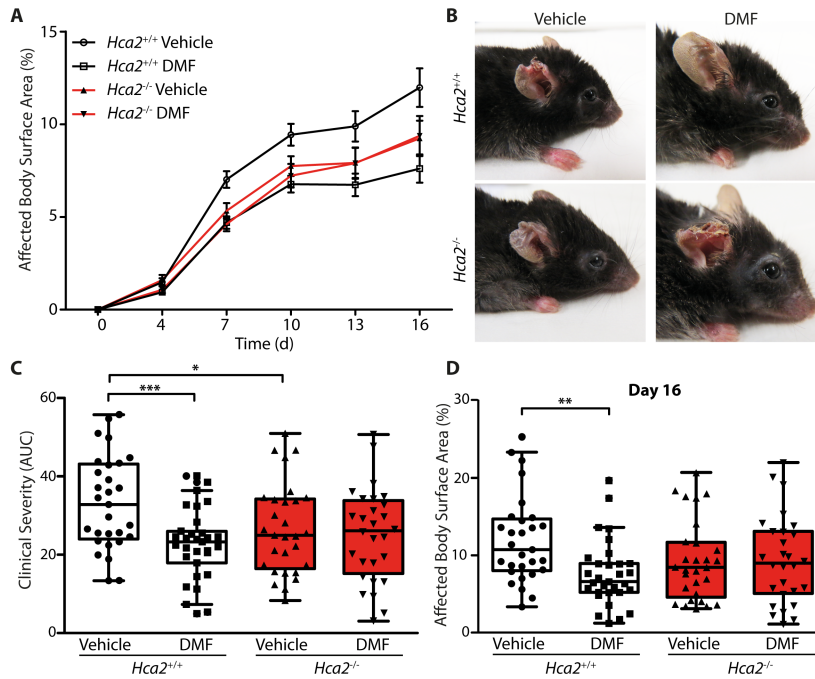


Figure 5.20: Therapeutic dimethyl fumarate (DMF) effects in experimental epidermolysis bullosa acquisita (EBA) depend on HCA₂.

(A) Clinical course of antibody transfer EBA in *Hca2*^{+/+} and *Hca2*^{-/-} mice that received oral vehicle or DMF treatment (50 mg/kg, p.o., twice per day). (B) Representative clinical presentation in the four experimental groups. (C) Clinical severity calculated as area under the curve of the data in (a). Two-way ANOVA, interaction between genotype and treatment $F(1/113) = 4.94$, $*p < 0.05$; $***p < 0.001$ ($n = 28-31$ mice, Bonferroni post hoc test) (D) Affected body surface area on day 16. ANOVA, interaction between genotype and treatment $F(1/113) = 5.75$, $**p < 0.01$ ($n = 28-31$ mice, Bonferroni post hoc test.)

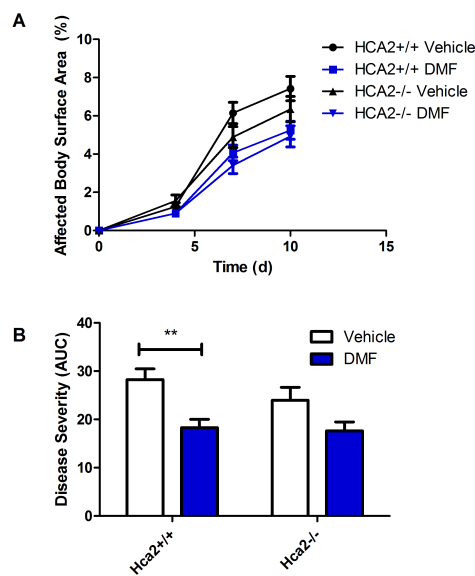


Figure 5.21: DMF effect in EBA is HCA₂-receptor dependent in male mice.

Male mice received a total of 3 i.p. injections of 100 μ g anti-collagen VII-IgG every second day. (A) Clinical manifestation was evaluated every third day starting on day 4 after EBA induction. (Degrees of freedom: 383; F-ratio: 2.323) (B) Disease severity. (Degrees of freedom: 95; F-ratio for treatment: 13.94) Data are shown as mean + SEM, $n = 22-26$ (2-way ANOVA with Bonferroni post-test was performed; $**p < 0.01$)

Sex dependency of DMF treatment

During FACS analysis for differentiating RFP⁺ subpopulations of immune cells, it seemed like female mice had fewer RFP expressing cells in comparison to their male equivalents (Figure 5.23).

Figure 5.22 depicts the cumulative data from the experiments in male mice. 2-way ANOVA with genotype and treatment as variables revealed, that a significant difference could be observed with regard to treatment in the wildtype group only. DMF showed no effect in HCA₂ deficient animals. These findings undergird the data from the experiments carried out before; stating that the DMF effect is receptor-dependent, also in male mice.

In consequence of these findings and already published data on differences in several immunological functions with regard to gender, further analysis of cell populations was carried out. For this purpose, RFP expression in total and for the cell populations of neutrophils (CD45+CD11b+Ly6G⁺), non-classical monocytes (CD45+CD11b+Ly6C^{Lo}), classical monocytes (CD45+CD11b+Ly6C^{Hi}), $\gamma\delta$ T cells (CD45+CD3+ $\gamma\delta$ TCR⁺), $\alpha\beta$ T cells (CD45+CD3+ $\gamma\delta$ TCR⁻) and NK cells (CD45+CD3-NK1.1⁺) was measured in blood of naïve animals.

Table 5.10 shows the antibody panels used for FACS analysis. For a precise evaluation, the reporter mouse line *Hca2^{mRFP} (Gpr109^{mRFP})* was used, in which mRFP is controlled by the *Gpr109* gene promoter. The expression pattern of the receptor can thus be quantified using FACS analysis:

First of all, the experiment showed, that male mice indeed have significantly more HCA₂ expressing cells in the population of viable single cells, compared to female animals (Figure 5.22 A). The quantification of RFP⁺ cells in each subpopulation is shown in Figure 5.22 C.

There was a gender dependency in the analysis of the Ly6C^{Lo} monocyte population with regard to receptor expression in blood, showing significantly higher counts in male mice (Figure 5.22 B). Only 61.4 % of female non-classical monocytes expressed the receptor, whereas 88.6 % of the male comparison group carried the receptor as indicated by the reporter expression (mean value).

For the neutrophil and non-classical monocyte populations, lower relative numbers were found in female animals. In fact, for both populations, female mice only showed about 1/3

of each population to be receptor positive compared to male animals (neutrophils: ♂ 17.1 % ♀ 4.7 %; Ly6C^{Lo} ♂ 17.9 % ♀ 6.9 %).

In NK, αβT and γδT cells, significantly higher expressions were observed in cells originating from the blood of female mice with the most considerable difference in both T cell populations. Here the relative amount of RFP expression was almost doubled (γδT cells: ♂ 0.3 % ♀ 0.6 %; αβT cells: ♂ 12.0 % ♀ 23.8 %).

With regard to classical monocytes (Ly6C^{Hi}) no difference in HCA₂ expression or relative number of cells could be found when comparing male and female gender in blood.

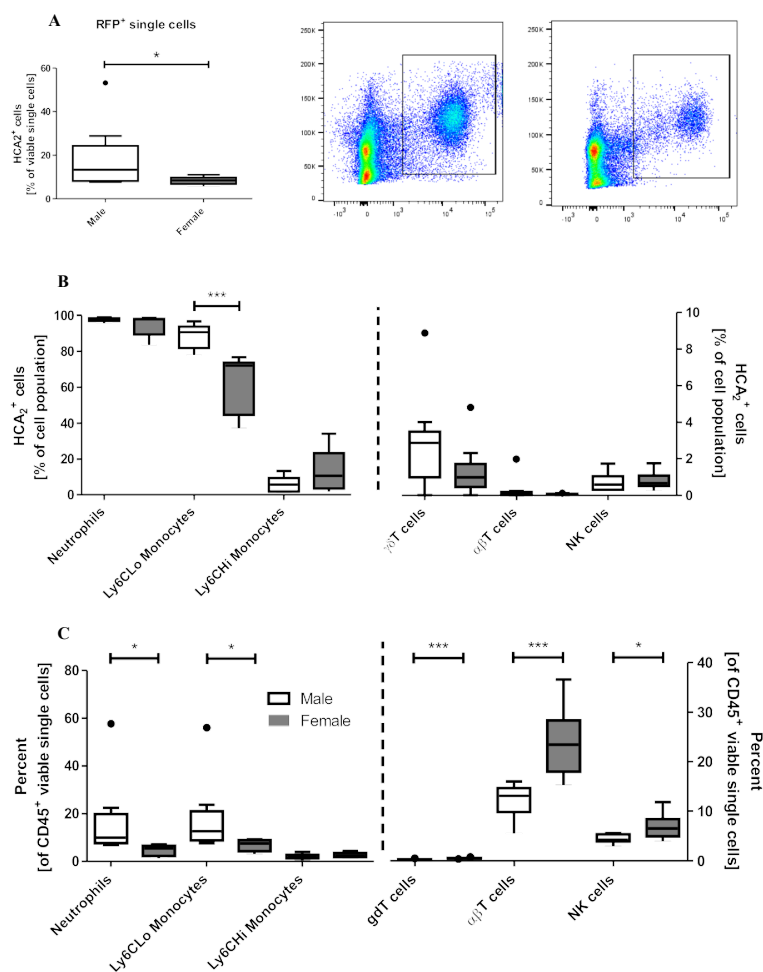


Figure 5.22: Higher HCA₂ expression in male mice.

Quantification of immune cell populations in blood of naive male and female HCA₂^{mRFP} mice. (A) The number of RFP⁺ cells is shown in percent of viable single cells. Representative dot plots are shown. (B) The number of RFP⁺ cells is shown in percent of cell population (C) The number of cells is shown in percent of CD45⁺ viable single cells. N = 9- 10 mice/group. Statistical analyses were performed using Student's t-Test (*p < 0.05; ***p < 0.001).

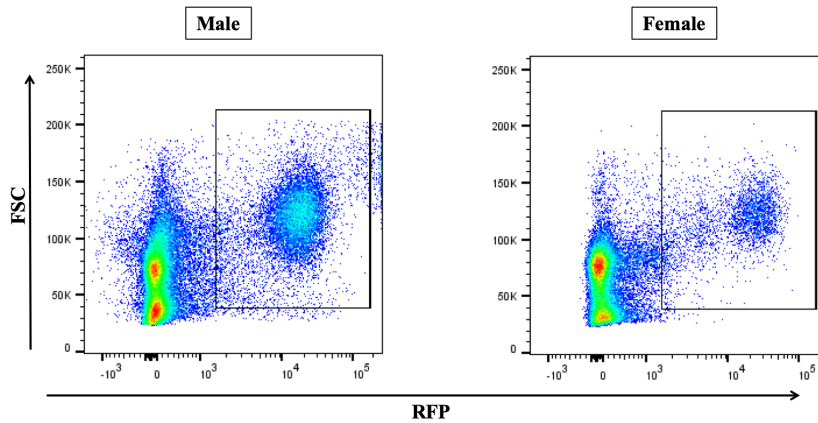


Figure 5.23: Higher RFP expression in male mice.

Quantification of immune cell populations in blood of naive male and female HCA₂^{mRFP} mice. Representative dot plots of FACS analysis of viable single cells are shown.

In conclusion, the immunological profile of mice on a cellular level varied significantly between the two genders. Whereas female animals showed lower counts of HCA₂-positive neutrophils and non-classical monocytes, HCA₂-positive NK, $\alpha\beta$ T and $\gamma\delta$ T cells were more abundant in blood.

5.9 Effects of ketogenic and niacin free diet on EBA

The two diets were chosen as nicotinic acid itself is an HCA₂ receptor agonist and during fasting or administration of a ketogenic diet, endogenous ligands of the receptor (mainly BHB) are produced by the body. Their potential impact on the course of EBA should thus be investigated.

Ketogenic diet

In order to assess the effect of nutritional baseline HCA₂ activation on the course of EBA, mice were either fed with a ketogenic or with a “normal”, control diet. In all animals fed with ketogenic diet, a shift to ketosis could be observed (representative pictures from test stripes depicted in Figure 5.24 E & F). Already on day 1 of disease (11 days of ketogenic diet only) a significant difference in urine levels of ketone bodies between the two feeding groups was observable which further increased during the course of the experiment. The average ketone body urine level of the control diet fed animals on day 11 was 1,67 mg/dl

compared to 134 mg/dl in the ketogenic diet group. In humans, urine levels of ketones exceeding 80 mg/dl mark a ketogenic metabolic state¹²⁶. For mice, no such specifications are available. The ketone body levels measured at different time points with regard to feeding are depicted in Figure 5.24 D.

In the course of the experiment, mice were weighed every third day. Even though food was provided *ad libitum*, a difference in body weight could be observed at 4 measuring points before disease induction. Here, ketogenic diet fed animals were significantly heavier than those in the control group. During EBA, the weight levels converged, and no significant difference became apparent. Furthermore, in both groups weight of the animals dropped after disease induction, a common observation in EBA mouse models. Figure 5.24 C shows the course of body weights.

Furthermore, Figure 5.24 shows the affected body surface area in % and disease severity as AUC. There was no significant difference between the two feeding groups with regard to disease severity at any time point. These findings suggest that a ketogenic diet provided no protective effect in EBA.

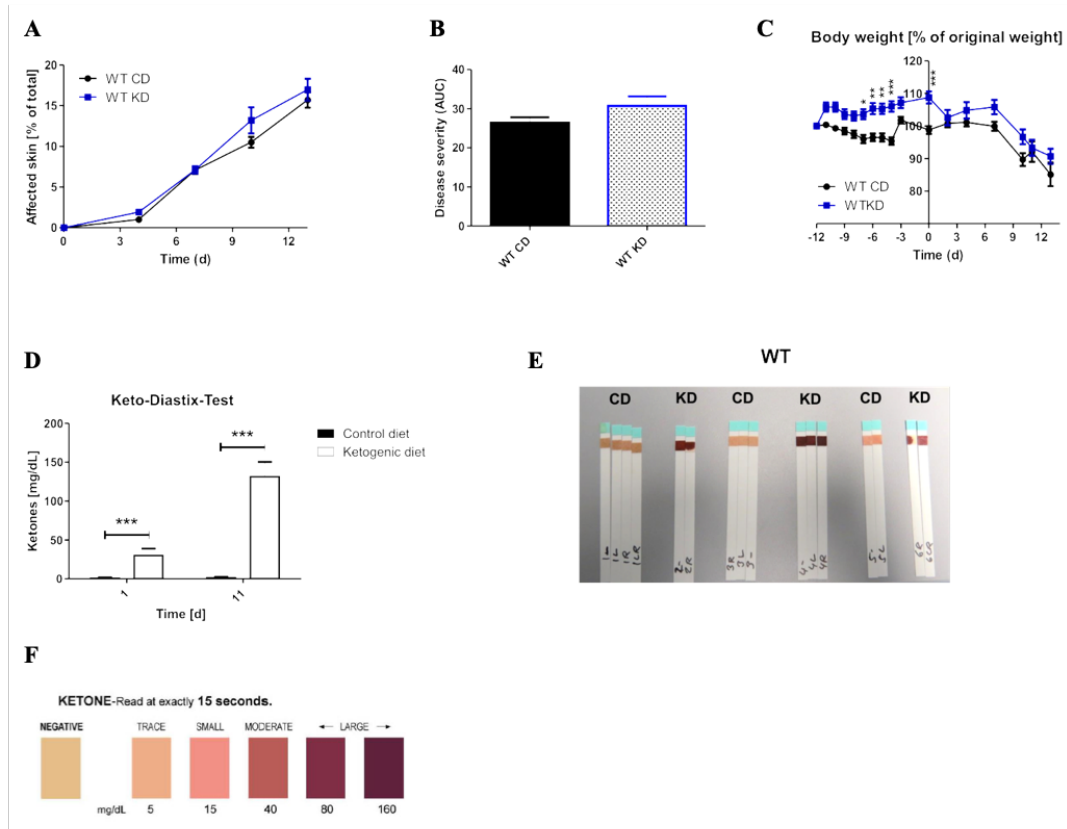


Figure 5.24: Ketogenic diet did not alter disease onset and disease severity in EBA.

Mice received a total of 3 i.p. injections of 100 μ g anti-collagen VII-IgG every second day. (A) Clinical manifestation was evaluated every third day starting on day 4 after EBA induction (degrees of freedom: 99; F-ration: 1.89) (B) Disease severity (degrees of freedom: 9; F-ration: 3.332). (C) Body weight in percent of original weight (-d12; degrees of freedom 339; F-ration: 10.42). (D) Ketosis test in spontaneous mouse urine. Ketone level before (day 1) and during (day 11) EBA experiment in control diet and ketogenic diet fed animals. (Keto-Diastix Test 5000, Roche). (E) Representative Ketosis-Test-Strips of mice (d11, CD = control diet: sniff M-Z, containing 48% carbohydrates, 15% fat and 37% protein; KD = ketogenic diet: sniff EF R/M ketogenic diet with 80% long-chain fatty acids in dry mass and 8% protein). (F) Keto-Diastix Test scale Data are shown as mean + SEM, n = 10 (1-way ANOVA with Bonferroni post-test was performed; *p < 0.05; **p < 0.01 ***p < 0.001).

Nicotinic acid free diet

In the second nutritional experiment carried out, mice were fed with either control diet or a nicotinic acid low diet for either 12 or 28 days. Plasma samples, analysed by the lab of Dr. Bayer after the feeding period, showed a significant difference in serum levels of nicotinic acid amongst the groups at both timepoints as depicted in Figure 5.25 B & D. This effect got more pronounced the longer the different diets were administered.

Furthermore, there seems to be a trend in body weight (Figure 5.25 A & C) towards lower weight in niacin-free diet fed animals, however there is no significant difference at any time point during the experiment.

In conclusion, dietary changes with regard to endogenous HCA₂-activation showed a significant effect on the plasma and urinary level of receptor ligands. However, the alteration in metabolism failed to have an impact on the clinical course of EBA with regard to ketogenic diet. The impact of the nicotinic acid reduction, observed in the serum of mice, on disease severity needs to be further elucidated.

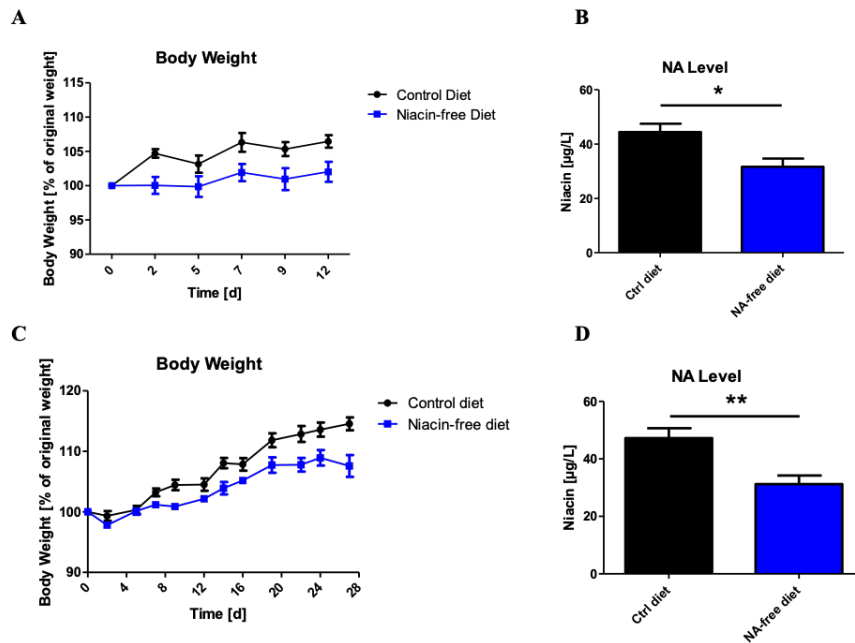


Figure 5.25: Niacin-free diet did alter Nicotinic acid level in plasma.

Mice received a Niacin-free diet (Altromin C 1025 Special Chow, Nicotinic acid low diet containing 0,05 mg/kg nicotinic acid) for (A+B) 12 days or (C+D) 28 days. Plasma samples were collected and NA level was analysed by Labor Dr. Bayer. (A+C) Body weight over time in percent of original weight (B+D) NA level of endpoint plasma sample. Data are shown as mean + SEM, n = 5 mice/ group. Statistics were performed using the Student's T-test; *p < 0.05 **p < 0.01; NA = nicotinic acid.

6.0 Discussion

The experiments described above were carried out to clarify the role of the HCA₂ receptor in autoimmune diseases. For this purpose, epidermolysis bullosa acquisita, a chronic blistering disease, was chosen as a model. In the course of the disease, subepidermal split formation occurs due to antibodies directed against collagen-type-VII which serves as an anchoring structure in the dermo-epidermal junction.

In mice, the autoimmune process is induced via antibody injection (anti-collagen-type-VII-IgG) which is a well-established model to mimic the effector phase of EBA¹²⁷.

Upon i.p. injection, the antibodies travel to the skin. The results described above, demonstrate that collagen-type-VII antibodies are spread evenly. Furthermore, levels of complement factor C3 in skin sections were equally distributed proving an organ wide and even immune response.

These findings are of fundamental importance for the interpretation of experimental results: Not only are IgG and C3 deposition used as diagnostic criteria in skin biopsies of patients⁷, also in studies where the mouse model of EBA was established, successful disease transmission was ascertained via these findings.

Despite the proof of immunohistochemical complement deposition, infiltration of immune cells is another, unspecific, marker for inflammation which can be assessed together with subepidermal split formation in histological samples.

In cryotome sections, epidermal thickening, as a result of inflammation, and split formation could be detected in all samples of mice on day 16. Successful disease induction was thus verified using the defined key findings in EBA⁶.

6.1 HCA₂ carrying cells and their importance in EBA

Even though the precise mechanisms by which receptor activation ameliorates diseases is still subject to current research, a number of different cells have been identified as targets: The expression on adipose tissue is a key to the anti-dyslipidemic effect of nicotinic acid which has been used intensively in the past to reduce the release of free fatty acids from fat cells¹²⁸. The receptor is thus involved in long-term regulation of lipolysis. Furthermore, anti-inflammatory- and tumour suppressing effects have been linked to receptor activation

on intestinal epithelial cells⁷⁴ whilst keratinocytes might convey an unwanted side effect of treatment, the flush reaction¹²⁹.

However, increasing interest has been drawn to the role of immune cells amongst which the receptor is expressed on monocytes and macrophages, neutrophils and Langerhans cells¹²⁹.

Monocytes

After migrating into tissue, monocytes can differentiate into macrophages and dendritic cells. These resident cells then carry out unique effector functions with macrophages being involved in host defence, for example via phagocytosis and cytokine production and dendritic cells participating in antigen presentation¹³⁰. The HCA₂ receptor has been found to play an important role in mediating these effector functions in a variety of diseases: Early research was directed towards atherosclerosis where migration of monocytes is altered upon niacin treatment⁹⁶. In obesity, treatment effects of niacin on macrophage function are also conveyed via the receptor⁷⁰. The importance of HCA₂ mediating effects on neuro-inflammation is still subject to current research, however it has been shown that it is required for the treatment effect of nicotinic acid on macrophages in a model of stroke. Ablation of monocytes led to a loss of the protective effect⁷³.

Concerning dermatological diseases, the treatment effects of the anti-psoriasis drugs containing fumaric acid esters have also been linked to the HCA₂ receptor, they were lost in knockout animals⁹⁹.

The role of monocytes in this association is not clear to date. Iwata et al. (2013) underlined the significance of monocytes for EBA as their presence is required during the induction phase of disease¹⁰. Spatiotemporal analysis of HCA₂ expression in the course of disease (Figure 5.10; 5.16; 5.17) indeed suggests that monocytes play an important role in conveying the treatment effect in this disease, as their abundance increases upon EBA induction.

Altogether, there is significant evidence underlining the importance of attenuated disease parameters through monocytes and macrophages carrying the HCA₂ receptor in a number of diseases. Despite their relevance in the course of each condition, the therapeutic potential mediated through the receptor becomes more apparent. Even though the precise mechanisms behind the signalling cascade remain to be explored, numerous approaches are made:

Monocytes in mice can be divided into two distinct subpopulations with regard to their activation status: activated, classical monocytes (CD45⁺CD11⁺Ly6C^{Hi}) and resting, non-classical monocytes (CD45⁺CD11⁺Ly6C^{Lo}). The effector functions are controlled diversely. It is known that chemokines, oligopeptides (produced by bacteria) and other microbial products (for example LPS) are important for the induction of defence mechanisms¹³⁰ as they promote the production of pro-inflammatory cytokines, such as TNF- α and IL-1. Subsequently, a cascade of intracellular signalling is activated in other immune cells, leading to an inflammatory response. Interestingly, recent data suggest a central role of the HCA₂ receptor in these regulatory pathways of macrophage function: The expression of the receptor on the cell surface is controlled by stimulation of LPS in a dose- and time dependent manner. Furthermore, Zandi-Nejad et al. (2013) found that the amount of TNF- α produced by macrophages upon activation correlates to LPS levels as expected, but also to HCA₂ expression, suggesting a role in early macrophage activation⁹⁶. In a second step, the impact of the receptor agonist nicotinic acid on activation of macrophages and their release of proinflammatory cytokines was investigated. The inhibition of activation observed was receptor-dependant. In addition, chemotaxis is inhibited in an HCA₂-dependant manner as treatment with nicotinic acid showed reduced migration in an *in vitro* experiment⁹⁶, as well as towards atherosclerotic lesions *in vivo*⁸⁶. In the experiments described above, corresponding data were acquired as the number of activated monocytes (Ly6C^{Hi}) was reduced in spleen and lymph node upon treatment with a receptor agonist (Figure 5.17 A & C).

A possible explanation for the underlying mechanism by which receptor activation inhibits macrophage function, is the reduction of nuclear factor kappa-light-chain-enhancer of activated B cells (NF- κ B⁹⁶): NF- κ B is a well described protein complex which controls the expression of inflammatory genes¹³¹, cytokine production and cell survival¹³⁰, thus serving a central position in regulating the immune response. However, how exactly the HCA₂-dependant effect on NF- κ B levels is mediated in macrophages remains unclear.

A different explanation of the reduced infiltration of monocytes is directed towards migration of cells. Reduced monocyte recruitment has been shown to be of potential relevance for the therapeutic effect of nicotinic acid in atherosclerosis¹³². In experimental models of this disease, it has already been established that reductions in chemokine signalling¹³³ or endothelial adhesion via VCAM-1¹³⁴ are centrally important for the effect observed. An explanation to the findings was put forth by Digby et al. (2012) who found the availability of a surface ligand (VLA-4) for VCAM-1 to be reduced upon treatment¹³⁵.

An almost total loss of antigen binding which in turn leads to a downregulation of integrin signalling, was observed as a consequence¹³⁶. As a result, the response to chemokine-induced signalling in monocytes is attenuated significantly and effector cells are less attracted to the site of inflammation. These *in vitro* data certainly need to be validated *in vivo* to prove their actual importance, however being confirmed in multiple setups enhances their plausibility in explaining the treatment effect of HCA₂ receptor agonists via macrophages and monocytes.

$\gamma\delta$ T cells

T cells are a type of leukocyte, playing a major role in controlling and shaping the immune response as they carry out a number of different effector functions, such as mediating cell death or recruitment of other effector cells. Traditionally T cells are characterised by expressing the T cell receptor on their surface delineating them from leukocytes¹⁰⁵ and enabling them to recognise antigen fragments bound to MCH molecules. The T cell receptor itself is made up from two different chains of proteins, either an alpha (α) and a beta (β) chain or a gamma (γ) and a delta (δ) chain. Under homeostasis, by far the largest number of T cells express a receptor composed of α and β chain (95%) and only a small proportion have a γ and δ chain¹³⁷. This ratio is unique to each species and also changes during diseases, such as leukaemia¹³⁸.

Even though, the functions of $\gamma\delta$ T cells still remain largely unknown and they cannot certainly be allocated to the adaptive, nor to the innate immune system¹³⁹, their particular distribution in epithelial and mucosal tissue suggests a role as the first line of defence against pathogens¹⁴⁰. This concept is underlined by their uniqueness in activation: Whilst other T cells ($\alpha\beta$ T cells) are solely activated through MHC presented antigens, most $\gamma\delta$ T cells respond in an MHC-independent manner: The $\gamma\delta$ TCR can directly bind to pyrophosphates or non-phosphorylated compounds¹⁴¹. Whereas these non-phosphorylated compounds are ubiquitously found in plants and bacteria¹⁴², phosphorylated antigens reflect raised metabolic stress and can be found on many tumour cells¹⁴³, for example. Upon activation, $\gamma\delta$ T cells carry out a number of immune response functions which enhance other components of the immune system: First of all, the secretion of chemokines and cytokines attracts $\alpha\beta$ T cells as well as natural killer cells to the site of inflammation¹⁴⁴. Furthermore, $\gamma\delta$ T cells themselves are capable of ingesting, processing and presenting antigens, functioning as professional antigen-presenting cells¹⁴⁵. Recent studies have shown that, despite already described effector functions, the cell lineage is also capable of

phagocytosis, a feature considered to be exclusive to myeloid cell types and not lymphocytes before¹⁴⁶.

Their uniqueness concerning cellular effector functions makes $\gamma\delta$ T cells an important research topic, especially in cancer as they are able to identify tumour cells by sensing cell stress¹⁴³, but also inflammatory autoimmune diseases.

For EAE, it has been shown that $\gamma\delta$ T cells are of high abundance in the CNS at the peak of inflammation and the chronic phase of the disease, accounting for about 10% of T cells at these timepoints¹⁴⁷. Two subpopulations can be distinguished with regard to their cytokine secretion (IL-17 or IFN- γ). Interestingly they seem to have opposing roles in the course of the disease, with the IL-17 secreting subset contributing to disease exacerbation whilst the other population may serve a protective role¹⁴⁸. Still a lot of research is needed, especially to clarify the role of this polarization. However, it seems like $\gamma\delta$ T cells are not required for disease onset or progression but related to the severity of EAE¹⁴⁹.

In dermatological diseases, the involvement of $\gamma\delta$ T cells is especially well investigated in psoriasis. Even though this skin disease largely relies on the function of CD4⁺ and CD8⁺ T cells¹⁵⁰ for the development of lesions, it has been shown that $\gamma\delta$ T cells also play a role as they seem to be necessary to drive plaque formation in mice, too¹⁵¹. In animals deficient of the T cell-receptor δ , inflammation and dermal hyperplasia was significantly reduced compared to wild-type littermates proposing a possible novel target in psoriasis treatment¹⁵².

In untreated BP in humans, the amount of circulating $\gamma\delta$ T cells is reduced and stays altered even when antibody titres decline during clinical remission¹⁵³. These observations suggest a potential role in both, disease development and possible treatment strategies. In contrast to these *in vivo* findings, contradictory *in vitro* data have been published stating that the involvement of this cell type can either dampen or enhance inflammatory processes¹⁵⁴, depending on the type, but also the current stage of the disease.

The involvement of $\gamma\delta$ T cells in autoantibody-induced skin inflammation has been studied intensively by Bieber et al. (2016) who propose a central role in EBA: Despite the activation of myeloid cells, e.g. neutrophils, which leads to reactive oxygen species and enzyme release, a pathway especially involving $\gamma\delta$ T- and natural killer cells is of major importance¹⁵⁵. These findings are very well compatible with the data shown above as higher relative amounts of this cell type during EBA and DMF administration suggest a central role (Figure 5.16 E). Recruitment of cells then leads to an activation of other cell types, especially neutrophils. How these interactions are conveyed is not yet elucidated on

a molecular level. Nevertheless, HCA₂ detection in $\gamma\delta$ T cells and the rise in receptor positive cells in response to EBA and DMF administration (Figure 5.16 E) suggest an effect mediated through the receptor. Similar changes to their effector functions as observed in other cell types, such as monocytes are conceivable but stay hypothetical until further research is conducted.

In conclusion, the role of this unique cell type is not yet fully understood, especially on a molecular level. Activation probably does not absolutely drive inflammation but as a regulatory element, a decisive effect is very likely. These findings may also explain why lesions in EBA and other autoantibody driven diseases occur at specific locations rather than continuously despite a uniform distribution of anti-collagen type VII IgG and C3 deposition (Figure 5.6 and 5.7). Interfering with $\gamma\delta$ T cell function thus provides a promising strategy in autoimmune diseases. However, few data exist on therapeutic approaches especially in humans. One example is Indirubin, a compound extracted from the leaves of the Chinese herb *Indigo naturalis*, which ameliorates skin pathology in mice suffering from psoriasis when administered orally. The authors state an inhibition of $\gamma\delta$ T cell mediated inflammatory responses especially involving the secretion of IL-17 as a central mechanism behind clinical remission¹⁵⁶. These results underline the therapeutic potential behind $\gamma\delta$ T cells in autoimmune diseases.

6.2 Neutrophil effector functions and L-selectin

Neutrophils play an important role in host defence as they carry out multiple effector functions serving as part of the innate immune system and are often the primary cell type recruited. In order to do so, migration to the site of inflammation is crucial.

In the experiments performed and described above, HCA₂ activation upon oral DMF treatment proved to significantly reduce infiltration of neutrophils into the skin (Figure 5.16 D). Neither in blood, spleen or lymph node, similar findings could be observed. These data underline the hypothesis that DMF exerts its anti-inflammatory effects via inhibiting neutrophil effector mechanisms at the site of inflammation, which has been described *in vitro* beforehand⁵². However, despite changes in specific effector mechanisms, a possible explanation for ameliorated skin pathology could be a decrease in the infiltration of immune cells, specifically neutrophils.

Many different parts of the diapedesis cascade have been shown to participate in the anti-inflammatory effect of the HCA₂ receptor in DMF treatment. However, few data exist on the *in vivo* effect of HCA₂ activation in EBA with regard to immune cell diapedesis. As a direct elaboration of neutrophil movement is difficult to obtain *in vivo*, an “indirect” approach was made using blood level measurement of L-selectin. As elucidated above, this transmembrane adhesion molecule is relevant for transendothelial migration of various leukocytes, such as neutrophils. A detailed look at the molecular structure has revealed that there is a cleavage site in the amino acid chains¹⁵⁷. The so called ectodomain can be separated from the cytoplasmic tail (“shedding”) under certain circumstances: Osmotic stress¹⁵⁸, exposure to LDL, various chemotactic factors or sulfonated glycoproteins possess the ability to elicit shedding for which multiple enzymes, such as the TNF- α converting enzyme¹⁵⁹, are responsible.

The consequence to this process is a rapid downregulation in L-selectin dependent effector functions, such as adhesion, cell migration and activation. Interestingly, older neutrophils express lower levels of L-selectin on their surface which is an important signal for macrophage executed cell clearance¹⁶⁰.

L-selectin has already been used as a drug target to interfere with massive infiltration of effector cells, for example in Crohn’s disease. The results from trials using inhibitory drugs have shown mixed results so that, according to a review article, a concluding remark on their significance cannot be drawn yet¹⁶¹.

In FACS-analysis, the hypothetical interference of anti-inflammatory treatment, using DMF, with cell migration could be validated in blood samples when analysing L-selectin levels. In neutrophils and non-classical monocytes, higher levels and thus reduced activation of cells could be detected upon DMF treatment (Figure 5.18 A, B). Classical monocytes were not affected (Figure 5.18 C). These findings are very well compatible with reduced clinical scores in the course of the EBA and summarise the reported anti-inflammatory impacts of DMF giving a molecular explanation for reduced cell infiltration. Even though it remains speculative to find a possible linkage between higher L-selectin levels in DMF treated animals, a potential explanation can be found in the signalling cascade downstream of the HCA₂ receptor. Activation of the receptor, via one of its agonists leads to a rise in intracellular calcium levels and furthermore a G_{ai} subunit mediated inhibition of the adenylate cyclase (Figure 2.3). Amongst others, a downstream effect in cells is an activation in various parts of the MAPK signalling pathway¹⁰². In leukocytes, these kinases play an important role in the regulation of L-selectin cleavage¹⁶²

as they control the dominant “shedase” (ADAM17¹⁶³). Through systemic MAPK activation, ADAM17-dependant cleavage of L-selectin is up-regulated¹⁶³ resulting in a higher proportion of non-activated immune cells. As fewer cells infiltrate the effector organs, such as the skin, the inflammatory response and thus skin pathology are ameliorated. However, as the precise control mechanism is not elucidated yet, these concepts remain theoretical.

6.3 Gender effects in immunology

The ability to defend oneself against foreign, but also self-antigens, is determined by various factors amongst which age, immunological status and sex are considered salient. Against common belief, women cannot generally be considered to have a weaker immune response and thus being more vulnerable to infectious diseases. Recent studies have shown that females in general react with a higher, possibly more robust cell-mediated and humoral response to antigenic contact¹⁶⁴. Especially during the reproductive years, women face lower amounts of viral, bacterial and also parasitic infections¹⁶⁵ thus being less susceptible to suffer from these diseases. A possible explanation for these observations are elevated immunoglobulin levels in the serum of women, indicating a superior antibody-driven immune response¹⁶⁶. The basis to these differences derives from the genetic differences between the two sexes and their influence on various immunological parameters: Gonadal hormones, such as androgens and oestrogens but also the unique distribution of genes on the two sex-determining chromosomes X and Y are primarily attributed to differences in the immune system. Numerous interleukins (such as IL-13, IL-10, IL-4), for example are primarily located on and controlled by expression of the X-chromosome¹⁶⁷. Furthermore, immune cell function, especially in myeloid cells and lymphocytes is shaped by surface receptors for oestrogen, progesterone and androgens¹⁶⁸. Following an infection and the subsequent immunological response, the body and its immune system returns back to resting state, homeostasis. Interestingly, in this step as well, differences with regard to gender can be observed. In males, the levels of different agents in the immune system drop faster and more consistently, leaving a certain risk of antigen persistence, whilst in women homeostasis is approached more gradually. This, however, bears the risk of tissue damage and thus long-lasting immunopathology¹⁶⁹.

Taken together, it is easily conceivable that the higher number of immunological agents circulating in the blood, ready to fight pathogens, and the longer lasting immunological process in women could lead to an exaggerated immune response. Autoimmune diseases, which are characterized by such excessive reactions to endogenous ligands, are indeed more prevalent in women than in men¹⁷⁰.

Intense research has been conducted on the influence of sex on MS: As shown above, women are generally more susceptible to the disease. Recently, the gap has been widened and large regional differences¹⁷¹ can be observed. As the changes occurred over a short period of time it is rather unlikely, that it is based on a genetic influence. Epigenetic factor as well as interactions with the environment differing between the sexes have been proposed as an explanation¹⁷².

From the data presented, one could assume that women generally have a poorer prognosis in MS, as the incidence is higher and the immune response more pronounced.

However, the disease course is more progressive in men and disabilities are acquired more quickly¹⁷³, even at an early stage of the disease, male individuals are affected more severely in comparison to their female counterparts with regard to mild cognitive impairment¹⁷⁴.

How exactly this gap is accomplished remains subject to research, but numerous observational studies have shown that sex hormones play an important role. First of all, the female specific increase in MS risk starts after puberty¹⁷⁵ and during the second half of pregnancy a decisive drop in progression frequency can be observed which is followed by a rise in relapses postpartum¹⁷⁶. Furthermore, men with lower levels of testosterone are more prone to accumulate disabilities¹⁷⁷. The role of hormones has then been tested in EAE with the results of testosterone, progesterone and estradiol (major oestrogen during pregnancy) to induce anti-inflammatory and neuroprotective effects¹⁷².

In contrast to the well-established and intensively studied gender effect in MS, few data exist on diseases of the skin and their relation to sex.

Hormonal effects on psoriasis have especially been studied in pregnant patients. Here, becoming pregnant is linked to a significant reduction in affected body surface area thus proving the beneficial effect described on an anecdotal level beforehand. Furthermore, oestrogen levels inversely correlate to disease activity; however, no effect can be observed for progesterone levels¹⁷⁸.

The only information on EBA, the model disease during our experiments, is derived from a meta-analysis of publications and state an equal gender distribution (54% women and 46% male⁴). Nevertheless, as this is a study population a recruitment bias for matching sexes might very well interfere with the selection of patients and the actual distribution might not be portrayed.

From the data gathered in our experiments it could be shown, that DMF treatment of EBA is HCA₂ receptor-dependant in both sexes. However, when only taking the results from the first experiment into account, male mice did not show a receptor-dependant effect (data not shown). With the studies presented above, a possible explanation could be a weaker manifestation of the disease in male animals, just like described for many other autoimmune diseases. If male animals would generally show a weaker manifestation of the disease, treatment and genotype effects could be less pronounced. However, this reasoning remains speculative as the actual degree of disease severity with regard to gender was not primarily part of our studies and thus the results ascertained need to be interpreted carefully.

Despite receptor dependency, further analysis of HCA₂ receptor carrying cell types with regard to gender was carried out. The results are depicted in Figure 5.22. Again, there are no data for comparison dealing with receptor expression of immune cells on the basis of gender.

In general, women show higher amounts of circulating immune cells in blood: A study comparing different ethnic backgrounds and gender found that blood counts for neutrophils and monocytes are higher in women compared to men in the Caucasian population and neutrophils are more present also in the Afro Caribbean study participants¹⁷⁹. Furthermore, monocytes are significantly more activated in women than in men as a different study found when dealing with blood counts in healthy participants and patients with SLE¹⁸⁰. For mice, very few data exist. However, Charles River, a large mice breeder offers a table with reference values¹⁸¹ and a study group also published results from blood count of mice used during their experiments¹⁸². In both analysis, male mice have higher levels of neutrophils and monocytes in their blood. These results correspond to the observations made in our own experiments, here male mice also had significantly more monocytes and neutrophils in their blood. The reason for the profound difference between human blood levels of

immune cells and the ones derived from mice remains unclear and so does the significance of the values with regard to interpreting the results in the context of gender differences. Regarding other populations of immune cells, no reference values could be found in the literature (Search date: 14th July 2019) so that unfortunately, a comparison and verification is not possible. From a methodological perspective however, the elevated counts of T cells, especially of $\gamma\delta$ T cells stand to reason as this cell type is typically associated with autoimmune diseases. Furthermore, they are HCA₂ receptor carrying and responsive to EBA, being recruited in high numbers to the site of inflammation. With this information in mind, the reduced treatment effect observed and described above could be explained: If male animals have lower counts of $\gamma\delta$ T cells which are also important for disease manifestation and treatment effect, the changes achieved by the treatment could be reduced in comparison to their female counterparts. However, as we did not primarily investigate the difference in cellular counts especially in the skin of EBA diseased mice and healthy controls with regard to gender, a conclusive evaluation cannot be drawn.

Altogether, the profound differences found in the blood counts of naïve mice are contrary to the findings in humans but consistent with literature. Currently, little is known about gender effects in mice, in particular with regard to disease models. Recently, an American study group established sex differences in their model of SLE which is a disease with strong gender-impacts in humans¹⁸³. In general, such approaches are very valuable as disease models mimicking human pathology as close as possible allow a more precise transfer of research results.

6.4 Effect of diets in EBA and DMF treatment

Dietary restrictions are not only used by many people to maintain a, according to their believe, healthy lifestyle, but also play an important role in treating innumerable medical conditions. Despite the difficulty of classifying a condition as a disease, which could benefit from a dietary treatment, it is particularly challenging to find appropriate information and well carried-out trials. There are many diseases where a direct link has been established between a food ingredient and illness, the most common ones being coeliac disease and lactose intolerance. On the other hand, depletion of certain ingredients

necessary to our body can obviously also culminate in diseases, such as Vitamin C deprivation leading to scurvy.

A prominent interaction, which has been used therapeutically since the early 1920s¹⁸⁴, is the benefit of ketogenic diets in neurological disorders, most importantly epilepsy. Fasting has proved to be effective historically, however, since it is limited to a certain time, alternative strategies were needed. Wilder et al. (1921)¹⁸⁵ found out that ketogenic diets, rich in fats and low in carbohydrates, reduce the amount epileptic seizures while still providing sufficient amounts of calories. This special formula mimics the metabolic situation during fasting, as the amount of carbohydrates available to cells is reduced dramatically. In order to carry out vital functions, fatty acids are burned, acetyl-CoA is generated in high amount and subsequently converted to ketone bodies, such as BHB, acetoacetate and acetone by the liver and released into the blood stream.

Ketone bodies, in contrast to fatty acids, can be used as an energy source by the brain due to their ability to cross the blood-brain barrier and compensate for reduced amounts of glucose which ordinarily is the sole source of fuel. Ketone bodies are degraded by specific enzymes (such as D- β -hydroxybutyrate dehydrogenases for BHB) to acetyl-CoA which can then enter the Krebs cycle to produce ATP in mitochondria of brain cells¹³⁰.

A variety of effector mechanisms of a ketogenic diet has been discussed recently:

In epilepsy, the anticonvulsant efficacy of the diet might be conveyed by increased γ -aminobutyric acid levels, an inhibitory neurotransmitter which prevents brain damage via limiting seizure-induced neuronal hyperexcitability¹⁸⁶. Furthermore, several antioxidant effector mechanisms were found, for examples changes in reactive oxygen species¹⁸⁷ and glutathione levels¹⁸⁸. Altogether, the mechanisms described comprise different ways in which inflammatory stress to the brain is reduced, making the ketogenic metabolism a potent modifier in neuroinflammation. Furthermore, due to the diverse effector mechanisms, the use of the diet and its potential effects have been studied extensively with preclinical trials running in a variety of neurological diseases, such as MS¹⁸⁹ and Parkinson's disease¹⁹⁰.

Only recently, it has been found out that the major ketone body retrieved from lipolysis during the diet, BHB, not only serves as an energy source for cells but also as a signalling molecule with a target being the HCA₂-receptor. From pharmacological approaches, it is known that the receptor possesses a rather low half maximal inhibitory concentration for BHB making it likely that effects reported with rising concentrations are due to activation

of this receptor¹⁹¹. Additionally, in a recent trial⁷³, associations between the HCA₂ receptor and supporting effects on neuroinflammation were ascertained: In a mouse model of ischemic stroke, infusion of BHB as well as a ketogenic diet significantly reduced the stroke-size in wild-type mice. However, no difference could be found when using a knockout strain (identical to the one used in the experiments described above), deficient in the HCA₂ receptor. These data reinforce the idea of neuroprotective effects on the basis of specific receptor activation, rather than due to BHB as an energy source solely.

In previous research, the effect of a ketogenic diet was examined in EAE, a mouse model for MS. The data collected in these experiments were in line with previously published ones from other EAE experiments, as far as the diet indeed reduced the overall score in mice and delayed disease onset¹⁹². However, the effect was not limited to the HCA₂ receptor wild-type group of animals, but also subsisted in the knockout cohort. In order to further characterize the role of the receptor, ketogenic diet experiments were thus carried out in a mouse model of EBA. In this bullous skin disease, as our data corroborate, the HCA₂ receptor also plays an important role.

In inflammatory dermatological diseases in general, much fewer data exist on the impact of a ketogenic diet. Just recently, a review article was published dealing with the potential role of the diet in treatment¹⁹³ which stated that no data were available on its efficacy. The potential effector mechanisms discussed above are certainly applicable for skin diseases as well and a number of them have already been linked: For example, amounts of ROS exceeding the antioxidant capacity of the cell are involved in the pathogenesis of psoriasis¹⁹⁴, varicose ulcers¹⁹⁵ and cutaneous malignancy¹⁹⁶. Despite these “general” effector mechanisms, receptor mediated ones could even play a more important role especially if the receptor could be addressed directly. In the experiments conducted, no difference could be found between animals treated with a ketogenic diet in comparison to those with regular chow (see Figure 5.24). These data could suggest the HCA₂ receptor activation triggered might not be sufficient to reduce the skin surface affected.

Furthermore, a possible explanation could be effects triggered by other ingredients of the feed which then influence the course of disease. Additionally, during the induction phase of ketosis, mice fed with KD showed a slower rise in body weight at the beginning of the experiment (see Figure 5.24 C) suggesting a certain caloric restriction. Malnutrition and undernourishment is not only a widespread problem in patients with EBA¹⁹⁷ but also affects the disease activity itself. Other than in patients suffering from MS, nutritional

compromise aggravates disease severity in Epidermolysis bullosa¹⁹⁸, which altogether might have limited the therapeutic effect of the feeding experiment.

A rather different explanation for absent effects of the diet deals with endogenic receptor activation: During ketosis, the HCA₂ receptor is believed to be mainly activated via BHB as this is the main product retrieved from lipolysis. Aside from this metabolite there are numerous other ligands capable of triggering the cascade such as butyric acid, MMF and nicotinic acid. Niacin is a form of vitamin B₃, which is essential to humans as it is needed as a precursor for the biosynthesis of nicotinamide adenine dinucleotide and nicotinamide adenine dinucleotide phosphate. Both are coenzymes for dehydrogenases in a variety of metabolic processes for the transfer of hydrogen¹³⁰. In order to prevent deficiencies, mice used for laboratory experiments are typically fed with a diet comprising a whole variety of vitamins and trace elements amongst which niacin is also included. The chow usually fed to the animals contains 36 mg/kg nicotinic acid and when analysing the plasma levels, the ones of nicotinic acid are within the “normal” range for humans, however, nicotinamide and total niacin were considerably elevated (see Figure 5.25).

When feeding the animals with a special, niacin “free” chow containing 0,05 mg/kg nicotinic acid, a significant reduction in plasma levels of the vitamin’s metabolites could be observed (Figure 5.25). The question underlying the experiment was to find out if plasma levels of niacin and its metabolite are directly dependant on the nutritional uptake. It could be shown during the feeding period, that a time of 12 days is already adequate to show a change in plasma levels. High amounts of receptor agonists present in the blood could lead to an increased baseline activation of HCA₂ carrying cells which, on the one hand would have a beneficial effect on the mice as it ameliorates disease severity. On the other hand, however, the response expected for those animals that received oral treatment would be attenuated. The basis to this hypothesis is the internalisation of the receptor after binding to nicotinic acid which has already been documented¹⁰¹. Furthermore, receptor carrying cells are desensitized after the first ligand-stimulation and can thus not be activated by other stimuli^{72,75}. Even though, plasma levels of niacin are not a reliable indicator of the niacin status in general¹⁹⁹, the changes detected upon different oral amounts of niacin in food could be a good explanation for the lower response in a series of EAE experiments conducted earlier. There are no reliable sources specifying the amount of niacin the food of mice should be containing, nor is there a protocol established to detect the current status of niacin and its metabolites in an animal. For further experiments, especially when comparing the results between different laboratories or trying to replicate

results acquired earlier, the niacin content of chow should be taken into account. A systematic analysis of animals fed with “normal” versus niacin-reduced chow with regard to their response rate to DMF in EAE or EBA could be a first step to prove the clinical significance of altered plasma concentrations.

7.0 References

1. Bertram, F., Bröcker, E.-B., Zillikens, D. & Schmidt, E. Prospective analysis of the incidence of autoimmune bullous disorders in Lower Franconia, Germany. *J. Dtsch. Dermatol. Ges. J. Ger. Soc. Dermatol. JDDG* **7**, 434–440 (2009).
2. Roenigk, H. H., Ryan, J. G. & Bergfeld, W. F. Epidermolysis bullosa acquisita. Report of three cases and review of all published cases. *Arch. Dermatol.* **103**, 1–10 (1971).
3. Woodley, D. T. *et al.* Epidermolysis bullosa acquisita antigen is the globular carboxyl terminus of type VII procollagen. *J. Clin. Invest.* **81**, 683–687 (1988).
4. Iwata, H. *et al.* Meta-analysis of the clinical and immunopathological characteristics and treatment outcomes in epidermolysis bullosa acquisita patients. *Orphanet J. Rare Dis.* **13**, (2018).
5. Buijsrogge, J. J. A., Diercks, G. F. H., Pas, H. H. & Jonkman, M. F. The many faces of epidermolysis bullosa acquisita after serration pattern analysis by direct immunofluorescence microscopy. *Br. J. Dermatol.* **165**, 92–98 (2011).
6. Ludwig, R. J. Clinical Presentation, Pathogenesis, Diagnosis, and Treatment of Epidermolysis Bullosa Acquisita. *ISRN Dermatol.* **2013**, (2013).
7. Vorobyev, A., Ludwig, R. J. & Schmidt, E. Clinical features and diagnosis of epidermolysis bullosa acquisita. *Expert Rev. Clin. Immunol.* **13**, 157–169 (2017).
8. Komorowski, L. *et al.* Sensitive and specific assays for routine serological diagnosis of epidermolysis bullosa acquisita. *J. Am. Acad. Dermatol.* **68**, e89-95 (2013).
9. Gammon, W. R. *et al.* Increased frequency of HLA-DR2 in patients with autoantibodies to epidermolysis bullosa acquisita antigen: evidence that the expression of autoimmunity to type VII collagen is HLA class II allele associated. *J. Invest. Dermatol.* **91**, 228–232 (1988).
10. Iwata, H. *et al.* B Cells, Dendritic Cells, and Macrophages Are Required To Induce an Autoreactive CD4 Helper T Cell Response in Experimental Epidermolysis Bullosa Acquisita. *J. Immunol.* **191**, 2978–2988 (2013).
11. Samavedam, U. K. S. R. L. *et al.* GM-CSF modulates autoantibody production and skin blistering in experimental epidermolysis bullosa acquisita. *J. Immunol. Baltim. Md 1950* **192**, 559–571 (2014).
12. Kasperkiewicz, M. *et al.* Clearance rates of circulating and tissue-bound autoantibodies to type VII collagen in experimental epidermolysis bullosa acquisita. *Br. J. Dermatol.* **162**, 1064–1070 (2010).
13. Challa, D. K., Velmurugan, R., Ober, R. J. & Sally Ward, E. FcRn: from molecular interactions to regulation of IgG pharmacokinetics and functions. *Curr. Top. Microbiol. Immunol.* **382**, 249–272 (2014).
14. Schmidt, E., Bröcker, E.-B. & Goebeler, M. Rituximab in treatment-resistant autoimmune blistering skin disorders. *Clin. Rev. Allergy Immunol.* **34**, 56–64 (2008).
15. Recke, A. *et al.* Pathogenicity of IgG subclass autoantibodies to type VII collagen: induction of dermal-epidermal separation. *J. Autoimmun.* **34**, 435–444 (2010).
16. Kovács, M. *et al.* The Src family kinases Hck, Fgr, and Lyn are critical for the generation of the in vivo inflammatory environment without a direct role in leukocyte recruitment. *J. Exp. Med.* **211**, 1993–2011 (2014).
17. Chiriac, M. T. *et al.* NADPH oxidase is required for neutrophil-dependent autoantibody-induced tissue damage. *J. Pathol.* **212**, 56–65 (2007).
18. Shimanovich, I. *et al.* Granulocyte-derived elastase and gelatinase B are required for dermal-epidermal separation induced by autoantibodies from patients with epidermolysis bullosa acquisita and bullous pemphigoid. *J. Pathol.* **204**, 519–527 (2004).
19. Hellberg, L. *et al.* Methylprednisolone blocks autoantibody-induced tissue damage in experimental models of bullous pemphigoid and epidermolysis bullosa acquisita through inhibition of neutrophil activation. *J. Invest. Dermatol.* **133**, 2390–2399 (2013).
20. Megahed, M. & Scharffetter-Kochanek, K. Epidermolysis bullosa acquisita--successful treatment with colchicine. *Arch. Dermatol. Res.* **286**, 35–46 (1994).
21. Khatri, M. L., Benghazeil, M. & Shafi, M. Epidermolysis bullosa acquisita responsive to cyclosporin therapy. *J. Eur. Acad. Dermatol. Venereol. JEADV* **15**, 182–184 (2001).
22. Ahmed, A. R. & Gürcan, H. M. Treatment of epidermolysis bullosa acquisita with intravenous immunoglobulin in patients non-responsive to conventional therapy: clinical outcome and post-treatment long-term follow-up. *J. Eur. Acad. Dermatol. Venereol. JEADV* **26**, 1074–1083 (2012).
23. McKinley, S. K., Huang, J. T., Tan, J., Kroshinsky, D. & Gellis, S. A case of recalcitrant epidermolysis bullosa acquisita responsive to rituximab therapy. *Pediatr. Dermatol.* **31**, 241–244 (2014).
24. Wegele, H., Müller, L. & Buchner, J. Hsp70 and Hsp90--a relay team for protein folding. *Rev. Physiol. Biochem. Pharmacol.* **151**, 1–44 (2004).
25. Kasperkiewicz, M. *et al.* Heat-shock protein 90 inhibition in autoimmunity to type VII collagen: evidence that nonmalignant plasma cells are not therapeutic targets. *Blood* **117**, 6135–6142 (2011).
26. Mihai, S. *et al.* The alternative pathway of complement activation is critical for blister induction in experimental epidermolysis bullosa acquisita. *J. Immunol. Baltim. Md 1950* **178**, 6514–6521 (2007).
27. Schweckendiek, W. [Treatment of psoriasis vulgaris]. *Med. Monatsschr.* **13**, 103–104 (1959).
28. Milo, R. & Kahana, E. Multiple sclerosis: geoepidemiology, genetics and the environment. *Autoimmun. Rev.* **9**, A387-394 (2010).
29. Browne, P. *et al.* Atlas of Multiple Sclerosis 2013: A growing global problem with widespread inequity. *Neurology* **83**, 1022–1024 (2014).
30. Compston, A. & Coles, A. Multiple sclerosis. *Lancet Lond. Engl.* **372**, 1502–1517 (2008).
31. Werdenberg, D., Joshi, R., Wolfram, S., Merkle, H. P. & Langguth, P. Presystemic metabolism and intestinal

- absorption of antipsoriatic fumaric acid esters. *Biopharm. Drug Dispos.* **24**, 259–273 (2003).
32. Rostami-Yazdi, M., Clement, B., Schmidt, T. J., Schinor, D. & Mrowietz, U. Detection of Metabolites of Fumaric Acid Esters in Human Urine: Implications for Their Mode of Action. *J. Invest. Dermatol.* **129**, 231–234 (2009).
 33. Dibbert, S., Clement, B., Skak-Nielsen, T., Mrowietz, U. & Rostami-Yazdi, M. Detection of fumarate–glutathione adducts in the portal vein blood of rats: evidence for rapid dimethylfumarate metabolism. *Arch. Dermatol. Res.* **305**, 447–451 (2013).
 34. Rostami-Yazdi, M., Clement, B. & Mrowietz, U. Pharmacokinetics of anti-psoriatic fumaric acid esters in psoriasis patients. *Arch. Dermatol. Res.* **302**, 531–538 (2010).
 35. Fachinfoservice. Tecfidera® 120 mg/240 mg, Biogen GmbH, Fachinfoservice Produktinformationen fachinfo.de. <https://www.fachinfo.de/api/fachinfo/pdf/020023>.
 36. Hanson, J., Gille, A. & Offermanns, S. Role of HCA(2) (GPR109A) in nicotinic acid and fumaric acid ester-induced effects on the skin. *Pharmacol. Ther.* **136**, 1–7 (2012).
 37. Drug Commission of the German Medical Association. Rote-Hand-Brief Tecfidera 2013. <https://www.akdae.de/Arzneimittelsicherheit/RHB/Archiv/2014/20141204.pdf>.
 38. Gilmore, T. D. Introduction to NF-kappaB: players, pathways, perspectives. *Oncogene* **25**, 6680–6684 (2006).
 39. Loewe, R. *et al.* Dimethylfumarate Inhibits TNF-Induced Nuclear Entry of NF-kB/p65 in Human Endothelial Cells. *J. Immunol.* **168**, 4781–4787 (2002).
 40. Stoof, T. J. *et al.* The antipsoriatic drug dimethylfumarate strongly suppresses chemokine production in human keratinocytes and peripheral blood mononuclear cells. *Br. J. Dermatol.* **144**, 1114–1120 (2001).
 41. Gerdes, S., Shakery, K. & Mrowietz, U. Dimethylfumarate inhibits nuclear binding of nuclear factor kappaB but not of nuclear factor of activated T cells and CCAAT/enhancer binding protein beta in activated human T cells. *Br. J. Dermatol.* **156**, 838–842 (2007).
 42. Gillard, G. O. *et al.* DMF, but not other fumarates, inhibits NF-kB activity in vitro in an Nrf2-independent manner. *J. Neuroimmunol.* **283**, 74–85 (2015).
 43. Takegawa, S. *et al.* Expression of CCL17 and CCL22 by latent membrane protein 1-positive tumor cells in age-related Epstein-Barr virus-associated B-cell lymphoproliferative disorder. *Cancer Sci.* **99**, 296–302 (2008).
 44. Venugopal, R. & Jaiswal, A. K. Nrf1 and Nrf2 positively and c-Fos and Fra1 negatively regulate the human antioxidant response element-mediated expression of NAD(P)H:quinone oxidoreductase1 gene. *Proc. Natl. Acad. Sci. U. S. A.* **93**, 14960–14965 (1996).
 45. Hayes, J. D. *et al.* The Nrf2 transcription factor contributes both to the basal expression of glutathione S-transferases in mouse liver and to their induction by the chemopreventive synthetic antioxidants, butylated hydroxyanisole and ethoxyquin. *Biochem. Soc. Trans.* **28**, 33–41 (2000).
 46. Yamamoto, T. *et al.* Physiological Significance of Reactive Cysteine Residues of Keap1 in Determining Nrf2 Activity. *Mol. Cell. Biol.* **28**, 2758–2770 (2008).
 47. Linker, R. A. *et al.* Fumaric acid esters exert neuroprotective effects in neuroinflammation via activation of the Nrf2 antioxidant pathway. *Brain* **134**, 678–92 (2011).
 48. Kees, F. Dimethyl fumarate : a Janus-faced substance? *Expert Opin. Pharmacother.* **14**, 1559–1567 (2013).
 49. Ghoreschi, K. *et al.* Fumarates improve psoriasis and multiple sclerosis by inducing type II dendritic cells. *J. Exp. Med.* **208**, 2291–303 (2011).
 50. McGuire, V. A. *et al.* Dimethyl fumarate blocks pro-inflammatory cytokine production via inhibition of TLR induced M1 and K63 ubiquitin chain formation. *Sci. Rep.* **6**, 31159 (2016).
 51. Eminel, S. *et al.* Dimethyl- and monomethylfumarate regulate indoleamine 2,3-dioxygenase (IDO) activity in human immune cells. *Exp. Dermatol.* **26**, 685–690 (2017).
 52. Müller, S. *et al.* Dimethylfumarate Impairs Neutrophil Functions. *J. Invest. Dermatol.* **136**, 117–126 (2016).
 53. Chen, H. *et al.* Hydroxycarboxylic acid receptor 2 mediates dimethyl fumarate’s protective effect in EAE. *J. Clin. Invest.* **124**, 2188–2192 (2014).
 54. Helwa, I. *et al.* The antipsoriatic agent monomethylfumarate has antiproliferative, prodifferentiative, and anti-inflammatory effects on keratinocytes. *J. Pharmacol. Exp. Ther.* **352**, 90–97 (2015).
 55. Gold, R., Linker, R. A. & Stangel, M. Fumaric acid and its esters: an emerging treatment for multiple sclerosis with antioxidative mechanism of action. *Clin Immunol* **142**, 44–8 (2012).
 56. Spencer, C. M., Crabtree-Hartman, E. C., Lehmann-Horn, K., Cree, B. A. C. & Zamvil, S. S. Reduction of CD8(+) T lymphocytes in multiple sclerosis patients treated with dimethyl fumarate. *Neurol. Neuroimmunol. Neuroinflammation* **2**, e76 (2015).
 57. Fleischer, V. *et al.* Treatment response to dimethyl fumarate is characterized by disproportionate CD8+ T cell reduction in MS. *Mult. Scler. Houndmills Basingstoke Engl.* **24**, 632–641 (2018).
 58. Diaz, G. M., Fraussen, J., Wijmeersch, B. V., Hupperts, R. & Somers, V. Dimethyl fumarate induces a persistent change in the composition of the innate and adaptive immune system in multiple sclerosis patients. *Sci. Rep.* **8**, 1–13 (2018).
 59. Li, R. *et al.* Dimethyl Fumarate Treatment Mediates an Anti-Inflammatory Shift in B Cell Subsets of Patients with Multiple Sclerosis. *J. Immunol. Baltim. Md 1950* **198**, 691–698 (2017).
 60. Diebold, M. *et al.* Dimethyl fumarate influences innate and adaptive immunity in multiple sclerosis. *J. Autoimmun.* **86**, 39–50 (2018).
 61. Ghadiri, M. *et al.* Dimethyl fumarate-induced lymphopenia in MS due to differential T-cell subset apoptosis. *Neurol. Neuroimmunol. Neuroinflammation* **4**, e340 (2017).
 62. Vandermeeren, M., Janssens, S., Borgers, M. & Geysen, J. Dimethylfumarate is an inhibitor of cytokine-induced E-selectin, VCAM-1, and ICAM-1 expression in human endothelial cells. *Biochem. Biophys. Res. Commun.* **234**, 19–23 (1997).

63. Arbiser, J. L. Fumarate esters as angiogenesis inhibitors: key to action in psoriasis? *J. Invest. Dermatol.* **131**, 1189–1191 (2011).
64. García-Caballero, M., Mari-Beffa, M., Medina, M. Á. & Quesada, A. R. Dimethylfumarate inhibits angiogenesis in vitro and in vivo: a possible role for its antipsoriatic effect? *J. Invest. Dermatol.* **131**, 1347–1355 (2011).
65. Meissner, M., Valesky, E. M., Kippenberger, S. & Kaufmann, R. Dimethyl fumarate – only an anti-psoriatic medication? *JDDG J. Dtsch. Dermatol. Ges.* **10**, 793–801 (2012).
66. Kiehl, R. & Ionescu, G. A defective purine nucleotide synthesis pathway in psoriatic patients. *Acta Derm. Venereol.* **72**, 253–255 (1992).
67. Nast, A. *et al.* S3-Leitlinie zur Therapie der Psoriasis vulgaris Update 10/2017. *JDDG J. Dtsch. Dermatol. Ges.* **9**, S1–S104 (2017).
68. Gold, R. *et al.* Long-term effects of delayed-release dimethyl fumarate in multiple sclerosis: Interim analysis of ENDORSE, a randomized extension study. *Mult. Scler. Houndmills Basingstoke Engl.* **23**, 253–265 (2017).
69. Montalban, X. *et al.*ECTRIMS/EAN guideline on the pharmacological treatment of people with multiple sclerosis. *Eur. J. Neurol.* **25**, 215–237 (2018).
70. Graff, E. C., Norris, O. C., Sandey, M., Kempainen, R. J. & Judd, R. L. Characterization of the hydroxycarboxylic acid receptor 2 in cats. *Domest. Anim. Endocrinol.* **53**, 88–94 (2015).
71. Titgemeyer, E. C., Mamedova, L. K., Spivey, K. S., Farney, J. K. & Bradford, B. J. An unusual distribution of the niacin receptor in cattle. *J Dairy Sci* **94**, 4962–7 (2011).
72. Kostylina, G., Simon, D., Fey, M. F., Yousefi, S. & Simon, H. U. Neutrophil apoptosis mediated by nicotinic acid receptors (GPR109A). *Cell Death Differ.* **15**, 134–142 (2008).
73. Rahman, M. *et al.* The β -hydroxybutyrate receptor HCA2 activates a neuroprotective subset of macrophages. *Nat. Commun.* **5**, 3944 (2014).
74. Singh, N. *et al.* Activation of Gpr109a, receptor for niacin and the commensal metabolite butyrate, suppresses colonic inflammation and carcinogenesis. *Immunity* **40**, 128–39 (2014).
75. Hanson, J. *et al.* Nicotinic acid- and monomethyl fumarate-induced flushing involves GPR109A expressed by keratinocytes and COX-2-dependent prostanoid formation in mice. *J Clin Invest* **120**, 2910–9 (2010).
76. Taggart, A. K. *et al.* (D)-beta-Hydroxybutyrate inhibits adipocyte lipolysis via the nicotinic acid receptor PUMA-G. *J Biol Chem* **280**, 26649–52 (2005).
77. Thangaraju, M. *et al.* GPR109A Is a G-protein–Coupled Receptor for the Bacterial Fermentation Product Butyrate and Functions as a Tumor Suppressor in Colon. *Cancer Res.* **69**, 2826–2832 (2009).
78. Li, Z. *et al.* Nicotinic Acid Receptor GPR109A Exerts Anti-Inflammatory Effects Through Inhibiting the Akt/mTOR Signaling Pathway in MIN6 Pancreatic β cells. *Ann. Clin. Lab. Sci.* **47**, 729–737 (2017).
79. Perry, R. J. *et al.* Acetate mediates a microbiome-brain- β -cell axis to promote metabolic syndrome. *Nature* **534**, 213–217 (2016).
80. Kim, C. H. Immune regulation by microbiome metabolites. *Immunology* **154**, 220–229 (2018).
81. Semple, G. *et al.* 3-(1H-tetrazol-5-yl)-1,4,5,6-tetrahydro-cyclopentapyrazole (MK-0354): a partial agonist of the nicotinic acid receptor, G-protein coupled receptor 109a, with antilipolytic but no vasodilatory activity in mice. *J. Med. Chem.* **51**, 5101–5108 (2008).
82. HCA2 receptor| Hydroxycarboxylic acid receptors | IUPHAR/BPS Guide to PHARMACOLOGY. <https://www.guidetopharmacology.org/GRAC/ObjectDisplayForward?objectId=312>.
83. Yang, R., He, J. & Wang, Y. Activation of the niacin receptor HCA2 reduces demyelination and neurofilament loss, and promotes functional recovery after spinal cord injury in mice. *Eur. J. Pharmacol.* **791**, 124–136 (2016).
84. Parodi, B. *et al.* Fumarates modulate microglia activation through a novel HCAR2 signaling pathway and rescue synaptic dysregulation in inflamed CNS. *Acta Neuropathol* (2015) doi:10.1007/s00401-015-1422-3.
85. Benyo, Z., Gille, A., Bennett, C. L., Clausen, B. E. & Offermanns, S. Nicotinic Acid-Induced Flushing Is Mediated by Activation of Epidermal Langerhans Cells. *Mol Pharmacol* **70**, 1844–1849 (2006).
86. Lukasova, M., Malaval, C., Gille, A., Kero, J. & Offermanns, S. Nicotinic acid inhibits progression of atherosclerosis in mice through its receptor GPR109A expressed by immune cells. *J. Clin. Invest.* **121**, 1163–1173 (2011).
87. Bermudez, Y. *et al.* Nicotinic acid receptor abnormalities in human skin cancer: implications for a role in epidermal differentiation. *PLoS One* **6**, e20487 (2011).
88. Ristic, B., Bhutia, Y. D. & Ganapathy, V. Cell-surface G-protein-coupled receptors for tumor-associated metabolites: A direct link to mitochondrial dysfunction in cancer. *Biochim. Biophys. Acta Rev. Cancer* **1868**, 246–257 (2017).
89. Pan, X. *et al.* Butyrate ameliorates caerulein-induced acute pancreatitis and associated intestinal injury by tissue specific mechanisms. *Br. J. Pharmacol.* (2019) doi:10.1111/bph.14806.
90. Felizardo, R. J. F. *et al.* Gut microbial metabolite butyrate protects against proteinuric kidney disease through epigenetic- and GPR109a-mediated mechanisms. *FASEB J. Off. Publ. Fed. Am. Soc. Exp. Biol.* fj201901080R (2019) doi:10.1096/fj.201901080R.
91. Jadeja, R. N. *et al.* Loss of GPR109A/HCAR2 induces aging-associated hepatic steatosis. *Aging* **11**, 386–400 (2019).
92. Parada Venegas, D. *et al.* Short Chain Fatty Acids (SCFAs)-Mediated Gut Epithelial and Immune Regulation and Its Relevance for Inflammatory Bowel Diseases. *Front. Immunol.* **10**, 277 (2019).
93. Offermanns, S. *et al.* International Union of Basic and Clinical Pharmacology. LXXXII: Nomenclature and Classification of Hydroxy-carboxylic Acid Receptors (GPR81, GPR109A, and GPR109B). *Pharmacol Rev* **63**, 269–90 (2011).
94. Duncan, R. E., Ahmadian, M., Jaworski, K., Sarkadi-Nagy, E. & Sul, H. S. Regulation of lipolysis in

- adipocytes. *Annu. Rev. Nutr.* **27**, 79–101 (2007).
95. Shi, Y. *et al.* Activated niacin receptor HCA2 inhibits chemoattractant-mediated macrophage migration via Gβγ/PKC/ERK1/2 pathway and heterologous receptor desensitization. *Sci. Rep.* **7**, 42279 (2017).
96. Zandi-Nejad, K. *et al.* The role of HCA2 (GPR109A) in regulating macrophage function. *FASEB J.* **27**, 4366–4374 (2013).
97. Knowles, H. J., te Poele, R. H., Workman, P. & Harris, A. L. Niacin induces PPARγ expression and transcriptional activation in macrophages via HM74 and HM74a-mediated induction of prostaglandin synthesis pathways. *Biochem. Pharmacol.* **71**, 646–56 (2006).
98. Exton, J. H. Regulation of phosphoinositide phospholipases by hormones, neurotransmitters, and other agonists linked to G proteins. *Annu. Rev. Pharmacol. Toxicol.* **36**, 481–509 (1996).
99. Tang, H., Lu, J. Y., Zheng, X., Yang, Y. & Reagan, J. D. The psoriasis drug monomethylfumarate is a potent nicotinic acid receptor agonist. *Biochem. Biophys. Res. Commun.* **375**, 562–5 (2008).
100. Sun, H. *et al.* Niacin Activates the PI3K/Akt Cascade via PKC- and EGFR-Transactivation-Dependent Pathways through Hydroxyl-Carboxylic Acid Receptor 2. *PLoS ONE* **9**, (2014).
101. Li, G. *et al.* Internalization of the Human Nicotinic Acid Receptor GPR109A Is Regulated by Gi, GRK2, and Arrestin3. *J. Biol. Chem.* **285**, 22605–22618 (2010).
102. Offermanns, S. & Schwaninger, M. Nutritional or pharmacological activation of HCA2 ameliorates neuroinflammation. *Trends Mol. Med.* **21**, 245–255 (2015).
103. Chai, J. T., Digby, J. E. & Choudhury, R. P. GPR109A and vascular inflammation. *Curr. Atheroscler. Rep.* **15**, 325 (2013).
104. Amulic, B., Cazalet, C., Hayes, G. L., Metzler, K. D. & Zychlinsky, A. Neutrophil Function: From Mechanisms to Disease. *Annu. Rev. Immunol.* **30**, 459–489 (2012).
105. Gulbins, E. & Lang, K. S. Immunsystem. in *Physiologie des Menschen: mit Pathophysiologie* (eds. Schmidt, R. F. & Lang, F.) 550–562 (Springer Berlin Heidelberg, 2007). doi:10.1007/978-3-540-32910-7_24.
106. Puga, I. *et al.* B cell-helper neutrophils stimulate the diversification and production of immunoglobulin in the marginal zone of the spleen. *Nat. Immunol.* **13**, 170–180 (2011).
107. Leiding, J. W. & Holland, S. M. Chronic Granulomatous Disease. in *GeneReviews®* (eds. Adam, M. P. *et al.*) (University of Washington, Seattle, 1993).
108. Fahy, J. V., Kim, K. W., Liu, J. & Boushey, H. A. Prominent neutrophilic inflammation in sputum from subjects with asthma exacerbation. *J. Allergy Clin. Immunol.* **95**, 843–852 (1995).
109. McColl, S. R. *et al.* Treatment with anti-granulocyte antibodies inhibits the effector phase of experimental autoimmune encephalomyelitis. *J. Immunol. Baltim. Md 1950* **161**, 6421–6426 (1998).
110. Miller, S. D., Karpus, W. J. & Davidson, T. S. Experimental Autoimmune Encephalomyelitis in the Mouse. *Curr. Protoc. Immunol. Ed. John E Coligan Al CHAPTER*, Unit-15.1 (2007).
111. Ludwig, R. J., Kalies, K., Köhl, J., Zillikens, D. & Schmidt, E. Emerging treatments for pemphigoid diseases. *Trends Mol. Med.* **19**, 501–512 (2013).
112. Liu, Z. *et al.* A major role for neutrophils in experimental bullous pemphigoid. *J. Clin. Invest.* **100**, 1256–1263 (1997).
113. Liu, Z. *et al.* Subepidermal Blistering Induced by Human Autoantibodies to BP180 Requires Innate Immune Players in a Humanized Bullous Pemphigoid Mouse Model. *J. Autoimmun.* **31**, 331–338 (2008).
114. Hoffmann, J. H. O., Schaekel, K., Hartl, D., Enk, A. H. & Hadaschik, E. N. Dimethyl fumarate modulates neutrophil extracellular trap formation in a glutathione- and superoxide-dependent manner. *Br. J. Dermatol.* **178**, 207–214 (2018).
115. Zarbock, A. & Ley, K. Mechanisms and Consequences of Neutrophil Interaction with the Endothelium. *Am. J. Pathol.* **172**, 1–7 (2008).
116. Spertini, O. *et al.* Leukocyte adhesion molecule-1 (LAM-1, L-selectin) interacts with an inducible endothelial cell ligand to support leukocyte adhesion. *J. Immunol. Baltim. Md 1950* **147**, 2565–2573 (1991).
117. Krauss, K. & Altevogt, P. Integrin Leukocyte Function-associated Antigen-1-mediated Cell Binding Can Be Activated by Clustering of Membrane Rafts. *J. Biol. Chem.* **274**, 36921–36927 (1999).
118. Christofidou-Solomidou, M., Nakada, M. T., Williams, J., Muller, W. A. & DeLisser, H. M. Neutrophil platelet endothelial cell adhesion molecule-1 participates in neutrophil recruitment at inflammatory sites and is down-regulated after leukocyte extravasation. *J. Immunol. Baltim. Md 1950* **158**, 4872–4878 (1997).
119. Seely, A. J., Pascual, J. L. & Christou, N. V. Science review: Cell membrane expression (connectivity) regulates neutrophil delivery, function and clearance. *Crit. Care* **7**, 291 (2003).
120. Ivetic, A. A head-to-tail view of L-selectin and its impact on neutrophil behaviour. *Cell Tissue Res.* **371**, 437–453 (2018).
121. Tunaru, S. *et al.* PUMA-G and HM74 are receptors for nicotinic acid and mediate its anti-lipolytic effect. *Nat Med* **9**, 352–5 (2003).
122. Tierärztliche Vereinigung für Tierschutz e.V. Empfehlungen zur Planung und Durchführung von Tierversuchen, Merkblatt Nr. 76. <https://www.tierschutz-tvt.de/alle-merkblaetter-und-stellungnahmen/#c306>.
123. Telford, W. G., Babin, S. A., Khorev, S. V. & Rowe, S. H. Green fiber lasers: An alternative to traditional DPSS green lasers for flow cytometry. *Cytometry A* **75A**, 1031–1039 (2009).
124. Bigos, M. Separation Index: An Easy-to-Use Metric for Evaluation of Different Configurations on the Same Flow Cytometer. in *Current Protocols in Cytometry* (eds. Robinson, J. P. *et al.*) (John Wiley & Sons, Inc., 2007). doi:10.1002/0471142956.cy0121s40.
125. Koga, H. *et al.* Epidermolysis Bullosa Acquisita: The 2019 Update. *Front. Med.* **5**, (2019).
126. Berry-Kravis, E., Booth, G., Sanchez, A. C. & Woodbury-Kolb, J. Carnitine levels and the ketogenic diet.

- Epilepsia* **42**, 1445–1451 (2001).
127. Sitaru, C. *et al.* Induction of dermal-epidermal separation in mice by passive transfer of antibodies specific to type VII collagen. *J. Clin. Invest.* **115**, 870–878 (2005).
 128. Carlson, L. A. Nicotinic acid: the broad-spectrum lipid drug. A 50th anniversary review. *J Intern Med* **258**, 94–114 (2005).
 129. Gille, A., Bodor, E. T., Ahmed, K. & Offermanns, S. Nicotinic Acid: Pharmacological Effects and Mechanisms of Action. *Ann Rev Pharmacol Toxicol* **48**, 79–106 (2008).
 130. *Löffler/Petrides Biochemie und Pathobiochemie.* (Springer-Verlag, 2014).
 131. Martin, W. J., Walton, M. & Harper, J. Resident macrophages initiating and driving inflammation in a monosodium urate monohydrate crystal-induced murine peritoneal model of acute gout. *Arthritis Rheum.* **60**, 281–289 (2009).
 132. Lee, J. M. S. *et al.* Effects of High-Dose Modified-Release Nicotinic Acid on Atherosclerosis and Vascular Function: A Randomized, Placebo-Controlled, Magnetic Resonance Imaging Study. *J. Am. Coll. Cardiol.* **54**, 1787–1794 (2009).
 133. Bursill, C. A., Choudhury, R. P., Ali, Z., Greaves, D. R. & Channon, K. M. Broad-spectrum CC-chemokine blockade by gene transfer inhibits macrophage recruitment and atherosclerotic plaque formation in apolipoprotein E-knockout mice. *Circulation* **110**, 2460–2466 (2004).
 134. Dansky, H. M. *et al.* Adhesion of monocytes to arterial endothelium and initiation of atherosclerosis are critically dependent on vascular cell adhesion molecule-1 gene dosage. *Arterioscler. Thromb. Vasc. Biol.* **21**, 1662–1667 (2001).
 135. Digby, J. E. *et al.* Anti-inflammatory effects of nicotinic acid in human monocytes are mediated by GPR109A dependent mechanisms. *Arterioscler. Thromb. Vasc. Biol.* **32**, 669–676 (2012).
 136. Chigaev, A., Waller, A., Zwartz, G. J., Buranda, T. & Sklar, L. A. Regulation of cell adhesion by affinity and conformational unbending of alpha4beta1 integrin. *J. Immunol. Baltim. Md 1950* **178**, 6828–6839 (2007).
 137. Deakin, J. E., Parra, Z. E., Graves, J. a. M. & Miller, R. D. Physical mapping of T cell receptor loci (TRA@, TRB@, TRD@ and TRG@) in the opossum (*Monodelphis domestica*). *Cytogenet. Genome Res.* **112**, 342K–342K (2006).
 138. Glusman, G. *et al.* Comparative Genomics of the Human and Mouse T Cell Receptor Loci. *Immunity* **15**, 337–349 (2001).
 139. Born, W. K., Reardon, C. L. & O'Brien, R. L. The function of $\gamma\delta$ T cells in innate immunity. *Curr. Opin. Immunol.* **18**, 31–38 (2006).
 140. Holtmeier, W. & Kabelitz, D. $\gamma\delta$ T Cells Link Innate and Adaptive Immune Responses. *Mech. Epithel. Def.* **86**, 151–183 (2005).
 141. Morita, C. T., Mariuzza, R. A. & Brenner, M. B. Antigen recognition by human $\gamma\delta$ T cells: pattern recognition by the adaptive immune system. *Springer Semin. Immunopathol.* **22**, 191–217 (2000).
 142. Kabelitz, D., Marischen, L., Oberg, H.-H., Holtmeier, W. & Wesch, D. Epithelial Defence by $\gamma\delta$ T Cells. *Int. Arch. Allergy Immunol.* **137**, 73–81 (2005).
 143. Bonneville, M. & Fournié, J.-J. Sensing cell stress and transformation through Vgamma9Vdelta2 T cell-mediated recognition of the isoprenoid pathway metabolites. *Microbes Infect.* **7**, 503–509 (2005).
 144. Smith, A. L. & Hayday, A. C. An $\alpha\beta$ T-cell-independent immunoprotective response towards gut coccidia is supported by $\gamma\delta$ cells. *Immunology* **101**, 325–332 (2000).
 145. Brandes, M., Willmann, K. & Moser, B. Professional antigen-presentation function by human gammadelta T Cells. *Science* **309**, 264–268 (2005).
 146. Wu, Y. *et al.* Human $\gamma\delta$ T Cells: A Lymphoid Lineage Cell Capable of Professional Phagocytosis. *J. Immunol.* **183**, 5622–5629 (2009).
 147. Rajan, A. J., Gao, Y. L., Raine, C. S. & Brosnan, C. F. A pathogenic role for gamma delta T cells in relapsing-remitting experimental allergic encephalomyelitis in the SJL mouse. *J. Immunol. Baltim. Md 1950* **157**, 941–949 (1996).
 148. Blink, S. E. *et al.* $\gamma\delta$ T cell subsets play opposing roles in regulating experimental autoimmune encephalomyelitis. *Cell. Immunol.* **290**, 39–51 (2014).
 149. Zarobkiewicz, M. K., Kowalska, W., Roliński, J. & Bojarska-Junak, A. A. $\gamma\delta$ T lymphocytes in the pathogenesis of multiple sclerosis and experimental autoimmune encephalomyelitis. *J. Neuroimmunol.* **330**, 67–73 (2019).
 150. Boyman, O. *et al.* Spontaneous development of psoriasis in a new animal model shows an essential role for resident T cells and tumor necrosis factor-alpha. *J. Exp. Med.* **199**, 731–736 (2004).
 151. Pantelyushin, S. *et al.* Ror γ t⁺ innate lymphocytes and $\gamma\delta$ T cells initiate psoriasiform plaque formation in mice. *J. Clin. Invest.* **122**, 2252–2256 (2012).
 152. Cai, Y. *et al.* Pivotal role of dermal IL-17-producing $\gamma\delta$ T cells in skin inflammation. *Immunity* **35**, 596–610 (2011).
 153. Oswald, E. *et al.* Reduced numbers of circulating gammadelta T cells in patients with bullous pemphigoid. *Exp. Dermatol.* **18**, 991–993 (2009).
 154. O'Brien, R. L. & Born, W. K. Dermal $\gamma\delta$ T Cells – What Have We Learned? *Cell. Immunol.* **296**, 62–69 (2015).
 155. Bieber, K. *et al.* T cells mediate autoantibody-induced cutaneous inflammation and blistering in epidermolysis bullosa acquisita. *Sci. Rep.* **6**, 38357 (2016).
 156. Xie, X.-J. *et al.* Indirubin ameliorates imiquimod-induced psoriasis-like skin lesions in mice by inhibiting inflammatory responses mediated by IL-17A-producing $\gamma\delta$ T cells. *Mol. Immunol.* **101**, 386–395 (2018).
 157. Mutational analysis of the membrane-proximal cleavage site of L-selectin: relaxed sequence specificity surrounding the cleavage site. *J. Exp. Med.* **182**, 549–557 (1995).

158. Rizoli, S. B., Rotstein, O. D. & Kapus, A. Cell Volume-dependent Regulation of L-selectin Shedding in Neutrophils A ROLE FOR p38 MITOGEN-ACTIVATED PROTEIN KINASE. *J. Biol. Chem.* **274**, 22072–22080 (1999).
159. Smalley, D. M. & Ley, K. L-selectin: mechanisms and physiological significance of ectodomain cleavage. *J. Cell. Mol. Med.* **9**, 255–266 (2005).
160. Casanova-Acebes, M. *et al.* Rhythmic modulation of the hematopoietic niche through neutrophil clearance. *Cell* **153**, 1025–1035 (2013).
161. Raffler, N. A., Rivera-Nieves, J. & Ley, K. L-selectin in inflammation, infection and immunity. *Drug Discov. Today Ther. Strateg.* **2**, 213–220 (2005).
162. Lee, D., Schultz, J. B., Knauf, P. A. & King, M. R. Mechanical Shedding of L-selectin from the Neutrophil Surface during Rolling on Sialyl Lewis x under Flow. *J. Biol. Chem.* **282**, 4812–4820 (2007).
163. Killock, D. J. & Ivetić, A. The cytoplasmic domains of TNF α -converting enzyme (TACE/ADAM17) and L-selectin are regulated differently by p38 MAPK and PKC to promote ectodomain shedding. *Biochem. J.* **428**, 293–304 (2010).
164. Klein, S. L. & Flanagan, K. L. Sex differences in immune responses. *Nat. Rev. Immunol.* **16**, 626–638 (2016).
165. Pennell, L. M., Galligan, C. L. & Fish, E. N. Sex affects immunity. *J. Autoimmun.* **38**, J282–291 (2012).
166. Verthelyi, D. Sex hormones as immunomodulators in health and disease. *Int. Immunopharmacol.* **1**, 983–993 (2001).
167. Wang, J. *et al.* Unusual maintenance of X chromosome inactivation predisposes female lymphocytes for increased expression from the inactive X. *Proc. Natl. Acad. Sci. U. S. A.* **113**, E2029–2038 (2016).
168. Kaushic, C., Roth, K. L., Anipindi, V. & Xiu, F. Increased prevalence of sexually transmitted viral infections in women: the role of female sex hormones in regulating susceptibility and immune responses. *J. Reprod. Immunol.* **88**, 204–209 (2011).
169. Klein, S. L. Sex influences immune responses to viruses, and efficacy of prophylaxis and treatments for viral diseases. *BioEssays News Rev. Mol. Cell. Dev. Biol.* **34**, 1050–1059 (2012).
170. Quintero, O. L., Amador-Patarroyo, M. J., Montoya-Ortiz, G., Rojas-Villarraga, A. & Anaya, J.-M. Autoimmune disease and gender: plausible mechanisms for the female predominance of autoimmunity. *J. Autoimmun.* **38**, J109–119 (2012).
171. Trojano, M. *et al.* Geographical variations in sex ratio trends over time in multiple sclerosis. *PLoS One* **7**, e48078 (2012).
172. Voskuhl, R. R. & Gold, S. M. Sex-related factors in multiple sclerosis susceptibility and progression. *Nat. Rev. Neurol.* **8**, 255–263 (2012).
173. Weinshenker, B. G. Natural history of multiple sclerosis. *Ann. Neurol.* **36 Suppl**, S6–11 (1994).
174. Beatty, W. W. & Aupperle, R. L. Sex differences in cognitive impairment in multiple sclerosis. *Clin. Neuropsychol.* **16**, 472–480 (2002).
175. Bove, R. & Chitnis, T. The role of gender and sex hormones in determining the onset and outcome of multiple sclerosis. *Mult. Scler. Houndmills Basingstoke Engl.* **20**, 520–526 (2014).
176. Pozzilli, C., Pugliatti, M. & ParadigMS Group. An overview of pregnancy-related issues in patients with multiple sclerosis. *Eur. J. Neurol.* **22 Suppl 2**, 34–39 (2015).
177. Bove, R. *et al.* Low testosterone is associated with disability in men with multiple sclerosis. *Mult. Scler. Houndmills Basingstoke Engl.* **20**, 1584–1592 (2014).
178. Murase, J. E., Chan, K. K., Garite, T. J., Cooper, D. M. & Weinstein, G. D. Hormonal effect on psoriasis in pregnancy and post partum. *Arch. Dermatol.* **141**, 601–606 (2005).
179. Bain, B. J. Ethnic and sex differences in the total and differential white cell count and platelet count. *J. Clin. Pathol.* **49**, 664–666 (1996).
180. Jiang, W., Zhang, L., Lang, R., Li, Z. & Gilkeson, G. Sex differences in monocyte activation in systemic lupus erythematosus (SLE). *PLoS One* **9**, e114589 (2014).
181. River, C. Biochemistry and Hematology for C57BL6NCrI Mouse Colonies in North American for January 2008-December 2012.pdf. http://animalab.eu/sites/all/pliki/produkty-dopobrania/Biochemistry_and_Hematology_for_C57BL6NCrI_Mouse_Colonies_in_North_American_for_January_2008_December_2012.pdf.
182. Vmd, L. M. S. Serum Clinical Chemistry and Hematology Reference Values in Outbred Stocks of Albino Mice from Three Commonly Used Vendors and Two Inbred Strains of Albino Mice. *White Blood Cells* **42**, 7 (2003).
183. Umiker, B. R. *et al.* Dosage of X-linked Toll-like receptor 8 determines gender differences in the development of systemic lupus erythematosus. *Eur. J. Immunol.* **44**, 1503–1516 (2014).
184. Hartman, A. L., Gasior, M., Vining, E. P. & Rogawski, M. A. The neuropharmacology of the ketogenic diet. *Pediatr Neurol* **36**, 281–92 (2007).
185. WILDER, R. The effects of ketonemia on the course of epilepsy. *Mayo Clin Proc* **2**, 307–308 (1921).
186. Maalouf, M., Rho, J. M. & Mattson, M. P. The neuroprotective properties of calorie restriction, the ketogenic diet, and ketone bodies. *Brain Res Rev* **59**, 293–315 (2009).
187. Sullivan, P. G. *et al.* The ketogenic diet increases mitochondrial uncoupling protein levels and activity. *Ann. Neurol.* **55**, 576–580 (2004).
188. Jarrett, S. G., Milder, J. B., Liang, L.-P. & Patel, M. The ketogenic diet increases mitochondrial glutathione levels. *J. Neurochem.* **106**, 1044–1051 (2008).
189. Kim do, Y. *et al.* Inflammation-mediated memory dysfunction and effects of a ketogenic diet in a murine model of multiple sclerosis. *PLoS ONE* **7**, e35476 (2012).
190. Yang, X. & Cheng, B. Neuroprotective and Anti-inflammatory Activities of Ketogenic Diet on MPTP-induced

Neurotoxicity. *J Mol Neurosci* **42**, 145–153 (2010).

191. Newman, J. C. & Verdin, E. Ketone bodies as signaling metabolites. *Trends Endocrinol Metab* **25**, 42–52 (2014).

192. Choi, I. Y. *et al.* A Diet Mimicking Fasting Promotes Regeneration and Reduces Autoimmunity and Multiple Sclerosis Symptoms. *Cell Rep.* **15**, 2136–2146 (2016).

193. Fomin, D. A., McDaniel, B. & Crane, J. The promising potential role of ketones in inflammatory dermatologic disease: a new frontier in treatment research. *J. Dermatol. Treat.* **28**, 484–487 (2017).

194. Okayama, Y. Oxidative stress in allergic and inflammatory skin diseases. *Curr. Drug Targets Inflamm. Allergy* **4**, 517–519 (2005).

195. Allhorn, M., Lundqvist, K., Schmidtchen, A. & Akerström, B. Heme-scavenging role of alpha1-microglobulin in chronic ulcers. *J. Invest. Dermatol.* **121**, 640–646 (2003).

196. Hiramoto, K., Kobayashi, H., Yamate, Y., Ishii, M. & Sato, E. F. Intercellular pathway through hyaluronic acid in UVB-induced inflammation. *Exp. Dermatol.* **21**, 911–914 (2012).

197. Birge, K. Nutrition Management of Patients with Epidermolysis Bullosa. *J. Am. Diet. Assoc.* **95**, 575–579 (1995).

198. Lakdawala, N. *et al.* The role of nutrition in dermatologic diseases: Facts and controversies. *Clin. Dermatol.* **31**, 677–700 (2013).

199. Institute of Medicine (US) Standing Committee on the Scientific Evaluation of Dietary Reference Intakes and its Panel on Folate, Other B Vitamins, and Choline. *Dietary Reference Intakes for Thiamin, Riboflavin, Niacin, Vitamin B6, Folate, Vitamin B12, Pantothenic Acid, Biotin, and Choline.* (National Academies Press (US), 1998).

8.0 Appendix

8.1 Abbreviations

↑	Elevation (for example in number of cells detected)
↓	Reduction (for example in number of cells detected)
♂	Male
♀	Female
AA	Arachidonic acid
AC	Adenylate cyclase
ALS	Amyotrophic lateral sclerosis
AMP	Adenosine monophosphate
ANOVA	Analysis of variance
APC	Allophycocyanin
ATP	Adenosine triphosphate
AUC	Area under the curve
AUT	Austria
BHB	β-hydroxybutyrate
BP	Bullous pemphigoid
BSA	Bovine serum albumin
BV	Brilliant™ violet
cAMP	Cyclic adenosine monophosphate
CD	Cluster of differentiation
CD	Cluster of differentiation
CH	Switzerland
CIS	Clinically isolated syndrome
CNS	Central nervous system
COL7	Collagen Type VII
COR	Corea
CTLD	Calcium-type lectin domain
Cy7	Cyanine dye 7
DABCO	1,4-Diazabicyclo[2.2.2]octane
DAPI	4',6-diamidino-2-phenylindole
DC	Dendritic cell
DECT	Dendritic epidermal T cell
DHEA-S	Dehydroepiandrosterone sulphate
DIF	Direct immunofluorescence
DMF	Dimethyl fumarate
DMSO	Dimethyl sulfoxide
EAE	Experimental autoimmune encephalomyelitis
EBA	Epidermolysis bullosa acquisita
EBA	Epidermolysis bullosa acquisita
EDTA	Ethylenediaminetetraacetate
$E_{n_{max}}$	Emission maximum
ERK1/2	Extracellular signal-regulating kinase 1/2
F	France
FACS	Fluorescence-activated cell scanning

FC	Fragment, crystallizable region
FCS	Fetal calf serum
FITC	Fluorescein isothiocyanate
FSC	Forward scatter
G	Germany
GABA	γ -aminobutyric acid
GB	Great Britain
GRK	G protein coupled receptor kinase
GRP109A	G-protein coupled receptor 109A, also HCA ₂ receptor
HBSS	Hank's Balanced Salt Solution
HCA ₂	Hydroxycarboxylic acid receptor 2
Hcar2	Hydroxycarboxylic acid receptor 2 (gene)
HLA	Human leukocyte antigen
HSP	Heat shock protein
i. p.	Intraperitoneal
IC ₅₀	half maximal inhibitory concentration
ICAM	Intracellular adhesion molecule
IEM	Immunolectron microscopy
IF microscopy	Immunofluorescence microscopy
IFN- β	Interferon- β
IFN- γ	Interferon- γ
Ig	Immunoglobulin
IL	Interleukin
ISEF	Institute for Systemic Inflammatory Research
IVIG	Intravenous Immunoglobulin
JP	Japan
KD	Ketogenic diet
KO	Knockout
LPS	Lipopolysaccharide
MAPK	Mitogen-activated protein kinase
MBP	Myelin basic protein
Med _{neg}	Medium fluorescent intensity of the negative population
Med _{pos}	Medium fluorescent intensity of the positive population
MFI	Medium fluorescent intensity
MHC	Major histocompatibility complex
Min	Minute
MMF	Monomethyl fumarate
MMPs	Matrix metalloproteinases
MOG	Myelin oligodendrocyte glycoprotein
mRFP	Monomeric red fluorescent protein
MRI	Magnetic resonance imaging
MS	Multiple sclerosis
NA	Nicotinic acid
NAD	Nicotinamide adenine dinucleotide
NADP	Nicotinamide adenine dinucleotide phosphate
NED	Netherlands
NET	Neutrophil extracellular trap
NF-kB	nuclear factor ' κ -light-chain-enhancer' of activated B-cells
NK cells	Natural killer cells
NKT cells	Natural killer T cells

P	Phosphorylation/ phosphorylated
p.o.	Per os
PBECs	Primary brain endothelial cells
PBMCs	Peripheral blood mononuclear cells
PBS	Phosphate buffered saline
PE	R-phycoerythrin
PECAM	Platelet-endothelial cell adhesion molecule
Per	Peridinin-Chlorophyll-protein
PFA	Paraformaldehyde
PGD ₂	Prostaglandin D ₂
PGE ₂	Prostaglandin E ₂
PI3K	Phosphoinositide 3-kinases
PKA	Protein kinase A
PLA ₂	Phospholipase A ₂
PMSF	Phenylmethylsulphonyl fluoride
PNS	Peripheral nervous system
PP-MS	Primary progressive multiple sclerosis
PPAR- γ	Peroxisome proliferator-activated receptor gamma
PTGS1	Prostaglandin synthase 1
RFP	Red fluorescent protein
ROS	Reactive oxygen species
RPMI	Roswell Park Memorial Institute buffer
RR-MS	Relapse remitting multiple sclerosis
RT	Room temperature
SEM	Standard error of the mean
SI	Staining index
SLE	Systemic lupus erythematosus
SP-MS	Secondary progressive multiple sclerosis
SSC	Side scatter
TAE	TRIS-acetate-EDTA
TBS	TRIS-buffered saline
TCR	T cell receptor
Th1/17	T helper cell type 1/17
TLCK	Tosyl-L-lysyl-chloromethane hydrochloride
TNF- α	Tumour necrosis factor - α
TRIS	tris(hydroxymethyl)aminomethane
UK	United Kingdom
USA	United States of America
VCAM-1	Vascular cell adhesion molecule 1
WT	Wildtype

8.2 List of tables

Table 4.1: Mouse lines used during the experiments and their specifications.	29
Table 4.2: Scoring of affected body surface area on day 13 of disease.	32
Table 5.10.: Antibody panel for HCA ₂ expression experiments.	54

8.3 List of figures

Figure 2.1: Clinical presentation of Epidermolysis bullosa acquisita	5
Figure 2.2: Effects of DMF on different cell types.	12
Figure 2.3: HCA ₂ receptor downstream cascade.	16
Figure 4.1: Course of bodyweight during EBA Experiment.	31
Figure 4.2: Gating strategy of flow cytometry analysis.	38
Figure 5.1: Antibody titration FACS L-selectin (CD62L) antibody.	44
Figure 5.2: Antibody titration T cell receptor gamma variable region 1 (Trgv1.1).	46
Figure 5.3: Antibody titration T cell receptor gamma variable 2 (Trgv2).	47
Figure 5.4: Antibody titration for the T cell receptor gamma variable 3 (Trgv3).	48
Figure 5.5: Representative immunohistochemical staining of anti-collagen VII-IgG and C3 depositions at the dermal–epidermal junction.	49
Figure 5.6: IgG deposition at the dermal-epidermal junction.	50
Figure 5.7: C3 deposition at the dermal-epidermal junction.	51
Figure 5.8: Average epidermal thickness measurement.	52
Figure 5.9: Epidermal thickness measurement.	52
Figure 5.10: HCA ₂ receptor expression in blood and skin in different cell types and with regard to treatment.	55
Figure 5.11: RFP ⁺ cells in spleen and lymph node.	55
Figure 5.12: DMF treatment of mice does not reduce elevated numbers of neutrophils in blood and lymphoid tissue.	56
Figure 5.13: DMF treatment of mice does not reduce elevated numbers of monocytes in blood.	57
Figure 5.14: DMF treatment of mice does not affect elevated numbers of NK cells.	59
Figure 5.15: DMF treatment of mice does not reduce elevated numbers of $\gamma\delta$ T cells in blood and lymphoid tissue.	60
Figure 5.16: Inflammatory cells in the skin.	62

Figure 5.17: Inflammatory cells in spleen and lymph node.	64
Figure 5.18: DMF treatment inhibits activation of neutrophils and non-classical monocytes.	66
Figure 5.19: DMF treatment does not affect CD62L expression on immune cells in secondary lymphoid tissues.	66
Figure 5.20: Therapeutic dimethyl fumarate (DMF) effects in experimental epidermolysis bullosa acquisita (EBA) depend on HCA ₂ .	68
Figure 5.21: DMF effect in EBA is HCA ₂ -receptor dependent in male mice.	68
Figure 5.22: Higher HCA ₂ expression in male mice.	70
Figure 5.23: Higher RFP expression in male mice.	71
Figure 5.24: Ketogenic diet did not alter disease onset and disease severity in EBA.	73
Figure 5.25: Niacin-free diet did alter Nicotinic acid level in plasma.	74

8.4 Tierversuchsgenehmigung

Zur Durchführung der Versuche erfolgte durch Herrn Dr. Julian Assmann, Arbeitsgruppenleiter AG Prof. Schwaninger, vor Beginn ein Tierversuchsantrag beim Umwelt- und Landwirtschaftsministerium Schleswig-Holstein in Kiel unter dem Aktenzeichen V 242-79898/2015 (110-8/15), welcher am 10.12.2012 genehmigt wurde und eine Verlängerung des Antrages, welche am 28. Juni 2017 (Aktenzeichen V241 – 34001/2017 (110-8/15) erteilt wurde.

9.0 Curriculum vitae



Jakob Friedrich Vielhauer

PERSÖNLICHE ANGABEN

Geburtsdatum/ -ort	20.04.1994 in Troisdorf
Anschrift	Osnabrücker Straße 3 57439 Attendorn
Telefon	+491707339623
E-Mail	jakobvielhauer@gmail.com

AUSBILDUNG

2004-2013	Bilinguales Abitur (Note 1.0), St. Ursula Gymnasium, Attendorn
01/2016-jetzt	Promotion Universität zu Lübeck Institut für Experimentelle und Klinische Pharmakologie und Toxikologie Direktor: Prof. Dr. med. M. Schwaninger „Therapeutic effects mediated through the Hydroxycarboxylic acid receptor 2 in an autoimmune blistering disease of the skin.“, Zeitraum der Versuchsdurchführung: 04/2016-06/2018
WiSe 2016/2017	Forschungssemester Unterstützung durch ein Stipendium der Deutschen Forschungsgesellschaft (DFG); Förderung in der klinischen Forschergruppe

(KFO/CRU) 303 sowie dem
Graduiertenkolleg 1727 der Universität zu
Lübeck

10/2013- 19.06.2020

Studium der Humanmedizin

Universität zu Lübeck

03.09.2015

Ablegen des „Ersten Abschnitts der
Ärztlichen Prüfung“ (Physikum), Note „gut“

11.04.2019

Ablegen des „Zweiten Abschnitts der
Ärztlichen Prüfung“ (StEx), Note „gut“

19.06.2020

Ablegen des „Dritten Abschnitts der
Ärztlichen Prüfung“ (mündliches
Staatsexamen), Note „sehr gut“

19.06.2020

Erteilung der Approbation als Arzt

Mitgliedschaft Fachgesellschaften

seit 5.3.2018

Mitglied in der Deutschen Gesellschaft für
Gastroenterologie, Verdauungs- und
Stoffwechselkrankheiten (DGVS),
Kongressbesuche: DGVS Jahreskongress
„Viszeralmedizin“ 2019, Wiesbaden;
EndoClub Nord in Hamburg 2018

seit 16.3.2018

Mitglied der Deutschen Gesellschaft für
Innere Medizin (DGIM)

Praktisches Jahr

20.05.- 08.09.2019

Klinik für Neurochirurgie -
Universitätsklinikum Schleswig-Holstein,

Campus Lübeck, Leiter: Prof. Tronnier

09.09.2019-29.12.2019

Chirurgische Klinik, St. Claraspital, Basel,
Schweiz, Lehrkrankenhaus der Universität
Basel, Leiter: Prof. von Flüe

30.12.2019-19.04.2020

Medizinische Kliniken, Sana Klinikum,
Lübeck, Lehrkrankenhaus der Universität zu
Lübeck, Leitung Prof. Weil, PD Dr.
Fetscher, PD Dr. Bahr

PUBLIKATION

Wannick M¹, Assmann JC¹, **Vielhauer JF**, Offermanns S, Zillikens D, Sadik CD and Schwaninger M: The Immunometabolomic Interface Receptor Hydroxycarboxylic Acid Receptor 2 Mediates the Therapeutic Effects of Dimethyl Fumarate in Autoantibody-Induced Skin Inflammation. *Front. Immunol.* 9:1890. doi: 10.3389/fimmu.2018.01890

¹: shared 1st authorship

POSTER- UND PROJEKTPRÄSENTATIONEN

11/2016

Graduiertenkolleg 1727/Klinische
Forschergruppe 303, Autumn Retreat

01/2017

Graduiertenkolleg 1727/ Klinische
Forschergruppe 303, Jour fixe

03/2017

Graduiertenkolleg 1727/ Klinische
Forschergruppe 303, Spring Retreat

Parts of the data have already been published: Wannick M¹, Assmann JC¹, **Vielhauer JF**, Offermanns S, Zillikens D, Sadik CD and Schwaninger M: The Immunometabolomic Interface Receptor Hydroxycarboxylic Acid Receptor 2 Mediates the Therapeutic Effects of Dimethyl Fumarate in Autoantibody-Induced Skin Inflammation. *Front. Immunol.* 9:1890. doi: 10.3389/fimmu.2018.01890

¹: shared 1st authorship

10.0 Danksagung

Zunächst möchte ich Herrn Prof. Schwaninger für die Möglichkeit danken, in der Pharmakologie promovieren zu dürfen. Nicht nur haben Sie mich enorm unterstützt bei der Planung und Auswertung des experimentellen Teils der Doktorarbeit, sondern auch dazu beigetragen meinen Wunsch später weiterhin in der Forschung tätig zu sein, zu festigen. Zudem danke ich Ihnen für die Ermöglichung der Assoziation des Projektes an die Klinische Forschergruppe 303. Der wissenschaftliche Austausch und die Möglichkeit das Projekt im Rahmen der wiederholten Treffen vorzustellen hat wesentlich zur Entwicklung meiner Dissertation beigetragen.

Herrn Prof. Zillikens und Herrn Prof. Sadik danke ich für die Assoziation des Projektes mit der Klinischen Forschergruppe 303, die regelmäßigen konstruktiven Diskussion zur weiteren Planung sowie Einladung zu den Retreats mit Vorstellung meiner jeweiligen Ergebnisse. Zudem möchte ich mich für die finanzielle Unterstützung durch das gewährte Stipendium bedanken.

Ebenfalls gilt mein Dank Frau PD Dr. K. Kalies und Prof Dr. Ludwig für die Übernahme des Zeitgutachtens und des Prüfungsvorsitzes für meine Promotion.

Ein außerordentlich großer Dank für die umfassende Betreuung und nicht ermüdenden Erklärungen zur genauen Ausführung und Planung der nächsten Experimente möchte ich an Herrn Dr. Julian Assmann und Frau Dr. Melanie Wannick richten! Danke Melanie, Danke Julian, ohne Eure enorme Unterstützung wäre die Anfertigung der Experimente nicht möglich gewesen. Ich betrachte es als großes Privileg, dass ihr mich so gut betreut und bei den Versuchen unterstützt habt!

Zudem möchte ich dem gesamten Team der Pharmakologie Lübeck für die stets konstruktiven Denkanstöße und Hilfestellung bei Experimenten danken, da es nicht selbstverständlich ist, jederzeit Unterstützung bei der Versuchsdurchführung zu erhalten. Zudem danke ich Ines, Frauke, Bea, Christine und Wiebke, ohne Euch wäre die tägliche Laborarbeit schlicht nicht möglich.

Meinen Eltern und meinem Bruder Julius danke ich, für all die Mühe und Zeit, die Ihr in mich investiert habt. Ohne Eure, nicht in Worten fassbare, Unterstützung hätte ich es nie dorthin geschafft, wo ich jetzt stehe. Danke, dass Ihr immer da seid, wenn ich Euch brauche! Auch meinen Großeltern, die mir so viel mitgegeben haben für mein Leben, möchte ich von Herzen danken, auch wenn Ihr es leider nicht mehr alle miterleben könnt.

Zuletzt möchte Dir, Inga, danken, dass Du mich stets begleitest und ich immer auf Dich zählen kann!

Eidesstattliche Erklärung

Erklärung

Hiermit versichere ich, dass ich die vorliegende Arbeit selbstständig verfasst und keine anderen als die angegebenen Hilfsmittel benutzt habe.

Lübeck, den ___13.06.2021___